NATIONAL ADVISORY COMMITTEE FOR AERONAUTICS

TECHNICAL NOTE 3839

EXPERIMENTAL DROPLET IMPINGEMENT ON SEVERAL TWO-

DIMENSIONAL AIRFOILS WITH THICKNESS

RATIOS OF 6 TO 16 PERCENT

By Thomas F. Gelder, William H. Smyers, Jr., and Uwe von Glahn

Lewis Flight Propulsion Laboratory
Cleveland, Ohio

NACA

TABLE OF CONTENTS

NATIONAL ADVISORY COMMITTEE FOR AERONAUTICS

TECHNICAL NOTE 3839

EXPERIMENTAL DROPLET IMPINGEMENT ON SEVERAL TWO-DIMENSIONAL

AIRFOILS WITH THICKNESS RATIOS OF 6 TO 16 PERCENT

By Thomas F. Gelder, William H. Smyers, Jr., and Uwe von Glahn

SUMMARY

The rate and area of cloud droplet impingement on several two-dimensional swept and unswept airfoils were obtained experimentally in the NACA Lewis icing tunnel with a dye-tracer technique. Airfoil thickness ratios of 6 to 16 percent, angles of attack from 0° to 12°, and chord sizes from 13 to 96 inches were included in the study. The data were obtained at 152 knots and are extended to other conditions by dimensionless impingement parameters.

In general, the data show that the total and local collection efficiencies and impingement limits are primary functions of the modified inertia parameter (in which airspeed, droplet size, and body size are the most significant variables) and the airfoil thickness ratio. Local collection efficiencies and impingement limits also depend on angle of attack. Secondary factors affecting impingement characteristics are airfoil shape, camber, and sweep angle. The impingement characteristics obtained experimentally for the airfoils were within ±10 percent on the average of the characteristics calculated from theoretical trajectories. Over the range of conditions studied, the experimental data demonstrate that a specific method can be used to predict the impingement characteristics of swept airfoils with large aspect ratios from the data for unswept airfoils of the same series.

INTRODUCTION

Knowledge of the local and total rates of cloud droplet impingement and of the surfacewise extent or limit of droplet impingement on bodies is required for the design and evaluation of icing-protection equipment for aircraft. These impingement characteristics are important factors in determining the extent of the surface to be protected, the shape and location of some ice formations on aircraft components, the aerodynamic penalties associated with icing of aircraft surfaces, and the local and total requirements for various thermal and fluid protection systems.

Previous studies (refs. 1 to 12) report the droplet trajectories about several two-dimensional bodies and bodies of revolution. These studies used differential analyzers for computing the droplet paths after the flow field about the body had been obtained. An empirical method for obtaining the impingement characteristics of airfoil sections is presented in reference 13. This method, however, is more suited to airfoils with blunt leading edges, because the basic data used in developing the method were obtained from four Joukowski airfoils and only one low-drag airfoil. For the two-dimensional case, a method for applying trajectory data from unswept airfoils to swept airfoils is presented in reference 14.

Droplet trajectories about bodies with unknown or complex flow fields are difficult to obtain with a differential analyzer. Therefore, a wind-tunnel method using a dye-tracer technique to obtain experimentally the impingement characteristics of bodies has been developed (ref. 15). In this technique water treated with known small quantities of a water-soluble dye is sprayed into the tunnel airstream by nozzles a large distance ahead of the body. The surface of the body is covered with blotter paper or a similar absorbent material upon which the dyed droplets impinge and are absorbed essentially upon contact. At the point of droplet impact and absorption, a permanent dye trace is deposited. The amount of dye deposited in a measured time interval can be determined by a colorimetric analysis of the blotter paper and can be converted into the amount of impinged water that produced the dye trace. From such an analysis and from known values of spray-cloud water content and droplet sizes, the impingement characteristics of a body can be determined readily, as discussed in reference 15.

In an extensive program of icing studies conducted in the NACA Lewis icing tunnel on various two- and three-dimensional bodies, experimental impingement data on six swept and two unswept airfoils (all two-dimensional) have been obtained. Although the airfoils used in these studies were a rather ad hoc collection of shapes and sizes, this report makes these data generally available and correlates the data as much as possible. The impingement data were obtained with airfoil chord sizes ranging from 13 to 96 inches, three volume-median droplet sizes ranging from 11 to 19 microns in diameter, and a nominal airspeed of 152 knots. The thickness ratio of the airfoils studied varied from 6 to 16 percent.

The airfoil impingement rates and limits obtained are presented in terms of dimensionless impingement parameters. These dimensionless parameters allow interpolation and extension of the experimental results over a wide range of operating conditions. The experimental impingement values for several airfoils are compared with values calculated from theoretically obtained trajectory data.

APPARATUS

Airfoil Models

This study of droplet impingement on various airfoil sections was conducted in the 6- by 9-foot test section of the NACA Lewis icing tunnel. The models, unless otherwise noted, were made of wood and spanned the 6-foot height of the tunnel (fig. 1). The airfoils are listed in the following table, and dimensionless streamwise sections are presented in figure 2.

Airfoil section (fig. 2)	Chord length in streamwise direction, in.	Remarks
(a) Joukowski 0015	13	
(b) Joukowski 0015	96	Smooth sheet-metal surface
(c) 63_2-015	13	
(d) 65_2-015	13	
(e) $65;2$-216	96	[1]Sheet-metal surface modified by 3/16-in.-thick de-icing boot extending from s_u of 0.156 to s_l of 0.250 (ref. 16)
(f) 65_1-212	13	
(g) 65_1-212	72	
(h) 65_1-206	72	Although the low-drag range for this series airfoil is <0.1 for thickness ratios <0.12 and thus the subscript 1 is usually omitted, it is retained herein to preserve similarity with the 65_1-212 section
(i) 65_1-212 (j) 65_1-206	87.9 87.9	Swept 35°, design section in plane perpendicular to leading edge

[1]Symbols are defined in appendix A.

The leading edge of the models was about 1.5 and 2.2 chord lengths from the entrance of the test section for the 96- and 72-inch-chord airfoils, respectively, and 9 chord lengths for the 13-inch-chord airfoils. These longitudinal locations indicate the length of the upstream flow field.

The local pressures on the surface of several models were obtained
by use of pressure belts. These experimental data, uncorrected for
tunnel wall effects, were used to indicate variations from the theoret-
ical pressure distributions.

Spray System and Related Equipment

The spray cloud was provided by air-water atomizing nozzles located
in the quieting chamber upstream of the tunnel test section. The noz-
zles were always positioned to provide a cloud that was relatively uni-
form in liquid-water content and droplet-size distribution in the test
section. The dye-water solution and air pressures to the nozzles were
set by means of pressure transmitters and manometers. The spray was
turned on and off by fast-action solenoid valves, while the spray dura-
tion was set and recorded by an electric timer. Further details of the
spray system are described in reference 15.

PROCEDURE

Blotter Mounting

For the larger models, a 3-inch-wide blotter was rubber-cemented to
a vellum strip, which in turn was cemented to the airfoil surface as
shown in figure 1. The cementing prevented the blotter from being lifted
from the airfoil surface by aerodynamic forces. The edges of the blotter
were also taped to the airfoil surface. The vellum strip prevented dam-
age to the blotter during removal from the model. After exposure to the
spray cloud the vellum and blotter were removed as a unit and later
separated carefully. For the small models a 2-inch-wide blotter was
stretched tightly over the leading edge and taped to the airfoil surface
along all the blotter edges.

Tunnel Conditioning and Blotter Exposure

In order to minimize the evaporation of the droplets during their
time of travel from the spray nozzles to the body (about 3/4 sec), the
entire tunnel airstream was nearly saturated before the body was exposed
to the dyed-water spray. Saturation of the test-section airstream was
achieved through the control of tunnel air temperature and the addition
of steam into the tunnel until a light condensation cloud resulted.

The studies reported herein were conducted at the following nominal
conditions: Free-stream velocity, 152 knots; static pressure, 28.1
inches of mercury; and static air temperature, 50° F.

3689

The procedure for each run was to preload the air and dyed-water
pressure in the spray system and preset the exposure time. (Air-water
gage pressure ratios similar to those used in ref. 15 - i.e., 0.5, 0.6,
and 0.8 - were used herein to obtain impingement data; low pressure ratio
was used to obtain large droplet sizes, while high pressure ratio was
used to obtain small droplets.) With the tunnel air properly conditioned
as to speed, temperature, and humidity, the blotter-wrapped model was ex-
posed to the dyed spray for the preset time interval. After tunnel shut-
down, the blotter was removed from the model.

In these studies the exposure time varied from 2 to 7 seconds for
the 13-inch-chord airfoils and from 3 to 12 seconds for the large-chord
airfoils at air-water pressure ratios of 0.5 to 0.8, respectively.

For each air-water pressure ratio, a relatively uniform cloud with
local liquid-water-content variations within ±10 percent and essentially
the same droplet-size distribution were obtained. The reproducibility
of the average liquid-water content from one model exposure to the next
was about ±5 percent.

Spray Cloud Properties

The cloud total liquid-water content was obtained by collecting dye
from the spray cloud in an aspirating device (a tube that draws in air
and liquid water at free-stream conditions, ref. 15). The inlet velocity
of the device was always within 1 percent of the free-stream value, denot-
ing theoretically a 100-percent collection efficiency.

The droplet-size distribution was determined by the method outlined
in reference 15, in which the experimental impingement rates for cylinders
are related to theoretical data for similar cylinders. In the present
study, however, small 36.5-percent-thick Joukowski airfoils were used
instead of cylinders. The absolute values of droplet size from this air-
foil section (see appendix B) generally confirm those obtained from the
cylinders of reference 15, but the body size trend is reduced from that
of reference 15.

The ratio of droplet diameter to volume-median diameter[1] is presented
in figure 3 as a function of the ratio of cumulative liquid-water content
to total liquid-water content. The volume-median droplet diameters are
believed accurate within ±6 percent. These data are from the aspirator
and 36.5-percent Joukowski airfoil analyses for the three spray conditions
(air-water pressure ratios) studied.

_____

[1]Volume-median droplet diameter is that diameter for which half the
total liquid-water content is contained in droplets larger than the vol-
ume median and half in droplets smaller than the volume median.

The pertinent spray cloud properties are summarized in the following table:

Air-water pressure ratio	Air pressure, lb/sq in. gage	Water (dye solution) pressure, lb/sq in. gage	Approx. max. droplet diam., d_{max}, microns	Range of total liquid-water content, w_t, g/cu m	Volume-median droplet diam., d_{med}, microns
0.5	60	120	59	0.46-0.65	18.6
.6	60	100	48	.37- .50	16.7
.8	80	100	29	.22- .33	11.5

The number and spacing of the spray nozzles varied during the course of the airfoil program because of other unrelated test programs interspersed between those reported herein. These changes resulted in a range of cloud liquid-water content, as noted in the previous table, and were accounted for in analyzing the experimental impingement data. Droplet-size distribution was not affected by these nozzle changes.

Colorimetric Analysis

In the colorimetric analysis of the dyed blotter, small $\left(\frac{1}{8} \times 1\frac{1}{2}\text{-in. or } \frac{1}{16} \times 1\text{-in.}\right)$ segments of area ΔA_s are punched from the blotter as shown in figure 4. The dye is dissolved out of each segment with a known quantity of distilled water (ref. 15). The concentration of this solution is determined by the amount of light of a suitable wavelength transmitted through the solution in a calibrated colorimeter. The amount of dye collected on the segment is converted into the weight of water (dye-water solution) that impinged on the blotter segment during the exposure. The local impingement rate $\overline{W}_\beta$ for a segment as given in reference 15 is expressed as

$$\overline{W}_\beta = \frac{0.794\ Pb}{t\mathscr{C}\Delta A_s}, \quad \frac{\text{lb water}}{(\text{hr})(\text{sq ft})} \tag{1}$$

ANALYSIS OF DATA

The analysis of the data obtained from the dye-impingement records consists in evaluating the local and total collection efficiencies of the airfoils and the extent or limit of impingement on the airfoil surfaces. In order to analyze the experimental data, the water content and

droplet-size distribution of the spray cloud also must be known. Final-
ly, methods of extending the data for conditions other than those used
in the tests must be employed in order to render the data generally use-
ful. A detailed discussion of the dye analysis is presented in reference
15 and reviewed herein for convenience in presenting the experimental
data.

The local rate of water-droplet impingement $\overline{W}_\beta$ and limit of im-
pingement s_{max} are obtained as a direct result of the dye-tracer tech-
nique used herein. The dimensionless impingement parameters $\overline{\beta}$ and $\overline{E}_m$
are obtained from the following equations (ref. 15):

$$\overline{\beta} = \frac{\overline{W}_\beta}{0.329 \ U_0 w_t} \qquad (2)$$

$$\overline{E}_m = \frac{\int_{s_{l,max}}^{s_{u,max}} \overline{W}_\beta \ dA_s}{0.329 \ U_0 w_t A_F} = \frac{1}{A_F} \int_{s_{l,max}}^{s_{u,max}} \overline{\beta} \ dA_s \qquad (3)$$

For a two-dimensional airfoil, equation (3) is rewritten for con-
venience as

$$\overline{E}_m = \frac{\int_{s_{l,max}}^{s_{u,max}} \overline{W}_\beta \ ds}{0.329 \ U_0 w_t h} = \frac{1}{h} \int_{s_{l,max}}^{s_{u,max}} \overline{\beta} \ ds \qquad (4)$$

Equation (4) is based on projected frontal height h rather than on the
airfoil thickness ratio used by some investigators. Figure 5 shows ratio
of projected frontal height to chord length h plotted against angle of
attack α for the airfoils used herein. For the swept airfoils, h and
s are referred to the free-stream direction.

Total collection efficiency and impingement limits are often pre-
sented in terms of K and φ, where K indicates the inertia of the
droplet and φ represents the deviation of the droplet drag forces from
Stokes' law, for correlating impingement characteristics. Reference 17
discusses and illustrates previously determined analytical airfoil im-
pingement data in terms of a modified K parameter defined as
$K_0 = K(\lambda/\lambda_s)$. The ratio λ/λ_s is a function of Re_0 as shown in fig-
ure 6 (data from ref. 12). Plotting a dependent impingement parameter
such as E_m or s_{max} as a function of K_0 yields a set of experiment-
ally or analytically determined points that can be essentially represented

by a single curve, independent of φ. This curve is approximately the
solution obtained using Stokes' law for sphere (droplet) drag. The ex-
tention or interpolation of experimental as well as analytical data
points over a wide range of the pertinent impingement variables (droplet
size, body size, speed, and altitude) is greatly facilitated by this K_0
parameter, even though no complete theoretical proof of its significance
or validity is available at this time.

The impingement parameters previously discussed are often presented
in the literature in terms of clouds containing droplets all of the same
size. Analytical calculations show that the presence of a droplet-size
distribution does not alter the usefulness of the K_0 parameter if it is
evaluated with the following droplet sizes: (1) The use of volume-median
droplet size to calculate a "weighted" K_0 will reduce weighted total
collection efficiency to data representable by a single curve; and (2) the
use of maximum droplet size in calculating K_0 will reduce limits of
impingement to data representable by a single curve. Reasonable exten-
sion and interpolation of experimental $\overline{E}_m$ and s_{max} data obtained with
droplet-size distribution for conditions other than those studied are
possible, therefore, with the $K_{0,med}$ or $K_{0,max}$ parameter, respectively.

Correlation of β (uniform droplet size) or $\overline{\beta}$ (distribution of drop-
let sizes) with $K_{0,med}$ was possible only if each value of β or $\overline{\beta}$
used was obtained for the same numerical value of s', where s' is the
dimensionless surface distance measured from the s location of β or $\overline{\beta}$
to the location of β_{max} or $\overline{\beta}_{max}$, respectively.

From the theoretical and experimental impingement results, it was
determined that the surface location of β_{max} or $\overline{\beta}_{max}$, measured from the
zero-chord point, denoted as s'', does not occur at the same s location
for various $K_{0,med}$ values except for symmetrical airfoils at zero angle
of attack. Generally, s'' occurs between the air stagnation point on the
airfoil (max. pressure point) and the foremost point on the airfoil. The
foremost point on the airfoil is where the airfoil surface is perpendicular
to the free-stream-velocity direction. As the value of the modified iner-
tia parameter $K_{0,med}$ increases, s'' moves toward the foremost point on
the airfoil, because the droplet paths approach straight-line trajectories.
As the value of $K_{0,med}$ decreases, s'' moves toward the maximum pressure
point, because the droplet inertia is approaching that of air particles.

The following empirical method of analysis was adopted for correlat-
ing $\overline{\beta}$ with $K_{0,med}$. From plots of the experimental data of $\overline{\beta}$ against
s, values of $\overline{\beta}$ were selected at specified values of $\overline{s}'$. Plotting $\overline{\beta}$
as a function of $K_{0,med}$ for various s' values yields points reasonably

represented by a single curve. The relation of these $\bar{\beta}$ values to their true surface location s is accomplished by a plot of s'' as a function of $K_{0,med}$ and the relation

$$s = s' + s'' \qquad (5)$$

A negative sign herein denotes the airfoil upper-surface values; a positive sign denotes the airfoil lower surface.

RESULTS

A complete tabulation of the local collection efficiency $\bar{\beta}$, the maximum extent of impingement on the airfoil surface s_{max}, and the total collection efficiency $\bar{E}_m$ for each airfoil and impingement condition studied is listed in table I. The $\bar{\beta}$ values are tabulated as a function of s, the surface distance from the zero-chord point on the airfoil divided by chord length. These $\bar{\beta}$ data are calculated from faired values of $\bar{W}_\beta$ and equation (2). Typical $\bar{W}_\beta$ values as a function of s are shown in figure 7 for several repeat runs. The data in this figure show a repeatability of better than ±10 percent.

In order to emphasize the significant trends and variables affecting the impingement characteristics of airfoils, this section of the report presents the experimental data in terms of (1) typical $\bar{\beta}$ curves as a function of s and (2) dimensionless $K_{0,med}$ and $K_{0,max}$ parameters. Part (1) consists in a general evaluation of the effect on impingement characteristics of the basic airfoil geometry, including such items as airfoil angle of attack, camber, thickness ratio, airfoil shape, and sweep angle. Part (2) presents the effects on airfoil impingement characteristics of varying the droplet size, airspeed, and model size as expressed by a variation of the dimensionless $K_{0,med}$ and $K_{0,max}$ parameters.

Effect of Airfoil Geometry on Impingement Characteristics

In order to illustrate the effect of airfoil geometry and attitude on typical values of local collection efficiency, $\bar{\beta}$ is presented as a function of surface distance divided by chord length s (fig. 8). The data used in figure 8 were obtained from table I.

Angle of attack. - An increase in angle of attack for the same spray cloud conditions will increase the extent of impingement on the lower surface of an airfoil $s_{l,max}$ and decrease the extent on the upper surface $s_{u,max}$. In figure 8(a) (Joukowski 0015 airfoil at angles of attack

of 0°, 4°, and 8°) the impingement limit on the lower surface increased from a value of $s_{l,max}$ of 0.158 to 0.379 as the angle of attack was increased from 0° to 8°. Concurrently, on the upper surface $s_{u,max}$ decreased from -0.158 to -0.058.

Generally, for a given s the local $\bar{\beta}$ values on the lower surface increase while those on the upper surface decrease as the angle of attack is increased. The value of $\bar{\beta}_{max}$ has a tendency (both from experimental and theoretical data) to decrease slightly (less than 10%) as the angle of attack is increased from 0° to 8°. As the angle of attack is increased, the $\bar{\beta}_{max}$ value is located farther aft along the lower surface, as shown in figure 8(a). At 8° angle of attack $\bar{\beta}_{max}$ occurs at s'' of 0.012 as compared with s'' of 0.005 and 0 at 4° and 0°, respectively. The shape of the local $\bar{\beta}$ curve is symmetrical or nearly symmetrical (depending on whether the airfoil is symmetrical or is cambered, respectively) at zero angle of attack. As the angle of attack is increased, the $\bar{\beta}$ curve has a steeper impingement gradient on the upper surface and a lesser gradient on the lower surface. For the airfoils, droplet sizes, and operating conditions used herein, the location of $\bar{\beta}_{max}$ occurs between the air stagnation region and the foremost point of the airfoil.

The $\bar{E}_m$ values for the 12- to 16-percent thick airfoils show no great change with an increase in angle of attack (table I) over the range of $K_{0,med}$ values studied (0.0057 to 0.093). However, these airfoils with increasing angle of attack will have an increased total water catch per foot of span almost proportional to the increased projected frontal height h of the airfoil (as will be discussed later). The total collection efficiency for the NACA 65_1-206 airfoil also does not vary appreciably for the limited range of angles of attack and $K_{0,med}$ values studied (0° to 4.3° and 0.0077 to 0.0167, respectively). According to theoretical data for a thin airfoil (ref. 11), however, the E_m for the NACA 65A-004 airfoil increased markedly between angles of attack of 0° and 8°, the E_m being 40 to 80 percent greater at 8° than at 0° for K_0 values of 0.01 and 0.10, respectively. Therefore, the $\bar{E}_m$ for the NACA 65_1-206 may increase for angles greater than 4° in the range of $0.01 < K_{0,med} < 0.10$ in a manner similar to that for the NACA 65A-004.

Airfoil thickness. - A change in airfoil thickness ratio (for the same airfoil series) has mixed effects. An increase in thickness ratio causes a decrease in $\bar{\beta}_{max}$ as shown in figure 8(b) (NACA 65_1-206 and 65_1-212 airfoils both at 0° angle of attack). The value of $\bar{\beta}_{max}$ for the thin 65_1-206 airfoil is 27 percent greater than that for the thicker 65_1-212 airfoil. Between the region of $\bar{\beta}_{max}$ and the limits of impingement, local $\bar{\beta}$ values for a thick airfoil are generally higher than those

of a thin one. In figure 8(b), the upper-surface limit of impingement $s_{u,max}$ on the 12-percent-thick airfoil is -0.06, while that on the 6-percent-thick airfoil is -0.09. The lower-surface limit of impingement $s_{l,max}$ is 0.03 for the thick airfoil compared with 0.02 for the thin airfoil. For the range of cloud properties, angle of attack, and airfoil series studied herein, the higher values of $\overline{\beta}_{max}$ and the smaller h of the 65_1-206 airfoil yielded a higher total collection efficiency than those of the 65_1-212 airfoil. (See table I, eq. (4), and subsequent discussion.)

   Airfoil shape. - The NACA 65_2-015 and 63_2-015 and the Joukowski 0015 airfoils are compared in the same cloud conditions and at 0° angle of attack in figure 8(c). These three airfoils are symmetrical and have a maximum thickness of 15 percent; they differ in the location of maximum thickness and leading-edge radius (see fig. 2). The Joukowski 0015 is the bluntest, with the maximum-thickness point at 25-percent chord; the 65_2-015 is the sharpest, with the maximum-thickness point at 40-percent chord; and the 63_2-015 airfoil is intermediate, with maximum thickness at 35-percent chord. The blunt Joukowski 0015 has a lower $\overline{\beta}_{max}$ value but higher local $\overline{\beta}$ values farther aft on the surface than the sharp, low-drag 65_2-015 airfoil. The value of $\overline{\beta}_{max}$ for the 65_2-015 airfoil was about 20 percent greater than for the Joukowski 0015. The 63_2-015 airfoil data show $\overline{\beta}_{max}$ values between those obtained for the other two 15-percent-thick airfoils. In addition, the limit of impingement on the bluff airfoil is less than that on the sharp low-drag airfoil, as shown in figure 8(c).

   The total collection efficiency of the blunt airfoil (Joukowski 0015) in the range of $K_{0,med}$ covered herein (0.04 to 0.1) is 20 to 40 percent higher than that of the low-drag airfoil (65_2-015) of the same thickness ratio (table I). In the determination of the $\overline{E}_m$ values for these airfoils, the higher $\overline{\beta}_{max}$ and greater total impingement area of the low-drag airfoil (fig. 8(c)) are insufficient to offset the generally higher $\overline{\beta}$ values (except near $\overline{\beta}_{max}$) of the blunt airfoils.

   Airfoil camber. - The extent of impingement at 0° angle of attack may be greater on the upper surface than on the lower surface for a cambered airfoil (fig. 8(b)); however, this is not generally true for angles greater than 0°. For the NACA 65_1-212 airfoil, the maximum impingement limit on the upper surface $s_{u,max}$ is -0.06, whereas on the lower surface the impingement limit is 0.03. No direct comparison of the effect of airfoil camber on local or total collection efficiency can be made with the

data available, because the same airfoil series was not studied with and
without camber. An interpolation, however, of the $\bar{E}_m$ data for the
cambered 65-series airfoils (65_1-206, 65_1-212, and $65,2$-216, the last
airfoil having similar geometric shape to the other two, (fig. 1)) to a
cambered 15-percent-thick airfoil can be made. Comparison of these in-
terpolated values of $\bar{E}_m$ with those of the uncambered 65_2-015 airfoil
indicates that the small camber involved has only a secondary effect on
the total collection efficiency.

Airfoil sweepback. - Sweeping back an airfoil and keeping the same
physical shape (yawing the airfoil) generally have only a small effect
on impingement limits and local and total collection efficiencies. Com-
paring the data for the unswept and swept 65-series airfoils (table I)
shows that the collection efficiencies and limits of impingement are a
little less, in general, on the yawed or swept airfoils than on the un-
swept airfoils. A correlation of swept- and unswept-airfoil impingement
data is presented later in the DISCUSSION.

Dimensionless Presentation of Data

The experimental impingement characteristics of airfoils $\bar{\beta}$, $\bar{E}_m$,
and s_{max} are conveniently presented as a function of the pertinent
modified inertia parameter $K_{0,med}$ or $K_{0,max}$ for purposes of extra-
polation and comparison in figures 9 to 12. Presentation of data in
this form permits a ready evaluation of airfoil impingement characteris-
tics in terms of droplet size, air temperature, altitude, component size,
and airspeed.

Variation of $\bar{\beta}$ with $K_{0,med}$. - In figure 9, average $\bar{\beta}$ values at
selected surface locations s' are shown as functions of $K_{0,med}$ for
all airfoils studied. These locations of $\bar{\beta}$ are referenced to the loca-
tion of $\bar{\beta}_{max}$ as discussed previously and were obtained from the origi-
nal curves of $\bar{\beta}$ against s. It is apparent from the curves shown in
figure 9 that the method of analysis for $\bar{\beta}$ (outlined in the ANALYSIS)
will produce data that can be essentially represented by a single curve
for particular s' locations.

In the range of $0.04 < K_{0,med} < 0.1$ (13-in.-chord airfoil data) the
point value of $\bar{\beta}_{max}$ could not be readily ascertained because of the
width of the blotter punch used. Generally, the $\bar{\beta}_{max}$ curve for the
13-inch-chord airfoils is estimated from the more reliable data in the
range of $0.001 < K_{0,med} < 0.01$ and from the shape of the $\bar{\beta}$ curves aft of
$\bar{\beta}_{max}$ ($s' = 0.01$, etc.) for the values of $K_{0,med}$ greater than 0.04.

3689

The local collection efficiency $\bar{\beta}$ increases with an increase in $K_{0,med}$ as shown in figure 9. The order of magnitude of the increase in $\bar{\beta}$ as $K_{0,med}$ increases depends on the surface location and is a complex function of the airfoil angle of attack and shape. In the range of $0.01 < K_{0,med} < 0.1$, the $\bar{\beta}$ values are believed accurate to ±10 percent; but, for $\bar{\beta}_{max}$ at $K_{0,med}$ greater than 0.02, a ±25-percent accuracy is estimated.

The curves of figure 10 present s" (the surface location of $\bar{\beta}_{max}$) as a function of $K_{0,med}$. Because of the width of the blotter punch used, s" could not be precisely established. Consequently, s" is represented in figure 10 by a dashed line.

Variation of s_{max} with $K_{0,max}$. - An increase in $K_{0,max}$ will increase the extent of impingement on both surfaces of the airfoil as shown in figure 11. With increasing $K_{0,max}$ there is a greater change in the lower-surface limit of impingement on a low-drag airfoil (NACA 65_1-212) than on a blunt airfoil (Joukowski 0015). On the upper surface no marked trends with airfoil shape are apparent except at 0° angle of attack. As previously discussed (fig. 8(a)), an increase in angle of attack will increase the extent of impingement on the lower surface and decrease the extent on the upper surface for all airfoils over the entire range of $K_{0,max}$ values.

Variation of $\bar{E}_m$ with $K_{0,med}$. - The total collection efficiency of an airfoil $\bar{E}_m$ increases as $K_{0,med}$ increases (fig. 12). These data are plotted from table I for an angle of attack of 0°. In the range of $K_{0,med} < 0.02$ the increase in $\bar{E}_m$ with a decrease in the thickness ratio is readily apparent in figure 12 for airfoils of the same series and camber. For example, at 0° angle of attack and $K_{0,med}$ of 0.01 the $\bar{E}_m$ values for the NACA 65_1-206, 65_1-212, and 65,2-216 airfoils are 0.105, 0.06, and 0.05, respectively. These airfoils, although their numbering systems are somewhat different, are of the same series, differing primarily in thickness ratio and only to a minor degree in leading-edge radius and location of maximum-thickness point. These latter differences are considered of secondary significance in the evaluation of total collection efficiency. Reversals of this change in $\bar{E}_m$ with thickness ratio may occur at high $K_{0,med}$ values ($K_{0,med} > 0.02$), especially as the thickness ratio approaches 6 or 4 percent.

The preceding $\overline{E}_m$ comparisons do not necessarily mean a similar comparison for total water caught on an airfoil. For a two-dimensional wing the total water catch per foot span $\overline{W}_m$ is

$$\overline{W}_m = 0.329 \ U_0 w_t \text{ch} \ \overline{E}_m \qquad (6)$$

Total catch is thus proportional to the product of $\overline{E}_m$, projected frontal height h, and chord length c. For example, at 0^0 angle of attack and $K_{0,\text{med}}$ of 0.007, the NACA 65,2-216 airfoil has an $\overline{E}_m$ value of 0.032 and a $\overline{W}_m$ value proportional to $0.16 \times 0.032 = 0.0051$ (values from figs. 5 and 12). In comparison, the NACA 65_1-206 has a higher $\overline{E}_m$ value of 0.085 but $\overline{W}_m$ proportional to $0.06 \times 0.085 = 0.0051$ is the same. A similar comparison at $K_{0,\text{med}}$ of 0.013 makes $\overline{W}_m$ proportional to 0.0109 and 0.0072 for the NACA 65,2-216 and 65_1-206, respectively, although $\overline{E}_m$ for the thicker airfoil is about 40 percent less than that for the thinner one.

The effect of angle of attack on $\overline{E}_m$ for all the airfoils studied at one spray condition is presented in figure 13. These data were obtained at a free-stream velocity U_0 of 152 knots and a volume-median droplet diameter d_{med} of 16.7 microns (air-water pressure ratio, 0.6) and are typical of the other spray cloud conditions. (Cross plots of these data, obtained from table I, yield curves of $\overline{E}_m$ against $K_{0,\text{med}}$ similar to those of fig. 12.) As previously discussed, $\overline{E}_m$ for the airfoils and spray conditions studied does not vary appreciably with angle of attack.

Because the h difference among the airfoils studied lessen as angle of attack increases (fig. 5), values of total water catch per foot span $\overline{W}_m$ (see eq. (6)) will depend largely on the values of $\overline{E}_m$ for angles of attack greater than 4^0.

DISCUSSION

The following discussion is based on comparison of the experimental results with available theoretical trajectory data. In order to compare experimental impingement data with that calculated from trajectory data for the same body, the flow fields in both cases must be similar. The local velocity distributions obtained experimentally on several of the airfoils are shown in figure 14. Also shown in this figure are the theoretical values used to set up the flow field for the trajectory calculations of reference 2. In general, the experimental results agree well

(especially near the leading edge) with the theoretical. The experimental velocity distributions are generally slightly high on both surfaces by an average of 5 percent. At angles of attack up to 4°, the local velocity data from the large-chord airfoils agrees well with those for the small-chord airfoils.

<div style="text-align:center">Impingement Characteristics</div>

The theoretical impingement characteristics for the Joukowski 0015 airfoil at angles of attack of 0° or 4° and the unswept NACA 65_1-212 airfoil at an angle of attack of 4° can be obtained from the trajectory studies of references 5 and 2, respectively. These trajectory results, when "weighted" (as described in ref. 1) for the droplet-size distribution of the tunnel spray cloud, can be used for a comparison between the experimental results obtained herein and the theoretical results.

The modified inertia parameter $K_{0,max}$ is the independent variable chosen as the basis for comparing the experimental limits of impingement s_{max} with the theoretical (fig. 15). For the Joukowski 0015 airfoil (fig. 15(a)) in the range of $K_{0,max}$ from 0.01 to 0.1, good agreement of the experimental impingement limits on both upper and lower surfaces with those of theory is obtained for angles of attack of 0° and 4°. Fair agreement is obtained for $K_{0,max}$ greater than 0.1. In this higher $K_{0,max}$ range the visual and colorimetric determinations of the experimental impingement limit, particularly on the lower surface, are more difficult than for $K_{0,max}$ less than 0.1 and may account for the lesser agreement with theoretical values when $K_{0,max}$ is greater than 0.1. For the NACA 65_1-212 airfoil at α of 4° (fig. 15(b)) there is poor agreement on both upper and lower surfaces between experiment and theory, the theoretical limits being twice the experimental. Even on the upper surface, where at 4° angle of attack the experimental limit is well defined, large discrepancies occur. As yet there is no reasonable explanation for these differences.

The experimental local collection efficiencies $\bar{\beta}$ as a function of s are in good agreement with those obtained from theory for the Joukowski 0015 airfoil at both 0° and 4° angles of attack (fig. 16). A similar comparison of $\bar{\beta}$ attempted for the NACA 65_1-212 airfoil at 4° angle of attack yielded very erratic results. The erratic nature of these data may be due in large part to the inconsistencies in the theoretical trajectory data. For a given impingement condition (Re_0 and K), total collection efficiency E_m obtained by the tangent trajectory data of

reference 2 differs by more than 30 percent, for example, from $\bar{E}_m$ determined from an integration of the local collection efficiency results of the same reference (see eq. (4) herein).

Theoretical and experimental values of total collection efficiency $\bar{E}_m$ for the Joukowski 0015 at angles of attack of 0^0 and 4^0 and the NACA 65_1-212 at an angle of attack of 4^0 are compared in figure 17. For the Joukowski 0015 (figs. 17(a) and (b)) good agreement ($\pm 10\%$) between theory and experiment is obtained over the entire $K_{0,med}$ range studied. The $\bar{E}_m$ value computed theoretically for the NACA 65_1-212 airfoil (fig. 17(c)) is 25 and 100 percent greater than that obtained experimentally for $K_{0,med}$ values of 0.09 and 0.008, respectively, because of the aforementioned discrepancies in s_{max} and $\bar{\beta}$. Similar comparisons between experiment and theory for the NACA 65_2-015 airfoil at α of 4^0 (theoretical in ref. 5) show the theoretical values to be 10 to 20 percent higher than the experimental values in the $K_{0,med}$ range tested.

The agreement between the theoretical and experimental evaluations of $\bar{E}_m$, $\bar{\beta}$, and s_{max} is considered good for the Joukowski 0015 and satisfactory for the NACA 65_2-015. No such agreement was obtained for the NACA 65_1-212 airfoil, as previously discussed. These three airfoils are the only ones available for comparison of experimental and theoretical impingement values at this time.

Correlation of Effect of Airfoil Sweepback

The experimental impingement data substantiate the method of reference 14 for predicting the impingement on a swept airfoil from data obtained on an unswept airfoil where (1) the wing can be considered two-dimensional or has a high aspect ratio and (2) the airfoil section in a plane perpendicular to the leading edge of the swept airfoil is the same section as that of the unswept airfoil. The application of the method of reference 14 to the experimental impingement data presented herein is discussed in appendix C. Typical experimental values of local collection efficiency $\bar{\beta}$ as a function of s for the 35^0 swept (NACA 65_1-212 and 65_1-206) airfoils are presented for angles of attack (referenced to free-stream velocity direction) of 0^0 and 4.3^0 in figures 18(a) and (b), respectively. The faired lines of figure 18 represent the $\bar{\beta}$ values calculated from the unswept experimental data by the method of reference 14. Good agreement between calculated swept and experimental swept values of $\bar{\beta}$ was obtained for the angles of attack and the airfoils studied. Similar good agreement was obtained for values of s_{max} and $\bar{E}_m$.

Application of Tunnel Impingement Data to Flight

Correlation of tunnel cloud characteristics with those reported in the literature for natural icing clouds. - Most of the reported data concerning droplet size and liquid-water content of natural icing clouds (refs. 18 to 20) have been obtained with rotating multicylinders that were permitted to ice for a known time interval. The rate of ice collection on various size cylinders is matched with the theoretical collection of these cylinders in a manner that determines the droplet size and liquid-water content of the cloud (ref. 1). Similarly, the dye catch on various size cylinders can be matched to the theoretical cylinder catch to evaluate the tunnel dyed-water spray cloud properties. Another method of using the theoretical cylinder data to determine cloud properties is that of reference 15, wherein the droplet sizes are determined from dye-tracer impingement rates on a single stationary cylinder or body for which theoretical trajectories are available. A modification of the method in reference 15 is the use of a 36.5-percent symmetrical Joukowski airfoil. Details of the dye-tracer droplet-size analysis using the 36.5-percent Joukowski are given in appendix B. The liquid-water content of the dyed-water spray cloud was obtained by an aspirating tube (ref. 15).

For droplets with diameters greater than 12 microns, the multicylinder matching, the single-cylinder solution, or the Joukowski airfoil solution each yield nearly the same absolute values of droplet size. Total liquid-water content, as measured by the aspirator, is nearly the same as that indicated by the multicylinder matching technique, and thus the volume-median droplet size is substantially the same for both the Joukowski-aspirator or multicylinder matching methods. The tunnel cloud properties and impingement data reported herein are based on the Joukowski-aspirator method. The difference or relation between the multicylinder matching and the Joukowski-aspirator evaluation of the tunnel spray cloud is illustrated in figure 19, which is a cross plot of the cloud properties as calibrated by the two techniques. The development of figure 19, a discussion of the relatively minor differences obtained, and the reasons for preferring the Joukowski-aspirator results over the multicylinder matching results are discussed in appendix B.

To apply the experimental data herein to flight conditions, a procedure is suggested and illustrated by a hypothetical problem, the conditions of which are as follows:

(1) Meteorological design conditions, based on multicylinder data:

   Cloud volume-median droplet diameter, 15 microns
   Cloud total liquid-water content, 0.5 g/cu m
   Cloud droplet-size distribution, Langmuir "D"

(2) Section characteristics:

    Airfoil section, NACA 65_1-212
    Airfoil chord length, 10 ft
    Airfoil angle of attack, 4°

(3) Operating conditions:

    True airspeed, 300 mph (261 knots)
    Pressure altitude, 10,000 ft
    Static air temperature, 12° F

For the example, it is desired to determine the local water collection rate at s_l of 0.02 and the lower surface limit of impingement $s_{l,max}$.

The meteorological conditions are converted from the multicylinder values to the Joukowski-aspirator values by using figure 19. The conversion results in a volume-median droplet size of 14.8 microns (Joukowski-aspirator value) and a water-content ratio of the aspirator to the multicylinder match of 1.12. This ratio yields an aspirator total liquid-water content w_t of 0.56 g/cu m. Values of K and Re_0 are then calculated (0.03242 and 111.3, respectively). With this Re_0, a λ/λ_s ratio of 0.325 is obtained (fig. 6). The $K_{0,med}$ calculated from K and λ/λ_s then amounts to 0.01054. In order to obtain $\bar{\beta}$ at the desired lower-surface location, s' and s" must be obtained. The value of s" obtained from figure 10(f) and (g) at a $K_{0,med}$ of 0.01054 is 0.0037. From equation (5), s' is then calculated to be 0.0163. The value of $\bar{\beta}$ is now determined from figure 9(f) and (g) using the curves for 4° angle of attack and $K_{0,med}$ of 0.01054; the result is a $\bar{\beta}$ of 0.14. The local collection rate at s_l of 0.02 is calculated from equation (2), which gives a value of $\bar{W}_\beta$ of 7.74 pounds per hour per square foot.

In order to determine the limit of impingement on the lower surface of the airfoil, the maximum droplet size in the cloud droplet distribution must be established. For the Langmuir "D" distribution as well as the tunnel spray distribution, an average ratio of d_{max}/d_{med} of 3.2 exists. Hence, the maximum droplet size for the example is 48 microns. A value of $K_{0,max}$ is now determined in a manner similar to that used to obtain $K_{0,med}$ (i.e., values of K_{max}, $Re_{0,max}$ and $\lambda/\lambda_{s,max}$ are determined). The result of these calculations is a $K_{0,max}$ value of 0.0692, from which a value of $s_{l,max}$ of 0.12 is obtained by use of figures 11(f) and (g).

Effect of droplet-size distribution on impingement characteristics. -
A natural icing cloud may contain a distribution of droplet sizes (perhaps
distribution types "B" to "E" defined in ref. 12), or the droplets in
a cloud may be all the same size ("A" distribution). Many current design
specifications are based on this assumption of an "A" distribution. For
large bodies, such as root sections of tapered wings or radomes (low
$K_{0,med}$ range), the wider droplet-size distributions will result in higher
values of $\bar{E}_m$ than will an "A" distribution. Therefore, icing-protection
equipment designed for large bodies and an "A" droplet-size distribution
may underestimate $\bar{E}_m$ and prove inadequate for some icing conditions.
On the other hand, in the high $K_{0,med}$ range typical for tip sections of
tapered wings, helicopter blades, and instruments, the assumption of an
"A" distribution may overestimate $\bar{E}_m$ slightly when compared with an as-
sumption of a wider droplet-size distribution.

Limit of impingement is a function only of the maximum droplet size
present in the distribution. Because typical distributions often contain
droplets 2 to 3 times larger than the uniform size of the "A" distribu-
tion, the extent or limit of impingement will be markedly increased if a
droplet-size distribution other than "A" is experienced. In addition,
the $\bar{\beta}$ profile will be altered by different droplet-size distributions.

Therefore, a droplet-size distribution that occurs relatively fre-
quently in nature should be considered in the design of all icing-
protection equipment. According to references 18 to 20, typical size
distributions in nature range from a Langmuir "C" to "E". As previously
discussed, the tunnel distribution of droplet sizes approximates a
Langmuir "D". Consequently, the droplet-size distribution inherent in
the data reported herein is typical of that in many natural icing clouds,
making these data suitable for design purposes.

CONCLUDING REMARKS

In an effort to obtain a general solution to the impingement char-
acteristics of various airfoils, some investigators have suggested that
correlation of impingement characteristics could be obtained if the body
dimension used in the independent impingement parameters were based on
airfoil thickness (ref. 21) or projected frontal height of the airfoil
(ref. 22). In both of these references relatively good correlation was
obtained for a limited number of airfoils at an angle of attack of 4°.
Subsequent data obtained at other angles of attack, particularly 0°, tend
to show that the correlation at 4° was fortuitous. Much of the available
theoretical E_m data at 0° angle of attack is shown in figure 20(a) as a
function of $K_{0,F}$, where $K_{0,F}$ is based on the projected height of the

airfoil rather than the chord. (At 0° angle of attack the projected height is equal to the airfoil thickness.) It is apparent that at values of $K_{0,F}$ greater than 0.2 a wide deviation in total collection efficiency occurs, and the thick airfoils (thickness ratios 15 to 36.5%) have a higher collection efficiency than the thin airfoils (thickness ratios 4 to 6%). Conversely, in the low ranges of $K_{0,F}$ the opposite trend is noted.

A similar plot of data at a 4° angle of attack in figure 20(b) shows the same good correlation of data for the various airfoils as noted in reference 22. The apparent good agreement at the 4° angle of attack may be due to the fact that at α of 4° compared with α of 0° the projected frontal height of the thin airfoils more nearly approaches that of the thick airfoils (see fig. 5), thereby reducing the effect of the thickness ratio on impingement characteristics and parameters. The experimental data for collection efficiency show trends similar to figure 20 when plotted in the $K_{0,F}$ form.

At present, there is no known parameter that accurately correlates all the available two-dimensional airfoil impingement data over realistic ranges of the independent variables.

SUMMARY OF RESULTS

The impingement characteristics of several airfoils obtained experimentally using a dye-tracer technique yield the following results:

1. In general, the data show that the local and total water catch and the limit of impingement of airfoils are primary functions of the modified inertia parameter (in which airspeed and droplet and body size are the most significant variables) and airfoil thickness ratio. In addition, the local water collection rate and the extent of impingement on the airfoil surfaces depend on the airfoil angle of attack. Secondary factors affecting airfoil impingement characteristics are airfoil shape (for a given thickness ratio), small camber, and sweep angle.

2. With an increase in the modified inertia parameter, the total and local collection efficiencies and the impingement limits also increase. For those airfoils of a comparable series operating at a typical flight value of the modified inertia parameter, a thickness ratio of 6 percent had total collection efficiencies of 1.7 and 2 times those of a 12- and 16-percent-thick airfoil, respectively. Airfoils with relatively blunt leading edges (Joukowski 0015) had higher total collection efficiencies than those with sharp leading edges (low-drag airfoils such as the NACA 65_2-015), although the impingement limits for the sharper airfoils were greater than those for the blunt airfoils.

3. The experimentally determined local and total collection efficiencies and impingement limits for the Joukowski 0015 and NACA 65_2-015 airfoils are in good agreement with the theoretical values. No such agreement is obtained for the NACA 65_1-212 airfoil.

4. Over the range of conditions studied, the experimental data substantiate a previous method of predicting the impingement characteristics of swept airfoils (design section laid out perpendicular to the leading edge) from data for the unswept design section.

5. Because of the typical droplet-size distribution of the tunnel spray, and the correlation of data by means of the modified inertia parameter, the experimental results herein may be applied over a wide range of flight conditions.

Lewis Flight Propulsion Laboratory
    National Advisory Committee for Aeronautics
        Cleveland, Ohio, August 13, 1956

APPENDIX A

SYMBOLS

A area, sq ft

b volume of distilled water used to dissolve dye from blotter segments, ml

$\mathscr{C}$ percent concentration by weight of dye in water solution used in spray system, $\dfrac{\text{lb dye}}{\text{lb solution}} \times 100\% \cong \dfrac{\text{lb dye}}{\text{lb water}} \times 100\%$

c airfoil chord length, ft

D cylinder diameter, in.

d droplet diameter, microns (3.28×10^{-6} ft)

E_m total collection efficiency in clouds of uniform droplet size, defined by eq. (3), dimensionless

h frontal height of airfoil projected parallel to free-stream velocity direction divided by chord length, dimensionless

K inertia parameter, $\dfrac{8.77 \times 10^{-13} \rho_d d^2 U_0}{\mu c}$, dimensionless

K_0 modified inertia parameter, $\dfrac{\lambda}{\lambda_s} K$, dimensionless

P concentration of solution obtained from blotter segments, mg dye/ml solution

Re_0 free-stream Reynolds number with respect to droplet, $\dfrac{4.81 \times 10^{-6} d \rho U_0}{\mu} = \sqrt{K\varphi}$, dimensionless

s distance along surface referenced from zero-chord point divided by chord length, dimensionless

t exposure time, sec

U_0 free-stream velocity, mi/hr or knots $\times$ 1.15

U_1 local velocity at outer edge of boundary layer, mi/hr or knots $\times$ 1.15

W_m total water impingement rate in cloud of uniform droplet size, lb/(hr)(ft span)

W_β local water impingement rate in cloud of uniform droplet size, lb/(hr)(sq ft)

w cumulative liquid-water content contained in droplets of sizes from d_{max} to any particular droplet size, g/cu m

w_t total liquid-water content of cloud, g/cu m

x distance along chord line from zero-chord point divided by chord length, dimensionless

y distance perpendicular to chord line divided by chord length, dimensionless

α airfoil angle of attack, deg

β local collection efficiency in cloud of uniform droplet size, defined by eq. (2), dimensionless

γ sweep angle, deg

θ cylinder central angle, deg

λ true range of droplet as projectile injected into still air, ft

λ_s range of droplet as a projectile following Stokes' law, ft

μ viscosity of air, lb/(ft)(sec)

ρ density of air, lb/cu ft

ρ_d density of droplet, 62.4 lb/cu ft

φ independent impingement parameter, $\dfrac{0.423\rho^2 U_0 c}{\mu}$, dimensionless

Subscripts:

F   frontal, projected parallel to free-stream-velocity direction

l lower surface

max   maximum

med   volume-median

n   normal plane

s   surface

u   upper surface

x   coordinate parallel to free-stream-velocity direction

Superscripts:

—   weighted value due to effects of more than one droplet size

'   referenced to surface location of $\bar{\beta}_{max}$

"   location of $\bar{\beta}_{max}$

APPENDIX B

DETERMINATION OF CLOUD DROPLET SIZE AND LIQUID-WATER

CONTENT FROM MEASURED IMPINGEMENT RATES ON BODIES

Cloud droplet size and liquid-water content can be obtained from measured impingement rates on a body for which theoretical trajectory data are known (ref. 15). Most of the published cloud characteristics have been obtained by collecting ice on various size cylinders and matching these data to theoretical collection rates (refs. 18 to 20). Similarly, the dye catch on various size cylinders can be matched with theory to evaluate the tunnel dyed-water spray cloud. A modification to the multicylinder technique is that of reference 15, wherein the impingement rates obtained by dye traces on one stationary cylinder suffice. A refinement to the method of reference 15 is the use of an airfoil (36.5% symmetrical Joukowski herein) instead of a cylinder. A discussion and comparison of these methods follow.

Multicylinder Matching

To calibrate the tunnel dyed-water spray cloud by the multicylinder matching technique, seven nonrotating cylinders (diam. of 1/8, 1/4, 1/2, 1, 2, 4, and 6 in.) were covered with absorbent material and separately exposed in the tunnel cloud. The total water catch (as measured by the dye collected) per unit time, frontal area, and velocity ($= \bar{E}_m w_t$) is plotted in figure 21 as a function of cylinder diameter including thickness of absorbent material. The log-log plot of figure 21 is the conventional presentation for analyzing multicylinder data (ref. 1). By the matching method described in reference 1, the tunnel data of figure 21 can be matched to a theoretical Langmuir "D" droplet-size distribution. As discussed in reference 1, there is usually considerable latitude in selecting the best theoretical fit to any multicylinder data. A Langmuir "D" distribution is selected for the tunnel data because it provides for the airfoils studied herein, the best over-all agreement of limits and rates of impingement with those calculated theoretically. This agreement was previously discussed and illustrated in figure 16, where experimental and theoretical impingement rates ($\bar{\beta}$) on the Joukowski 0015 airfoil are compared. Matching the tunnel multicylinder data to a Langmuir "D" droplet-size distribution yields the following spray cloud characteristics:

Air-water pressure ratio	Volume-median droplet diameter, d_{med}, microns	Liquid-water content, w_t, g/cu m
0.5	. 21.2	0.54 .
.6	16.8	.43
.8	11.6	.25

Single Cylinders or 36.5-Percent Joukowski Airfoils

In reference 15 a method for determining droplet-size distribution is described in which the theoretical trajectory results for cylinders (ref. 1) are applied to experimental impingement obtained on cylinders with the dye-tracer technique. Reference 15 shows that the experimental pressure distribution about cylinders deviates considerably from theory; these surface pressure differences probably reflect unknown differences in the flow field ahead of cylinders and hence droplet trajectories about cylinders. In order to eliminate or reduce these unknown effects, a 36.5-percent-thick symmetrical Joukowski airfoil (coordinates listed in table II) has been selected herein for which the experimental pressure and thus velocity distributions are in good agreement with the theoretical values (shown in fig. 22). In addition, a bluff configuration like the 36.5-percent Joukowski lends itself to accurate determination of the point where a droplet impinges on the surface, a critical factor in evaluating experimentally as well as theoretically the pertinent impingement variables s_{max}, β, and E_m. The 36.5-percent Joukowski was studied theoretically (unpublished trajectory data) and with the dye-tracer technique. For the 36.5-percent Joukowski experimental studies, airfoils of 5.47- and 16.32-inch chord were used. These chord sizes gave about the same leading-edge diameters as the 2- and 6-inch cylinders of reference 15 and thereby provided a dimensional similarity for comparing the results from the two types of bodies.

The experimental techniques and methods of determining droplet size from 36.5-percent Joukowski dye traces are identical to those detailed for cylinders in reference 15. In the Joukowski analysis, the surface distance from the zero-chord point is denoted as s, whereas in the cylinder analysis surface distance is given by the central angle θ. Curves of s_{max} as a function of K and φ, and β as a function of s_{max} and s are given for the 36.5-percent Joukowski airfoil in figures 23 and 24, respectively. These theoretical Joukowski results were obtained at the Lewis laboratory with the mechanical analog described in reference 23. Figures 23 and 24 for the 36.5-percent Joukowski airfoil are comparable to figures 15 and 16, respectively, of reference 15 and are used with the experimental results (unpublished) in the same manner.

From such a procedure dimensional plots of droplet diameter as a function of cumulative liquid-water content can be obtained.

Comparison of Multicylinder, Single-Cylinder,

and 36.5-Percent Joukowski Airfoil Solutions

A curve of droplet diameter against cumulative liquid-water content based on data obtained from the Joukowski airfoils for each of the three tunnel spray conditions used herein is shown in figure 25(a). In addition to the 36.5-percent Joukowski solution of droplet sizes, the multicylinder matching the Langmuir "D" solution obtained from figure 21 and the single-cylinder solutions of reference 15 are presented for comparison. The average solution from each of the three methods is represented by the faired curves of figure 25. These averages are adjusted to common liquid-water contents. This adjustment is necessary for comparison on a dimensional basis, because data for the three methods of resolution were not obtained from the identical array (number and spacing) of spray nozzles. It is apparent from the curves that the solutions are in reasonable agreement.

Further comparisons of the methods of determining droplet size are presented in figure 25(b). For convenience, the cylinder size results of reference 15 are reproduced together with the 36.5-percent Joukowski results for the two chord sizes studied. The 36.5-percent Joukowski airfoil solutions in figure 25(b) are considered first, and each chord size gives a slightly different droplet-size distribution. However, the consistent body-size trend for droplet diameters less than 16 microns noted in the cylinder data (ref. 15) no longer exists. In addition, the over-all spread in droplet size at a particular liquid-water content value w is markedly reduced for droplet diameters greater than 16 microns. Ideally, different body sizes exposed to the same cloud should indicate the same droplet-size distribution. However, as discussed in reference 15, the consistent body-size trend for cylinders may be the result of nonideal flow about cylinders or unaccounted-for droplet drag increments due to droplet acceleration. Furthermore, difficulties encountered in calculating accurately the theoretical trajectories in the range of low K values (less than about 0.7) also may contribute to the cylinder size trend when the theoretical data are applied in the analysis of the experimental data. The air flow about the 36.5-percent Joukowski is nearly ideal, as previously discussed and illustrated in figure 22. This improved air flow and an increased accuracy of the theoretical trajectory data in the low K range for the 36.5-percent Joukowski airfoil evidently yield results nearer the ideal than those from cylinders, as shown in figure 25(b).

In summary, the 36.5-percent Joukowski solution of droplet size is preferred over a single or multicylinder solution because (1) the consistent body-size trend noted for cylinders is absent, and (2) the body-size spread throughout the droplet-size range is reduced. An aspirating tube (ref. 15) is the preferred instrument in measuring total liquid-water content, because its collection efficiency is adjusted to be 100 percent whereas the calculated efficiency for cylinders may be inaccurate in the low K range.

Joukowski-aspirator values of volume-median droplet size and liquid-water content comparable to those previously tabulated in this appendix for the multicylinder matching method are as follows:

Air-water pressure ratio	Volume-median droplet diameter, d_{med}, microns	Liquid-water content, w_t, g/cu m
0.5	18.6	0.60
.6	16.7	.47
.8	11.5	.30

A dimensionless droplet-size distribution as obtained by the Joukowski-aspirator method is discussed in the text and is presented in figure 3.

Although the Joukowski-aspirator method of determining droplet size and liquid-water content of the dyed spray cloud is used to present the airfoil impingement characteristics herein, most of the published data on cloud characteristics have been obtained by the multicylinder matching method. The relation between the two methods for the range of conditions studied is obtained by a cross plot of the droplet sizes and liquid-water contents obtained by the two techniques. This cross plot, consisting of the data tabulated in this appendix, is shown as figure 19, and its use discussed in the text.

Values of Total Liquid-Water Content Reported in Reference 15

The aspirator values of total liquid-water content as reported in reference 15 are in error because of an undetected recirculation of the dyed spray cloud. The error was incurred by operating the aspirator for a longer time than required for the air and dyed droplets in the tunnel to recirculate. This phenomenon resulted in aspirator values of total liquid-water content higher than the true value by the amount of recirculated dye. Recent studies have evaluated the effect of recirculation for all spray conditions, and the effect is only significant for values of total liquid-water content (and thus by definition volume-median droplet size). The corrections to liquid-water content and

volume-median droplet size (the latter based on analysis of cylinder im-
pingement data) given in reference 15 are tabulated as follows:

Air-water pressure ratio	Liquid-water content, w_t, g/cu m		Volume-median droplet diameter, d_{med}, microns	
	Reference 15	Reference 15 corrected	Reference 15	Reference 15 corrected
0.5	0.70	0.46	14.8	20.4
.6	.58	.37	12.0	16.6
.8	.43	.22	7.6	12.0

The cylinder impingement, techniques, and method of solution for
droplet size are unchanged from those reported in reference 15. The
cylinders were exposed to the dyed spray cloud and then withdrawn from
the tunnel before the circuit time of the tunnel air was complete (approx.
14 sec at an airspeed in the test section of 152 knots). The recirculated
spray cloud for all conditions studied contains droplets less than 5 mi-
crons in diameter with recirculation dying out completely in a few minutes.
Even for the 13-inch-chord airfoils, these small droplets impinge in a
very narrow band (less than 1/16 in.) at or near the leading edge. The
effect of these recirculated droplets on all the airfoil impingement
characteristics is considered negligible. Total liquid-water contents
for the airfoils studied herein are measured with aspirator exposure
times significantly less than the tunnel air circuit time.

APPENDIX C

PREDICTION OF IMPINGEMENT ON SWEPT AIRFOIL

FROM RESULTS OBTAINED ON UNSWEPT AIRFOIL

Reference 14 presents a method for predicting the impingement on a swept wing from impingement data for an unswept airfoil section if the unswept airfoil section is in the plane perpendicular to the leading edge of the swept wing. Limit of impingement and local and total collection efficiency are first determined with respect to flow conditions in the normal plane of the swept wing and then by geometry into the free-stream plane.

The 35° swept NACA 65_1-212 and 65_1-206 models studied herein were layed out with the sections in a plane perpendicular to the leading edge. Data from these swept airfoils are therefore directly comparable with the data from the unswept airfoils modified by the method of reference 14. Application of the unswept data as discussed in reference 14 to the swept airfoils is as follows (the NACA 65_1-212 airfoil is used as an example):

(1) For a particular value of $K_{0,med}$, $\bar{\beta}$ is obtained from figure 9(f) and (g) for several values of s' and angles of attack α. By using figure 10 and equation (5), s' is converted to s. The $K_{0,med}$ value used to enter figure 9(f) and (g) is smaller than that at which the data were obtained. The value of $K_{0,med}$ is smaller because $U_{0,x}$ is replaced by $U_{0,n}$, where $U_{0,n} = U_{0,x} \cos \gamma$; this has a greater effect on $K_{0,med}$ than the accompanying increase in λ/λ_s (a function of Re_0 and also decreased by $\cos \gamma$).

(2) The values of $\bar{\beta}$ obtained from step (1) are plotted against angle of attack α for constant values of s.

(3) The $\bar{\beta}$ values are read from the plot described in step (2) at $\alpha_n = \alpha/\cos \gamma$ for several values of s. The $\bar{\beta}$ values thus obtained $(\bar{\beta}_n)$ are in terms of a plane perpendicular to the leading edge of the swept airfoil.

(4) The $\bar{\beta}_n$ values from step (3) are multiplied by $\cos \gamma$ to obtain $\bar{\beta}_x$ values on the swept airfoil. Therefore, $\bar{\beta}_x$ is in terms of a plane perpendicular to the free-stream-velocity direction. This latter definition of $\bar{\beta}$ (actually $\bar{\beta}_x$) is identical to the conventional one for unswept bodies.

(5) The s (actually s_n) values of steps (1) to (3) are in terms of a plane perpendicular to the leading edge of the swept airfoil. These s_n values are converted to corresponding s_x values from the geometry of the "stretched" airfoil (the NACA 65_1-212 section in plane perpendicular to leading edge stretched to a thinner section in the free-stream plane). For the NACA 65_1-212 and 65_1-206, the difference between s_n and s_x is of secondary importance.

Unswept experimental $\bar{\beta}$ values modified by the preceding procedure are compared with experimental swept data in figure 18, and discussed in the text.

REFERENCES

1. Brun, R. J., Lewis, W., Perkins, P. J., and Serafini, J. S.: Impingement of Cloud Droplets on a Cylinder and Procedure for Measuring Liquid-Water Content and Droplet Sizes in Supercooled Clouds by Rotating Multicylinder Method. NACA Rep. 1215, 1955. (Supersedes NACA TN's 2903 and 2904, and RM E53D23.)

2. Brun, Rinaldo J., Serafini, John S., and Moshos, George J.: Impingement of Water Droplets on an NACA 65_1-212 Airfoil at an Angle of Attack of 4°. NACA RM E52B12, 1952.

3. Brun, Rinaldo J., Gallagher, Helen M., and Vogt, Dorothea E.: Impingement of Water Droplets on NACA 65A004 Airfoil and Effect of Change in Airfoil Thickness from 12 to 4 Percent at 4° Angle of Attack. NACA TN 3047, 1953.

4. Brun, Rinaldo J., Gallagher, Helen M., and Vogt, Dorothea E.: Impingement of Water Droplets on NACA 65_1-208 and 65_1-212 Airfoils at 4° Angle of Attack. NACA TN 2952, 1953.

5. Guibert, A. G., Janssen, E., and Robbins, W. M.: Determination of Rate, Area, and Distribution of Impingement of Waterdrops on Various Airfoils from Trajectories Obtained on the Differential Analyzer. NACA RM 9A05, 1949. (Addendum I by A. G. Guibert, Apr. 1949.)

6. Brun, Rinaldo J., and Dorsch, Robert G.: Impingement of Water Droplets on an Ellipsoid with Fineness Ratio 10 in Axisymmetric Flow. NACA TN 3147, 1954.

7. Dorsch, Robert G., Brun, Rinaldo J., and Gregg, John L.: Impingement of Water Droplets on an Ellipsoid with Fineness Ratio 5 in Axisymmetric Flow. NACA TN 3099, 1954.

8. Brun, Rinaldo J., Gallagher, Helen M., and Vogt, Dorothea E.: Impingement of Water Droplets on NACA 65A004 Airfoil at 8° Angle of Attack. NACA TN 3155, 1954.

9. Dorsch, Robert G., Saper, Paul G., and Kadow, Charles F.: Impingement of Water Droplets on a Sphere. NACA TN 3587, 1955.

10. Lewis, William, and Brun, Rinaldo J.: Impingement of Water Droplets on a Rectangular Half Body in a Two-Dimensional Incompressible Flow Field. NACA TN 3658, 1956.

11. Brun, Rinaldo J., and Vogt, Dorothea E.: Impingement of Water Droplets on NACA 65A004 Airfoil at 0° Angle of Attack. NACA TN 3586, 1955.

12. Langmuir, Irving, and Blodgett, Katherine B.: A Mathematical Investigation of Water Droplet Trajectories. Tech. Rep. No. 5418, Air Materiel Command, AAF, Feb. 19, 1946. (Contract No. W-33-038-ac-9151 with General Electric Co.)

13. Bergrun, Norman R.: An Empirical Method Permitting Rapid Determination of the Area, Rate, and Distribution of Water-Drop Impingement on an Airfoil of Arbitrary Section at Subsonic Speeds. NACA TN 2476, 1951.

14. Dorsch, Robert G., and Brun, Rinaldo J.: A Method for Determining Cloud-Droplet Impingement on Swept Wings. NACA TN 2931, 1953.

15. von Glahn, Uwe, Gelder, Thomas F., and Smyers, William H., Jr.: A Dye-Tracer Technique for Experimentally Obtaining Impingement Characteristics of Arbitrary Bodies and a Method for Determining Droplet Size Distribution. NACA TN 3338, 1955.

16. Lewis, James P., and Bowden, Dean T.: Preliminary Investigation of Cyclic De-Icing of an Airfoil Using an External Electric Heater. NACA RM E51J30, 1952.

17. Sherman, P., Klein, J. S., and Tribus, M.: Determination of Drop Trajectories by Means of an Extension of Stokes' Law. Eng. Res. Inst., Univ. of Mich., Apr. 1952. (Air Res. and Dev. Command, USAF, Contract AF 18(600)-51, Proj. M992-D.)

18. Kline, Dwight B., and Walker, Joseph A.: Meteorological Analysis of
    Icing Conditions Encountered in Low-Altitude Stratiform Clouds.
    NACA TN 2306, 1951.

19. Lewis, William, Kline, Dwight B., and Steinmetz, Charles P.: A
    Further Investigation of the Meteorological Conditions Conducive
    to Aircraft Icing. NACA TN 1424, 1947.

20. Lewis, William, and Hoecker, Walter H., Jr.: Observations of Icing
    Conditions Encountered in Flight During 1948. NACA TN 1904, 1949.

21. Drell, H., and Valentine, P. J.: Comments on Methods of Calculating
    Water Catch and a Correlation of Some New Data. Rep. No. 8552,
    Lockheed Aircraft Corp., Apr. 16, 1952.

22. Schwartz, Herman: A Modified Method of Determining the Rate of Ice
    Accretion of an Airfoil in an Icing Condition. Tech. Note WCT
    54-106, Directorate of Flight and All-Weather Testing, Wright Air
    Dev. Center, Air Res. and Dev. Command, Wright-Patterson Air Force
    Base, Oct. 1954.

23. Brun, Rinaldo J., and Mergler, Harry W.: Impingement of Water Drop-
    lets on Cylinder in an Incompressible Flow Field and Evaluation
    of Rotating Multicylinder Method for Measurement of Droplet-Size
    Distribution, Volume Median Droplet Size, and Liquid-Water Content
    in Clouds. NACA TN 2904, 1953.

24. Abbott, Ira H., and von Doenhoff, Albert E.: Theory of Wing Sections.
    McGraw-Hill Book Co., Inc., 1949.

3689

CT-5

TABLE I. - IMPINGEMENT CHARACTERISTICS OF AIRFOILS

Air-water pressure ratio	s	Joukowski 0015; chord, 13 in.				NACA 63$_2$-015; chord, 13 in.			
		Local efficiency, $\bar{\beta}$, for angle of attack, α, of -							
		0°	2°	4°	8°	0°	4°	8°	12°
0.5	-0.08	0.070	0.035	0.014	<0.01	0.044	<0.01	-----	-----
	-.06	.133	.087	.040	<.01	.089	.014	-----	-----
	-.04	.265	.216	.140	.026	.170	.056	-----	-----
	-.02	.540	.547	.477	.235	.371	.212	0.035	0.000
	-.01	.657	.663	.603	.392	.518	.432	.212	.042
	0	.688	.733	.687	.547	.770	.735	.525	.335
	.01	.657	.697	.673	.605	.518	.629	.581	.546
	.02	.540	.572	.575	.590	.371	.511	.546	.588
	.04	.265	.350	.377	.461	.170	.335	.410	.476
	.06	.133	.217	.253	.353	.089	.210	.294	.364
	.08	.070	.127	.165	.262	.044	.140	.224	.301
	.10	.034	.072	.104	.195	.021	.115	.182	.252
	.15	.010	.021	.037	.081	-----	.056	.115	.168
	.20	<.01	<.01	.017	.047	-----	.027	.056	.115
	$\bar{E}_m$	0.378	0.400	0.392	0.350	0.302	0.354	0.340	0.315
	$s_{u,max}$	-0.189	-0.167	-0.117	-0.075	-0.199	-0.108	-0.029	-0.032
	$s_{l,max}$	.189	.240	.292	.435	.199	.350	.453	.623
0.6	-0.08	0.045		<0.01	<0.01	0.030	-----	-----	-----
	-.06	.105		.020	<.01	.066	<0.01	-----	-----
	-.04	.235		.075	<.01	.144	.015	-----	-----
	-.02	.485		.385	.185	.336	.121	0.021	-----
	-.01	.601		.520	.354	.489	.292	.156	0.029
	0	.637		.623	.520	.725	.664	.489	.285
	.01	.601		.614	.590	.489	.605	.547	.497
	.02	.485		.523	.570	.336	.489	.518	.526
	.04	.235		.347	.445	.144	.307	.389	.437
	.06	.105		.225	.336	.066	.179	.281	.336
	.08	.045		.133	.240	.030	.109	.204	.262
	.10	.020		.077	.175	.015	.072	.161	.223
	.15	.010		.022	.070	-----	.037	.088	.132
	.20	<.01		<.01	.032	-----	.011	.049	.015
	$\bar{E}_m$	0.310		0.317	0.313	0.252	0.279	0.295	0.254
	$s_{u,max}$	-0.158		-0.105	-0.058	-0.186	-0.073	-0.027	-0.028
	$s_{l,max}$	.158		.246	.379	.186	.315	.442	.508
0.8	-0.08	<0.01	<0.01	<0.01	<0.01	0.008	-----	-----	-----
	-.06	.037	.011	<.01	<.01	.022	-----	-----	-----
	-.04	.115	.051	.017	<.01	.071	-----	-----	-----
	-.02	.380	.287	.207	.057	.212	0.049	-----	-----
	-.01	.490	.415	.355	.201	.367	.183	0.033	0.017
	0	.553	.521	.467	.365	.679	.501	.267	.200
	.01	.490	.505	.484	.453	.367	.516	.449	.383
	.02	.380	.398	.415	.448	.212	.384	.467	.434
	.04	.115	.203	.257	.353	.071	.203	.333	.347
	.06	.037	.090	.135	.241	.022	.100	.200	.242
	.08	<.01	.037	.055	.150	.008	.049	.133	.175
	.10	<.01	.014	.027	.087	-----	.033	.100	.133
	.15	<.01	<.01	<.01	.025	-----	.011	.033	.059
	.20	<.01	<.01	<.01	<.01	-----	-----	.017	.017
	$\bar{E}_m$	0.219	0.213	0.197	0.198	0.157	0.169	0.193	0.156
	$s_{u,max}$	-0.095	-0.069	-0.054	-0.032	-0.107	-0.034	-0.019	-0.020
	$s_{l,max}$	.095	.119	.154	.234	.107	.192	.280	.319

3689

CT-5 back

TABLE I. - Continued. IMPINGEMENT CHARACTERISTICS OF AIRFOILS

Air-water pressure ratio	s	NACA 65$_2$-015; chord, 13 in.				NACA 65$_1$-212; chord, 13 in.			
		Local efficiency, $\bar{\beta}$, for angle of attack, α, of -							
		0°	4°	8°	12°	0°	2°	4°	8°
0.5	-0.08	0.039	<0.01	-----	-----	0.035	0.014	<0.01	-----
	-.06	.072	.011	-----	-----	.070	.040	.014	-----
	-.04	.157	.038	-----	-----	.154	.084	.035	-----
	-.02	.345	.168	0.039	0.014	.336	.224	.113	0.021
	-.01	.542	.378	.280	.085	.537	.490	.301	.168
	0	.821	.749	.638	.329	.757	.770	.699	.546
	.01	.542	.629	.651	.582	.336	.505	.531	.560
	.02	.345	.480	.562	.550	.197	.308	.349	.453
	.04	.157	.294	.413	.440	.084	.168	.197	.322
	.06	.072	.182	.301	.344	.037	.097	.154	.252
	.08	.039	.126	.238	.270	.014	.070	.115	.201
	.10	.024	.104	.191	.224	<.01	.049	:084	.168
	.15	<.010	.070	.126	.154	<.01	.028	.057	.105
	.20	-----	.033	.085	.115	<.01	.014	.028	.070
	$\bar{E}_m$	0.289	0.339	0.384	0.316	0.274	0.326	0.327	0.344
	$s_{u,max}$	-0.280	-0.095	-0.035	-0.027	-0.250	-0.176	-0.109	-0.036
	$s_{l,max}$	.280	.422	.527	.600	.202	.350	.460	.580
0.6	-0.08	0.021	-----	-----	-----	0.029	<0.01	<0.01	-----
	-.06	.045	<0.01	-----	-----	.058	.022	<.01	-----
	-.04	.113	<.01	-----	-----	.121	.058	.015	-----
	-.02	.287	.088	0.023	<0.01	.307	.205	.073	0.014
	-.01	.467	.248	.117	.044	.482	.464	.226	.117
	0	.759	.608	.518	.258	.715	.737	.562	.512
	.01	.467	.606	.574	.508	.365	.473	.502	.554
	.02	.287	.467	.489	.497	.161	.292	.336	.454
	.04	.113	.258	.347	.394	.058	.153	.190	.322
	.06	.045	.150	.248	.307	.029	.088	.132	.242
	.08	.021	.099	.183	.233	.011	.044	.103	.190
	.10	.012	.072	.146	.177	<.01	.029	.073	.146
	.15	-----	.043	.072	.117	<.01	.011	.037	.088
	.20	-----	.022	.044	.072	-----	<.01	.015	.051
	$\bar{E}_m$	0.216	0.270	0.275	0.243	0.237	0.268	0.267	0.302
	$s_{u,max}$	-0.200	-0.069	-0.032	-0.024	-0.199	-0.129	-0.085	-0.029
	$s_{l,max}$	.200	.373	.473	.520	.170	,288	.394	.534
0.8	-0.08	-----	-----	-----	-----	<0.01	-----	-----	-----
	-.06	0.013	-----	-----	-----	.017	<0.01	-----	-----
	-.04	.058	-----	-----	-----	.051	.017	-----	-----
	-.02	.195	0.040	0.01	-----	.201	.092	0.025	-----
	-.01	.359	.175	.049	<0.01	.425	.300	.141	0.025
	0	.724	.515	.283	.149	.699	.674	.567	.416
	.01	.359	.549	.471	.379	.316	.376	.500	.532
	.02	.195	.372	.400	.400	.116	.191	.327	.425
	.04	.058	.172	.266	.300	.033	.081	.159	.259
	.06	.013	.092	.167	.216	<.01	.033	.092	.175
	.08	-----	.049	.116	.149	<.01	.017	.059	.122
	.10	-----	.025	.083	.116	-----	.011	.033	.083
	.15	-----	.013	.033	.049	-----	<.01	.013	.033
	.20	-----	<.01	.01	.025	-----	-----	<.01	.017
	$\bar{E}_m$	0.147	0.167	0.167	0.143	0.186	0.186	0.200	0.191
	$s_{u,max}$	-0.120	-0.037	-0.024	-0.012	-0.121	-0.070	-0.041	-0.015
	$s_{l,max}$	.120	.214	.285	.346	.081	.152	.248	.302

TABLE I. - Continued.   IMPINGEMENT CHARACTERISTICS OF AIRFOILS

Air-water pressure ratio	s	Joukowski 0015; chord, 96 in.			NACA 65,2-216; chord, 96 in.	
		Local efficiency, $\bar{\beta}$, for angle of attack, α, of -				
		0°	2°	4°	0°	4°
0.5	-0.03	0.057	0.031	0.015	0.031	0.00
	-.02	.139	.083	.031	.077	<.01
	-.015	.206	.137	.061	.152	.015
	-.010	.274	.229	.121	.282	.036
	-.005	.334	.305	.213	.395	.164
	0	.368	.365	.320	.442	.317
	.005	.334	.400	.383	.371	.466
	.010	.274	.336	.397	.243	.437
	.015	.206	.275	.350	.131	.334
	.02	.139	.229	.294	.059	.268
	.03	.057	.118	.187	.015	.146
	.04	.015	.046	.095	<.01	.077
	.06	<.01	<.01	.020	<.01	.031
	.08	.0	<.01	<.01	.0	.015
	$\bar{E}_m$	0.092	0.096	0.098	0.075	0.078
	$s_{u,max}$	-0.08	-0.06	-0.05	-0.09	-0.03
	$s_{l,max}$	.08	.10	.13	.08	.13
0.6	-0.03	0.015	<0.01	0.0	<0.01	-----
	-.02	.078	.031	<.01	.034	0.0
	-.015	.141	.063	.015	.069	<.01
	-.010	.203	.141	.051	.234	.020
	-.005	.266	.221	.123	.350	.058
	0	.297	.282	.210	.397	.266
	.005	.266	.311	.277	.314	.360
	.010	.203	.263	.292	.191	.354
	.015	.141	.203	.251	.051	.275
	.02	.078	.141	.203	.022	.203
	.03	.015	.053	.109	<.010	.088
	.04	<.01	.015	.040	.0	.031
	.06	.0	<.01	<.01	-----	<.01
	.08	-----	-----	<.01	-----	<.01
	$\bar{E}_m$	0.060	0.063	0.059	0.055	0.057
	$s_{u,max}$	-0.055	-0.04	-0.03	-0.07	-0.02
	$s_{l,max}$	.055	.07	.09	.04	.10
0.8	-0.03	0.0	-----	-----	-----	-----
	-.02	.011	0.0	-----	-----	-----
	-.015	.030	<.01	-----	-----	-----
	-.010	.079	.027	-----	0.0	-----
	-.005	.146	.091	0.023	.206	<0.01
	0	.176	.145	.068	.256	.066
	.005	.146	.174	.137	.175	.198
	.010	.079	.145	.160	.061	.221
	.015	.030	.079	.136	<.01	.152
	.02	.011	.039	.079	.0	.089
	.03	.0	<.01	.020	-----	<.01
	.04	-----	.0	<.01	-----	<.01
	.06	-----	-----	-----	-----	-----
	.08	-----	-----	-----	-----	-----
	$\bar{E}_m$	0.025	0.025	0.023	0.026	0.023
	$s_{u,max}$	-0.03	-0.02	<-0.01	-0.01	<-0.01
	$s_{l,max}$	.03	.04	.05	.02	.05

3689

TABLE I. - Concluded. IMPINGEMENT CHARACTERISTICS OF AIRFOILS

Air-water pres-sure ratio	s	NACA 65₁-212; chord, 72 in.			NACA 65₁-206; chord, 72 in.			[a]NACA 65₁-212; chord, 87.9 in.; swept 35°			[a]NACA 65₁-206; chord, 87.9 in.; swept 35°		
		Local collection efficiency, β, for angle of attack, α, of -											
		0°	2°	4°	0°	2°	4°	0°	2°	4.3°	0°	2°	4.3°
0.5	-0.03	0.038	<0.01	0.000	0.034	<0.01	-----	0.017	0.0	-----	0.013	-----	-----
	-.02	.085	.020	<.01	.059	<.01	0.0	.040	<.01	0.0	.024	0.0	-----
	-.015	.187	.062	.019	.095	<.01	<.01	.092	.015	<.01	.040	<.01	-----
	-.010	.311	.230	.053	.178	.034	<.01	.215	.070	.015	.099	<.01	<0.01
	-.005	.492	.438	.266	.426	.187	.034	.365	.202	.096	.294	.091	<.01
	0	.599	.592	.492	.795	.720	.620	.472	.337	.270	.605	.629	.394
	.005	.382	.507	.559	.117	.328	.486	.290	.321	.415	.075	.238	.397
	.010	.170	.322	.433	.016	.105	.276	.129	.196	.337	.021	.117	.246
	.015	.058	.164	.302	<.01	.057	.189	.042	.115	.242	<.01	.070	.174
	.020	.024	.098	.202	<.01	.043	.147	.019	.068	.170	<.01	.049	.132
	.03	.013	.038	.115	-----	.030	.098	<.01	.028	.098	0	.036	.087
	.04	<.01	.014	.071	-----	.022	.067	<.01	.019	.064	-----	.026	.062
	.06	.0	<.01	.031	-----	.011	.037	.0	<.01	.030	-----	.011	.035
	.08	-----	<.01	.015	-----	<.01	.027	-----	<.01	.018	-----	<.01	.019
	$\overline{E}_m$	0.106	0.106	0.122	0.158	0.132	0.147	0.092	0.077	0.108	0.127	0.129	0.128
	$s_{u,max}$	-0.10	-0.06	-0.03	-0.13	-0.04	-0.02	-0.08	-0.03	-0.02	-0.09	-0.02	<-0.01
	$s_{l,max}$	.07	.12	.18	.025	.16	.25	.06	.18	.13	.03	.20	>.25
0.6	-0.03	0.011	<0.01	-----	0.019	0.00	-----	<0.01	-----	-----	<0.01	-----	-----
	-.02	.043	<.01	0.0	.032	<.01	-----	.023	0.0	-----	.015	-----	-----
	-.015	.115	.028	<.01	.054	<.01	-----	.059	<.01	-----	.024	-----	-----
	-.010	.262	.124	.028	.129	.019	0.000	.157	.028	0.0	.070	0.0	-----
	-.005	.426	.342	.178	.352	.152	.019	.320	.143	.037	.249	.059	<0.01
	0	.527	.502	.438	.661	.671	.506	.420	.280	.174	.615	.555	.324
	.005	.312	.433	.501	.087	.280	.455	.236	.280	.336	.052	.221	.383
	.010	.108	.231	.380	<.01	.080	.246	.082	.169	.277	.013	.087	.232
	.015	.031	.115	.257	<.01	.037	.162	.019	.089	.196	<.01	.049	.155
	.020	<.01	.063	.173	.0	.027	.117	<.01	.047	.123	.0	.037	.111
	.03	.0	.015	.079	-----	.018	.067	<.01	.023	.066	-----	.027	.068
	.04	-----	<.01	.044	-----	.010	.040	.0	.014	.038	-----	.019	.045
	.06	-----	<.01	.011	-----	<.01	.020	-----	<.01	<.014	-----	<.01	.019
	.08	-----	<.01	<.01	-----	<.01	.012	-----	<.01	<.01	-----	<.01	<.01
	$\overline{E}_m$	0.078	0.077	0.092	0.118	0.107	0.117	0.072	0.059	0.068	0.096	0.100	< 0.101
	$s_{u,max}$	-0.06	-0.04	-0.02	-0.09	-0.03	-0.01	-0.05	-0.02	-0.01	-0.05	-0.01	<-0.01
	$s_{l,max}$	.03	.08	.13	.02	.12	.17	.04	.09	.14	.02	.14	>.20
0.8	-0.03	<0.01	-----	-----	<0.010	-----	-----	0	-----	-----	<0.01	-----	-----
	-.02	<.01	0.00	<0.01	.016	-----	-----	<0.01	0	-----	<.01	-----	-----
	-.015	.038	<.01	<.01	.025	-----	-----	<.01	<0.01	-----	.016	-----	-----
	-.010	.146	.029	<.01	.091	0.000	<.01	.071	<.01	-----	.030	-----	-----
	-.005	.328	.203	.043	.324	.063	<.01	.215	.071	<0.01	.193	0.012	-----
	0	.433	.380	.262	.645	.624	.383	.333	.221	.075	.545	.490	0.217
	.005	.193	.306	.382	.022	.241	.415	.122	.237	.237	.028	.193	.312
	.010	.025	.124	.279	<.01	.042	.197	.024	.118	.198	.0	.063	.166
	.015	<.01	.039	.155	-----	.018	.106	<.01	.043	.114	-----	.030	.091
	.020	.0	<.01	.073	-----	.014	.065	.0	.016	.063	-----	.020	.054
	.03	-----	.0	.020	-----	<.01	.038	-----	<.01	.022	-----	.016	.029
	.04	-----	-----	<.01	-----	<.01	.023	-----	<.01	<.01	-----	.014	.016
	.06	-----	-----	<.01	-----	-----	<.01	-----	-----	<.01	-----	<.010	<.01
	.08	-----	-----	-----	-----	-----	.0	-----	-----	<.01	-----	-----	<.01
	$\overline{E}_m$	0.048	0.045	0.050	0.094	0.084	0.077	0.042	0.040	0.038	0.076	0.071	0.065
	$s_{u,max}$	-0.04	-0.02	-0.01	-0.05	-0.01	<-0.01	-0.03	-0.02	<-0.01	-0.04	<-0.01	<-0.01
	$s_{l,max}$	.02	.03	.07	<.01	.05	.08	.02	.05	.09	.01	.07	.14

[a]Design section in plane normal to leading edge.

TABLE II. - COORDINATES OF 36.5-=

PERCENT-THICK JOUKOWSKI AIRFOIL

x	y	s
0.0000	0.0000	0.000
.0024	.0248	.025
.0095	.0492	.050
.021	.0726	.078
.0372	.0945	.104
.0575	.1146	.132
.0816	.1325	.161
.1094	.1479	.194
.1404	.1606	.227
.1741	.1704	.262
.1884	.1734	.275
.2029	.1760	.291
.2104	.1771	.299
.2400	.1810	.328
.2803	.1818	.368
.2884	.1817	.376
.3713	.1752	.458
.4563	.1594	.548
.5408	.1369	.633
.6229	.1106	.723
.7008	.0834	.800
.7729	.0580	.879
.8376	.0364	.948
.8934	.0199	1.003
.9388	.0088	1.049
.9724	.0027	1.082
.9931	.0003	1.103
1.0000	.0000	1.110

3689
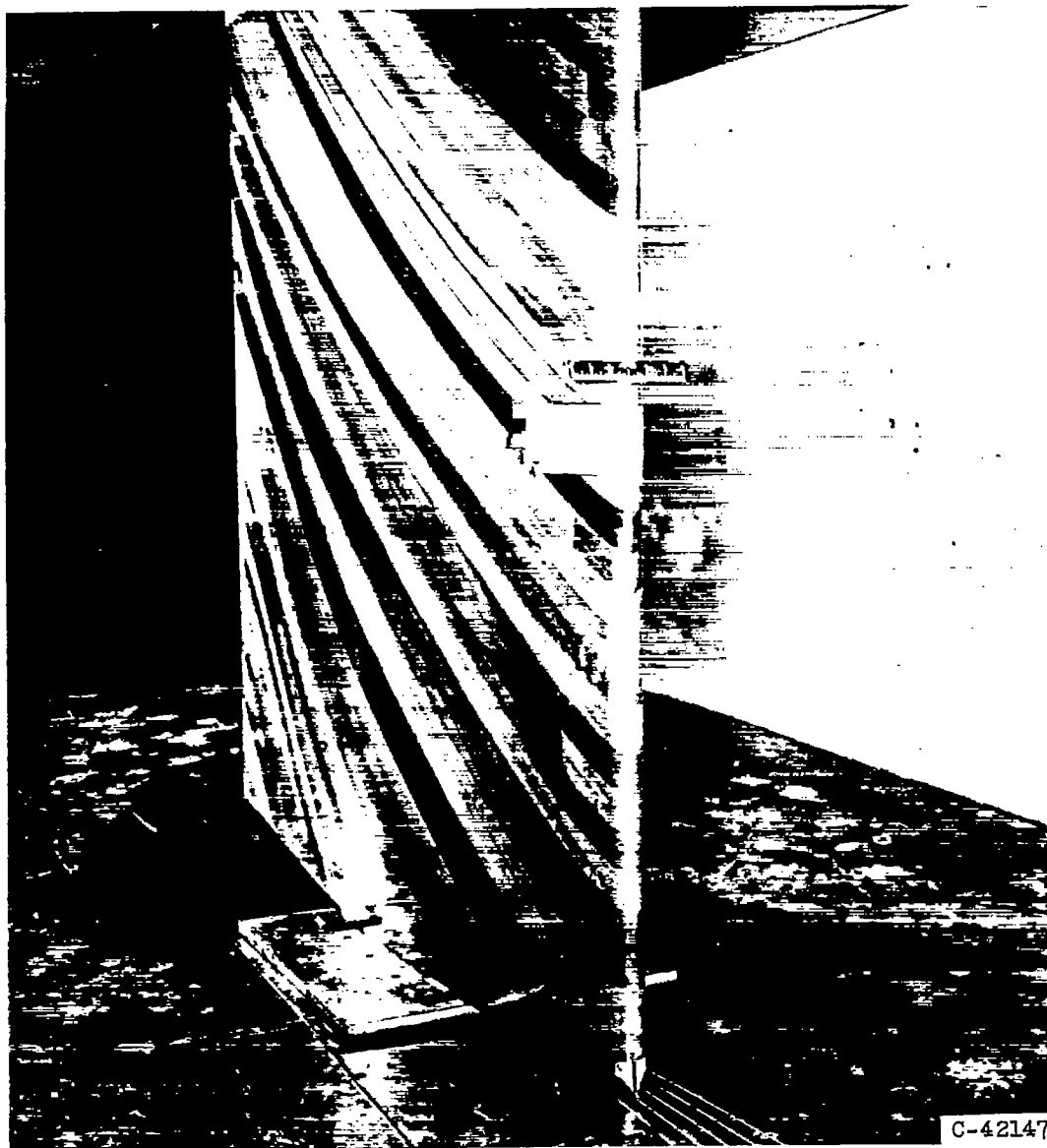
Figure 1. - Typical installation of airfoil (NACA 65_1-212) with blotter attached, in 6- by 9-foot test section of icing tunnel.
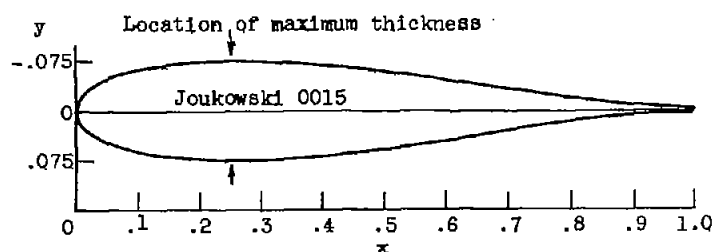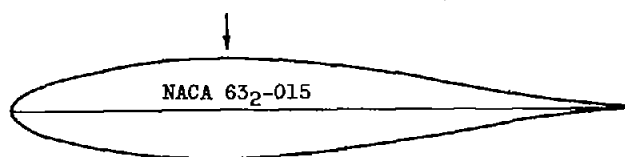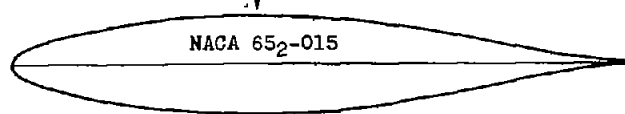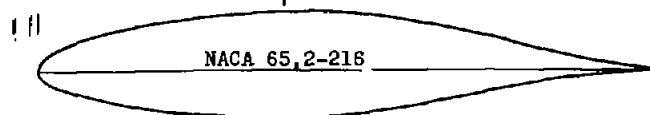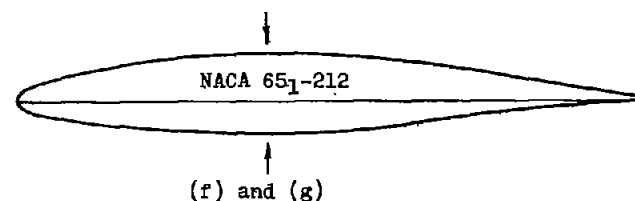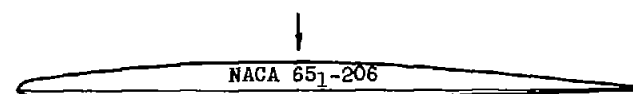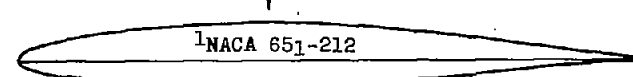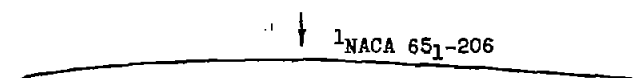
Figure 2. - Airfoil sections studied with dye-tracer technique. Sections laid out in free-stream direction.
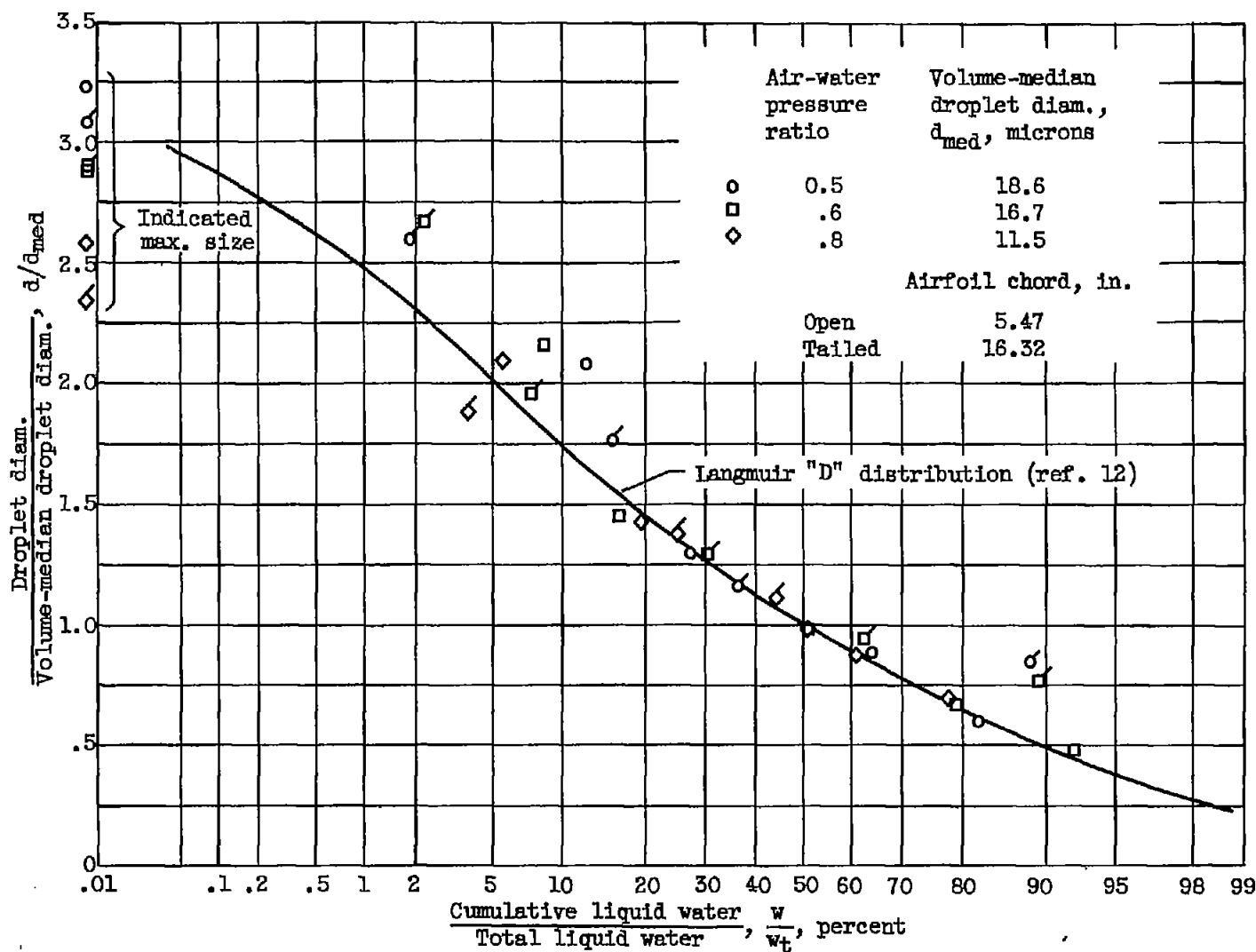
Figure 3. – Dimensionless droplet-size distribution of tunnel spray obtained on 36.5-percent Joukowski airfoil (see appendix B).
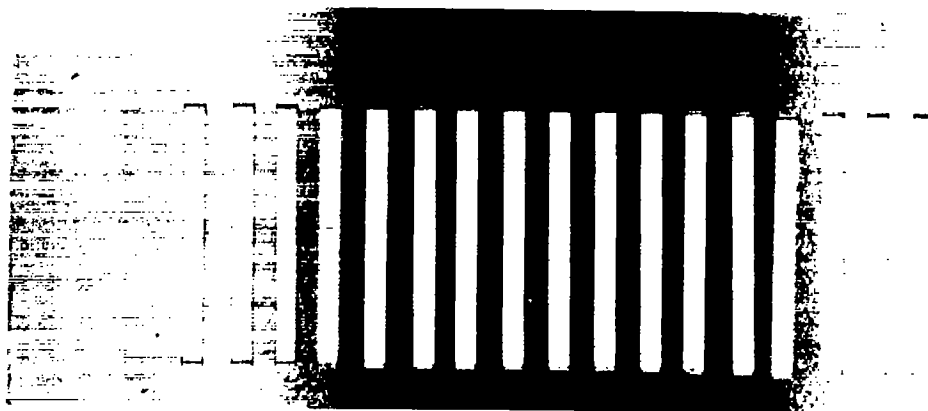
(a) $\frac{1}{8}$ - By $1\frac{1}{2}$-inch segments.
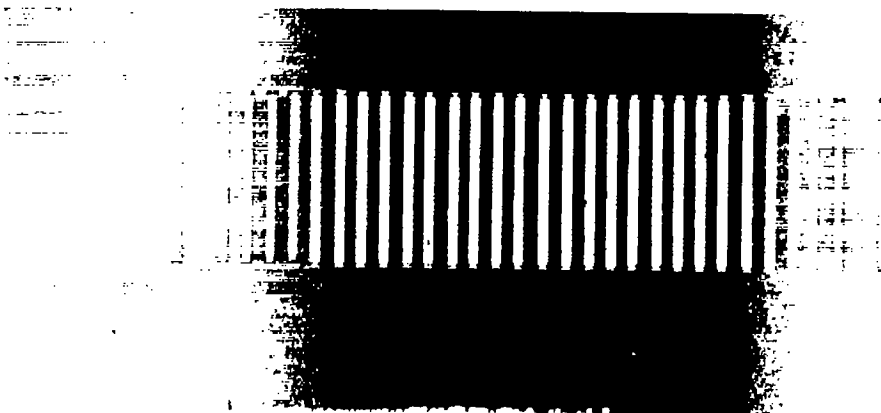
C-42776

(b) $\frac{1}{16}$ - By 1-inch segments.

Figure 4. - Typical blotter records from airfoils after exposure to dye cloud with punched segments removed for colorimetric analysis.
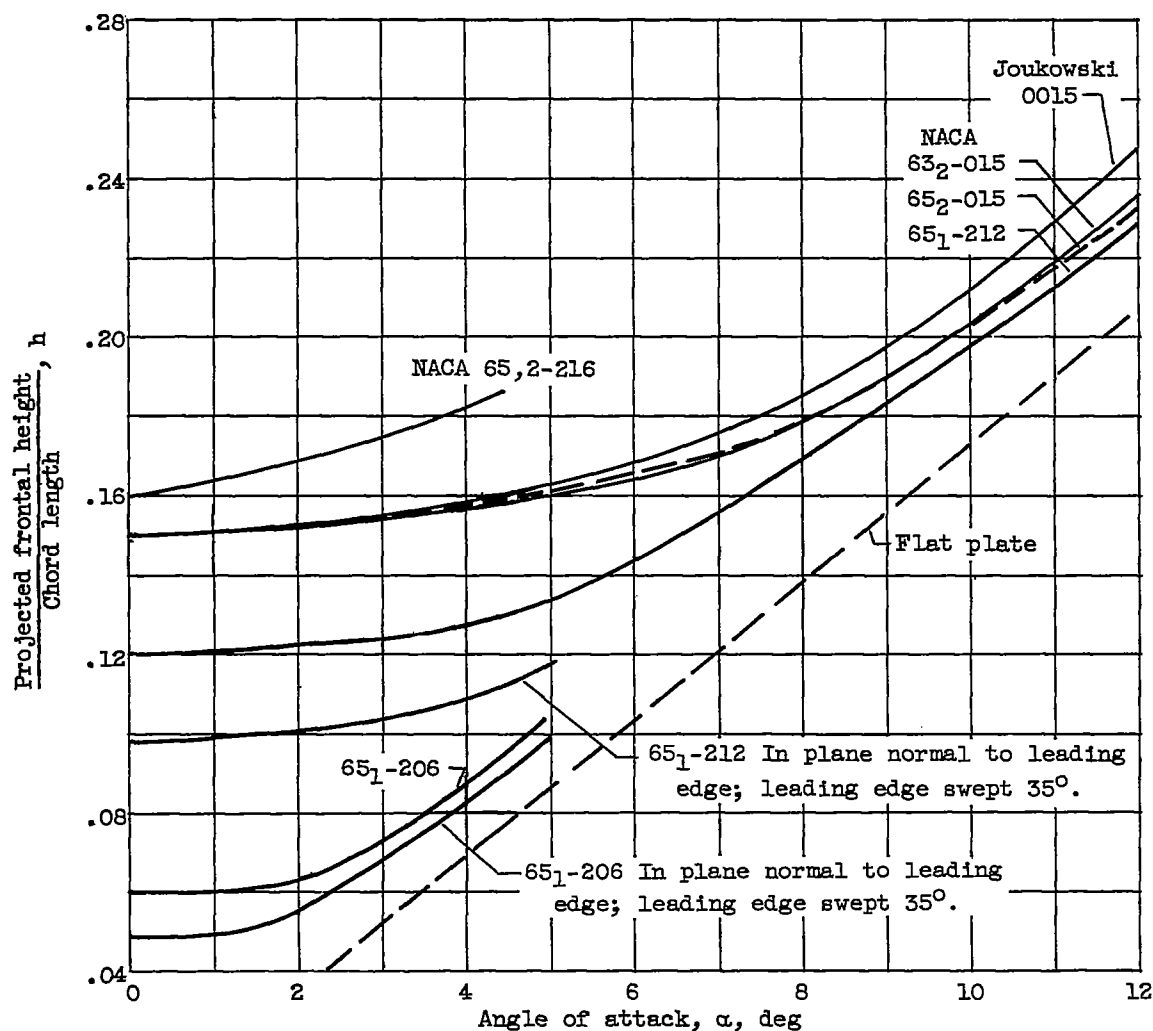
Figure 5. - Effect of angle of attack on ratio of projected height to chord length of various airfoils. (Reference is free-stream-velocity direction.)
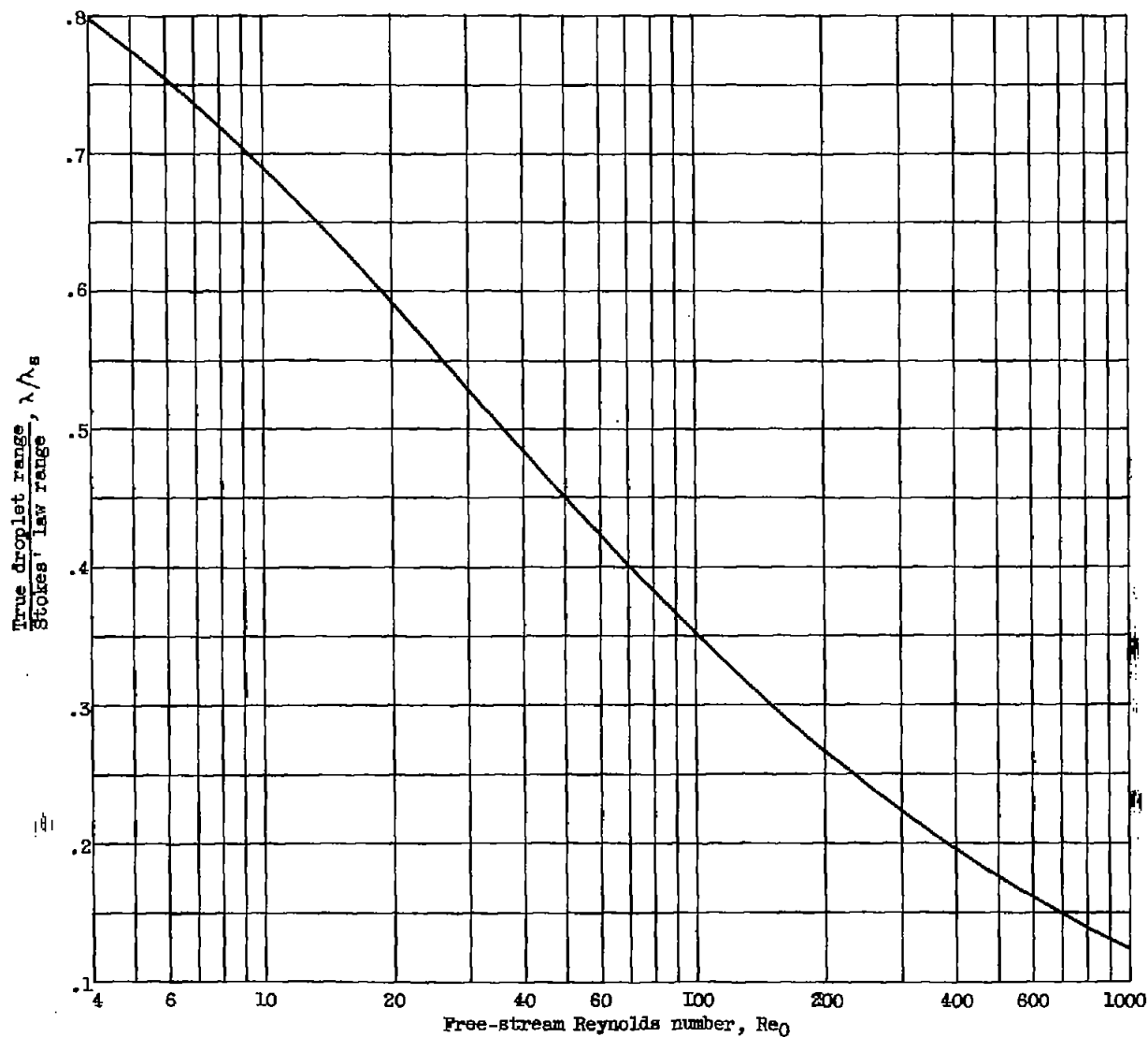
Figure 6. - Droplet range ratio as function of droplet Reynolds number (data from ref. 12).
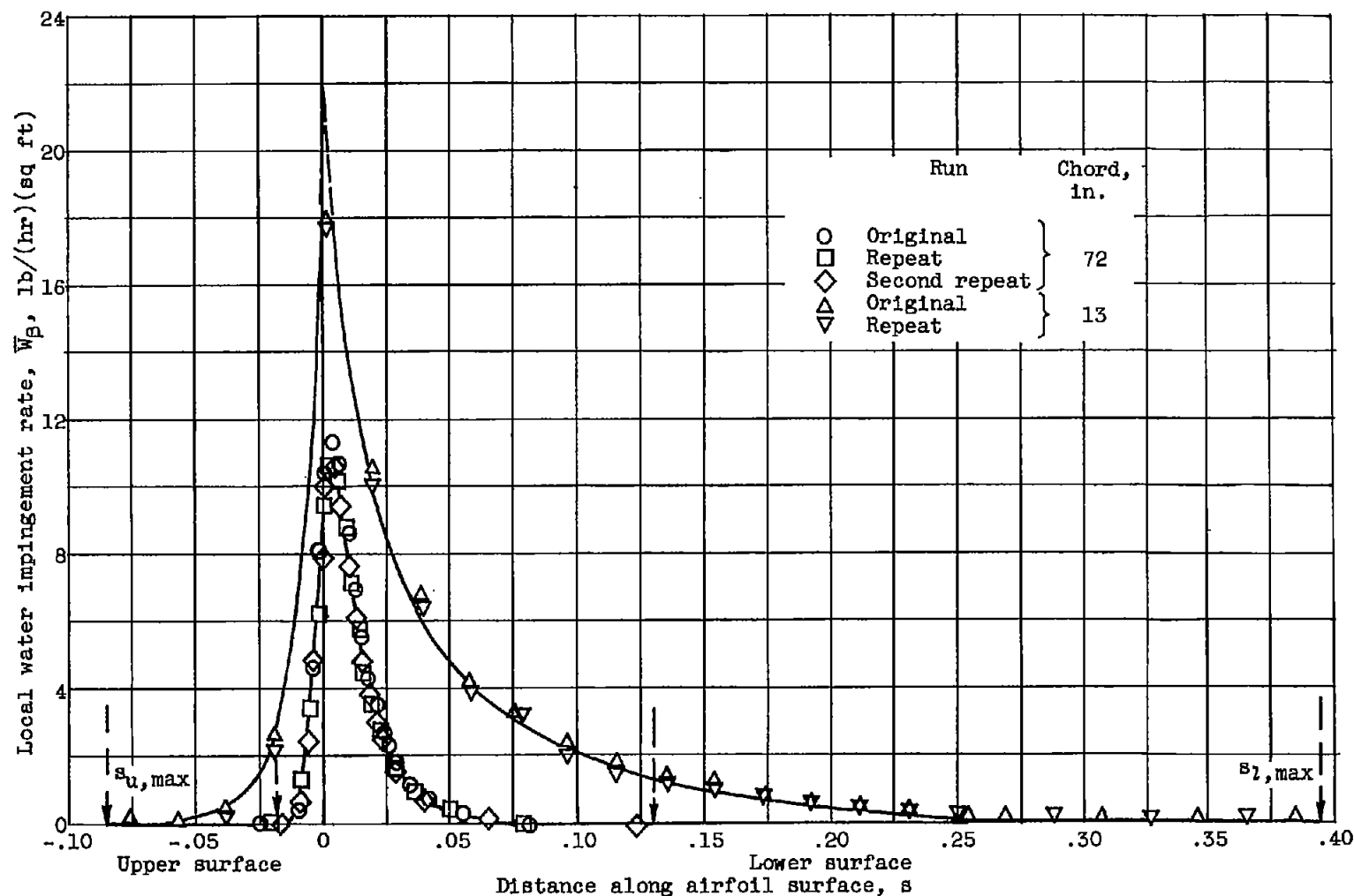
Figure 7. - Typical water impingement rates on NACA 65_1-212 airfoil. Airspeed, 152 knots; volume-median droplet diameter, 16.7 microns; angle of attack, 4^0.
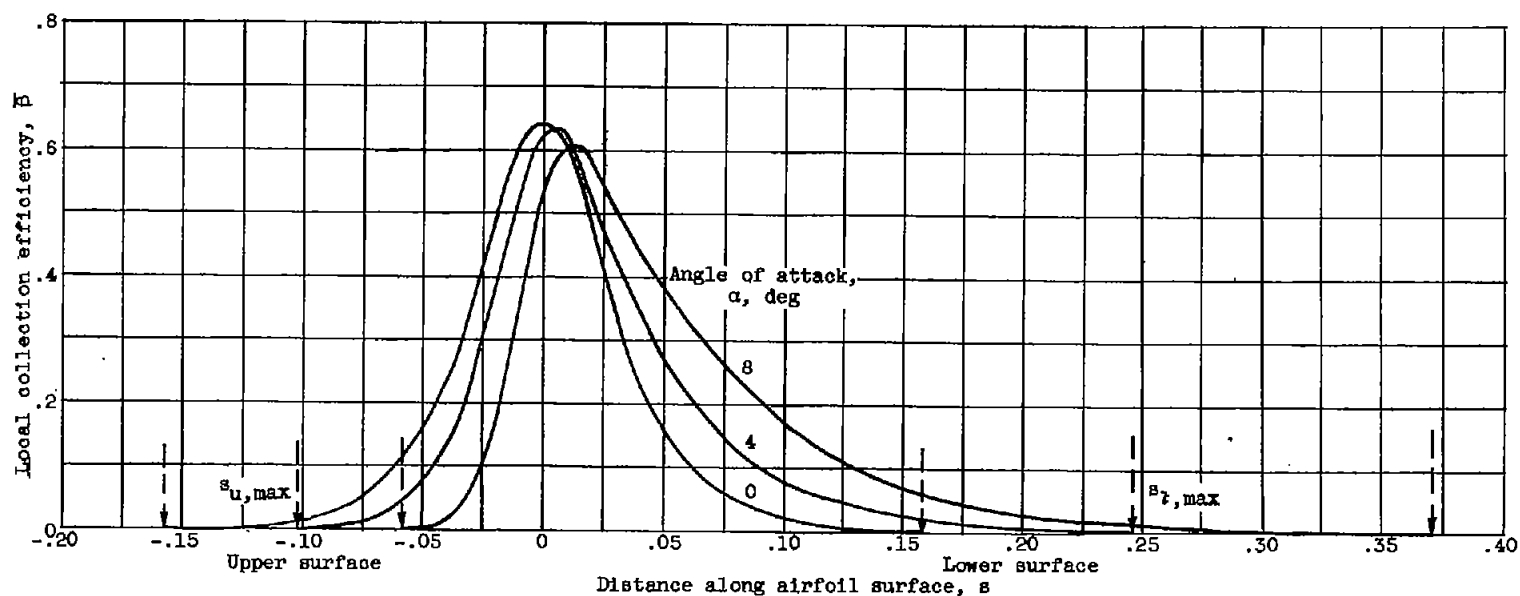
(a) Angle of attack effect. Joukowski 0015 airfoil; 13-inch chord.

Figure 8. - Effect of airfoil geometry and angle of attack on local collection efficiency. Airspeed, 152 knots; volume-median droplet diameter, 16.7 microns.
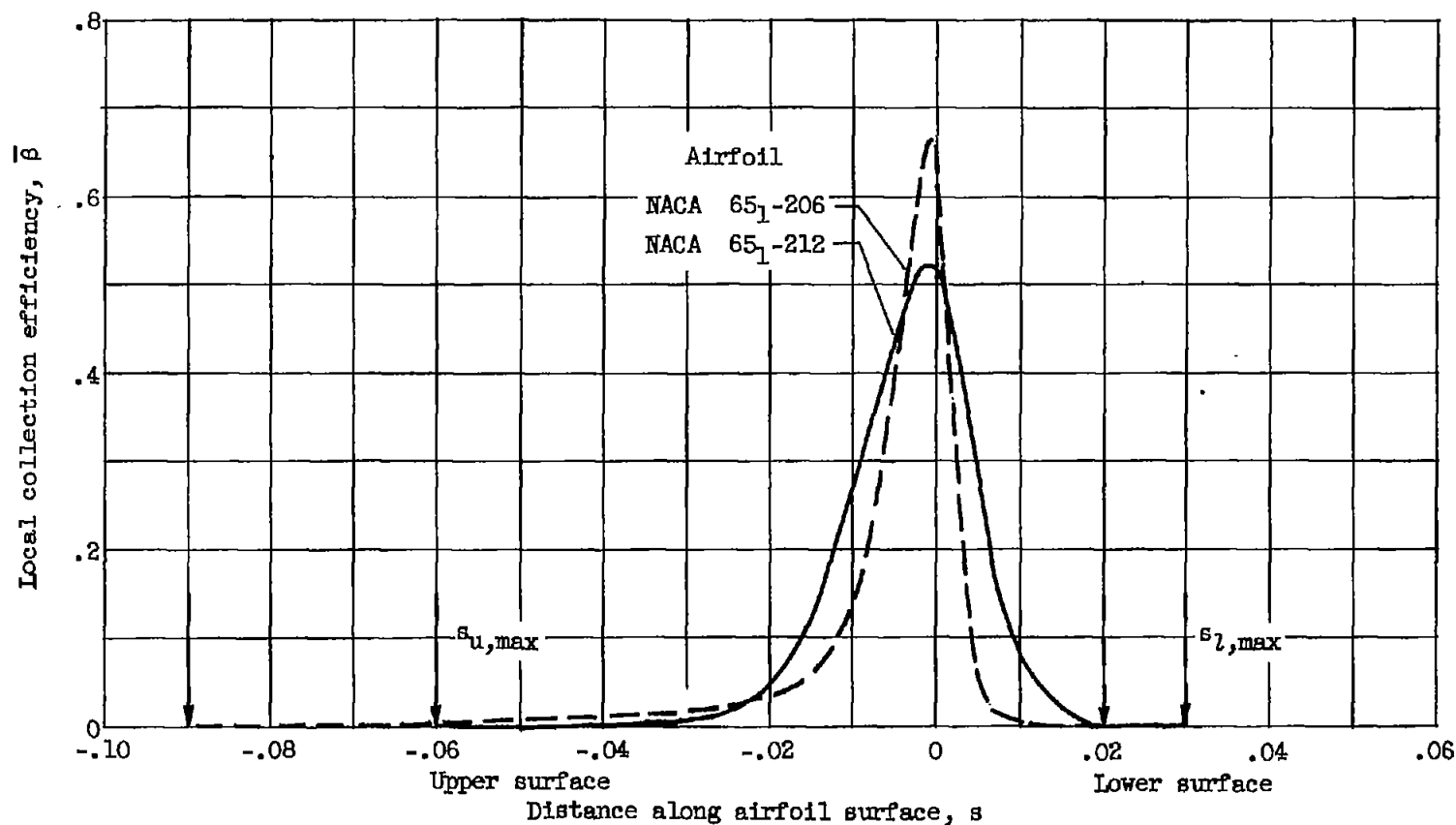
(b) Thickness effect. Angle of attack, $0°$; 72-inch chord.

Figure 8. - Continued. Effect of airfoil geometry and angle of attack on local collection efficiency. Airspeed, 152 knots; volume-median droplet diameter, 16.7 microns.
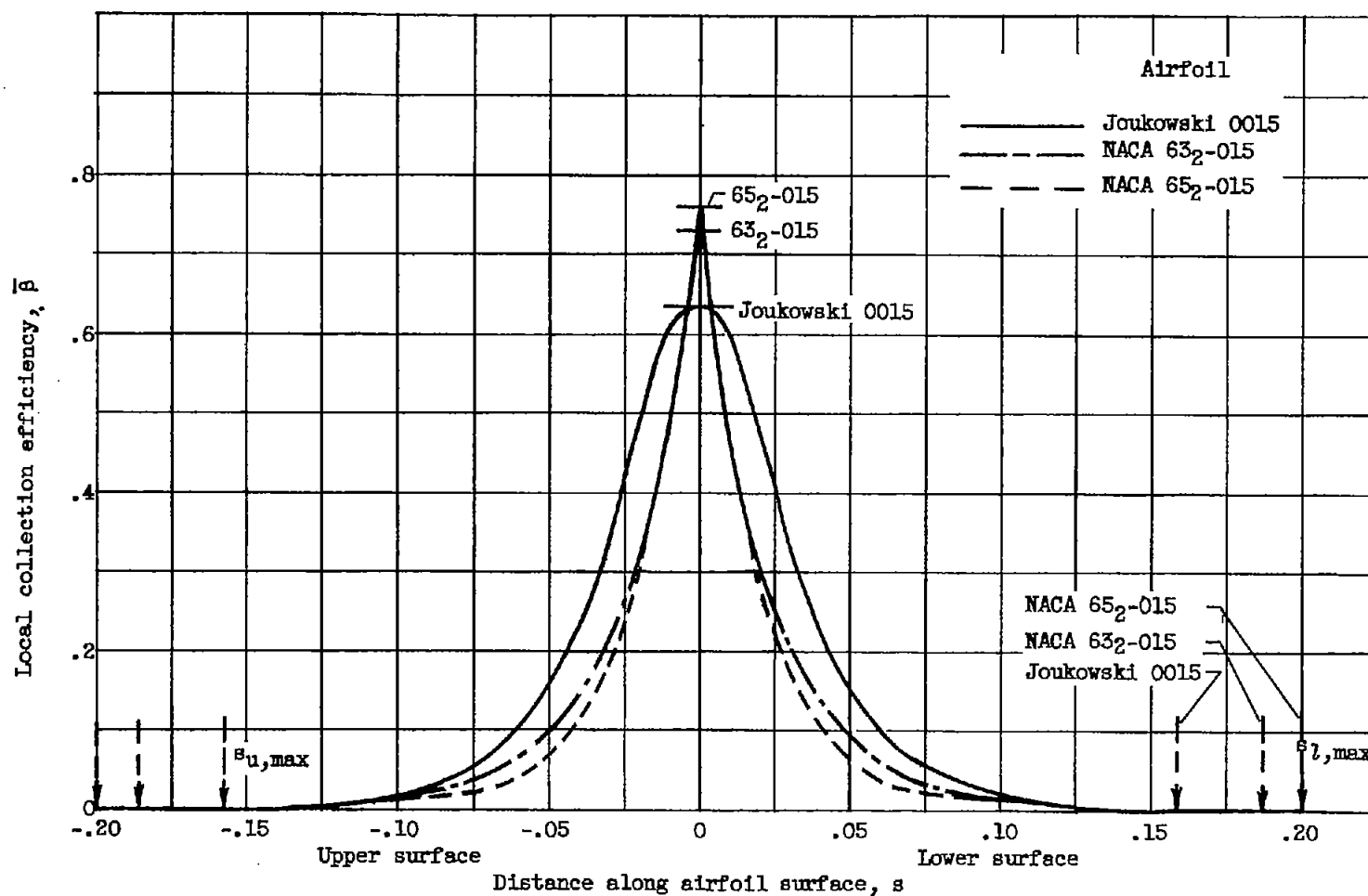
(c) Shape effect. Angle of attack, 0°; 13-inch chord.

Figure 8. - Concluded. Effect of airfoil geometry and angle of attack on local collection efficiency. Airspeed, 152 knots; volume-median droplet diameter, 16.7 microns.
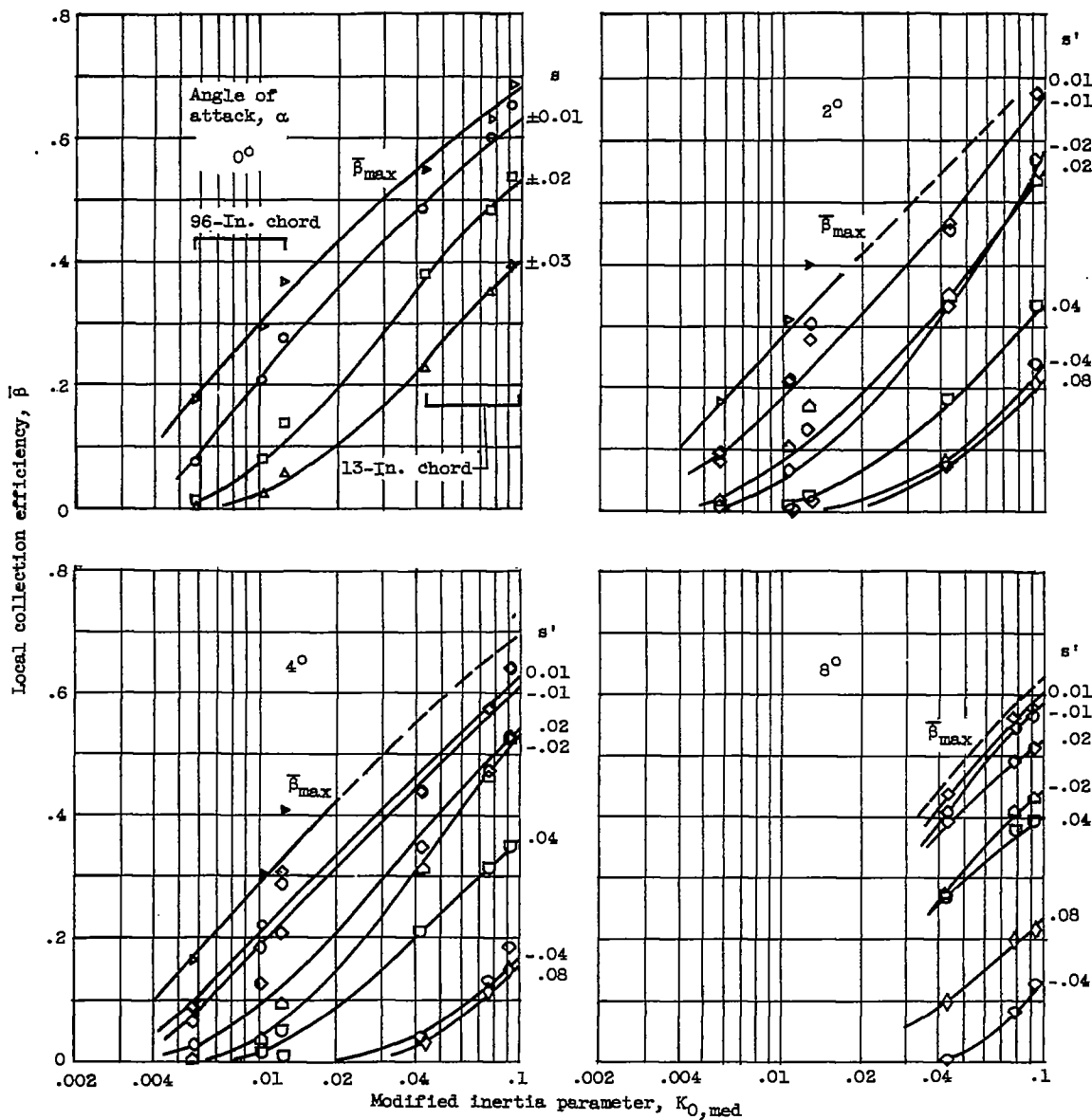
(a) and (b) Joukowski 0015 airfoils. Chord, 13 and 96 inches.

Figure 9. - Local collection efficiency of airfoils as function of modified inertia parameter and surface location.
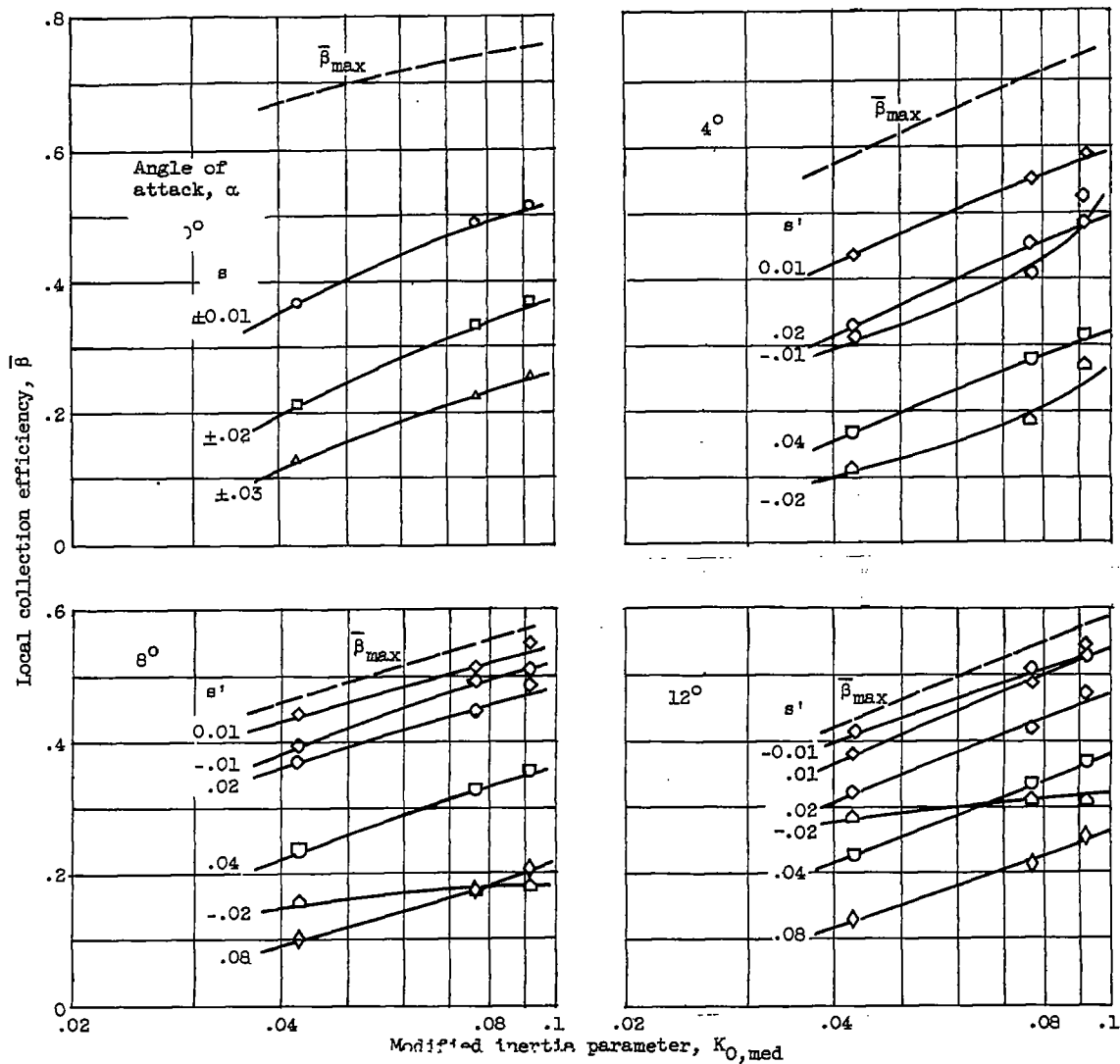
(c) NACA 63_2-015 airfoil. Chord, 13 inches.

Figure 9. - Continued. Local collection efficiency of airfoils as function of modified inertia parameter and surface location.
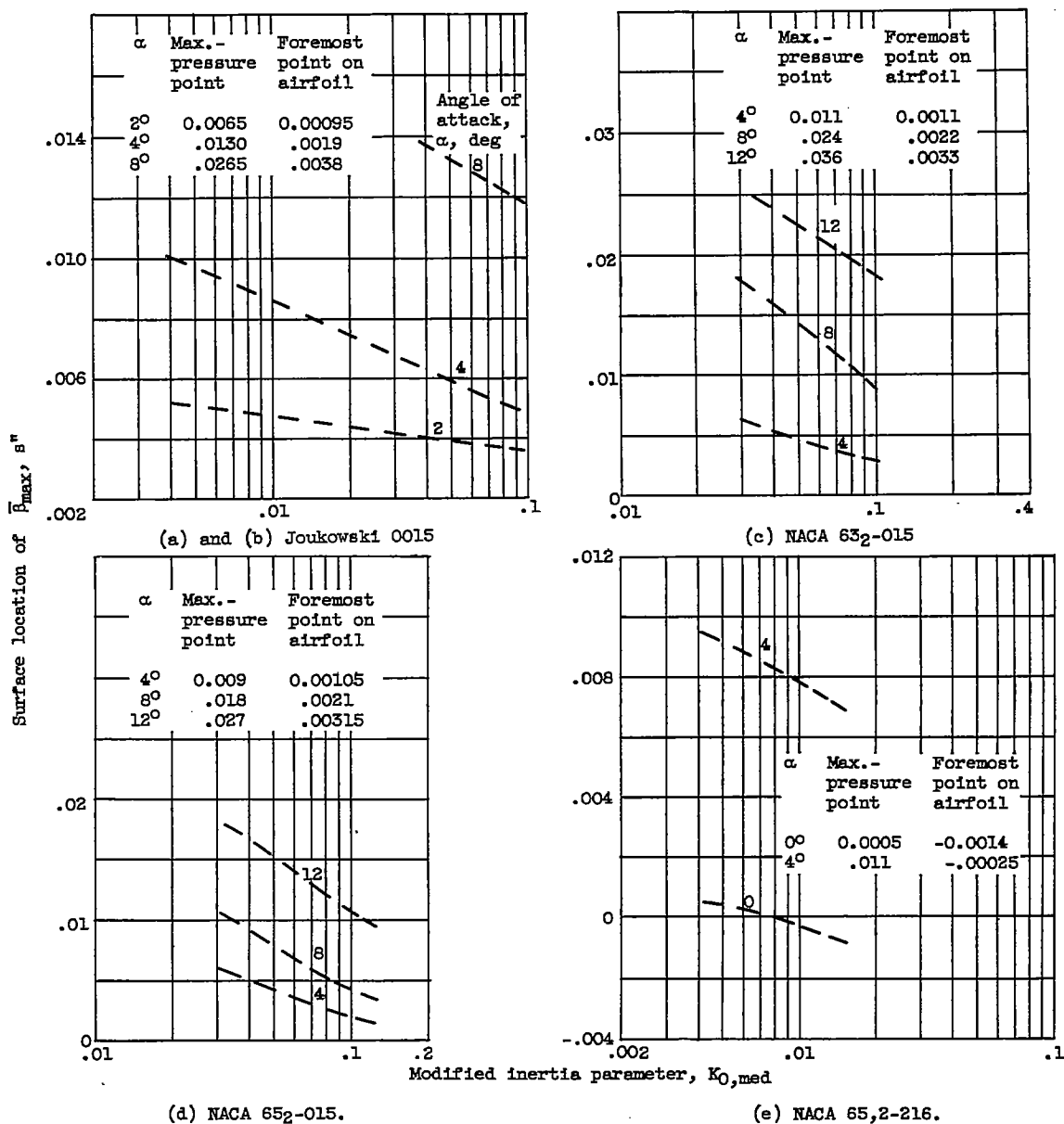
3689

CT-7 back
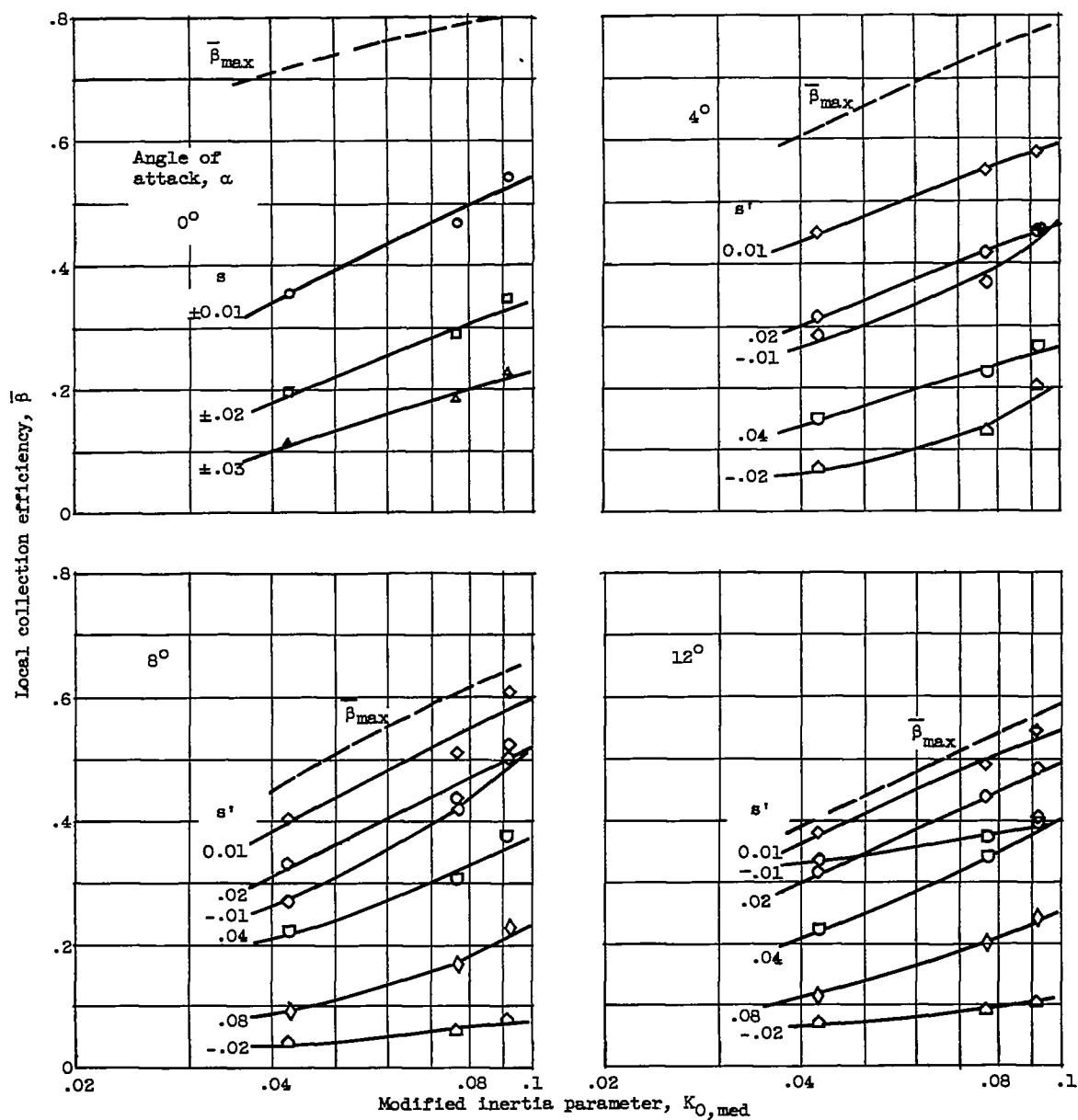
(d) NACA 65₂-015 airfoil. Chord, 13 inches.

Figure 9. - Continued. Local collection efficiency of airfoils as function of modified
    inertia parameter and surface location.
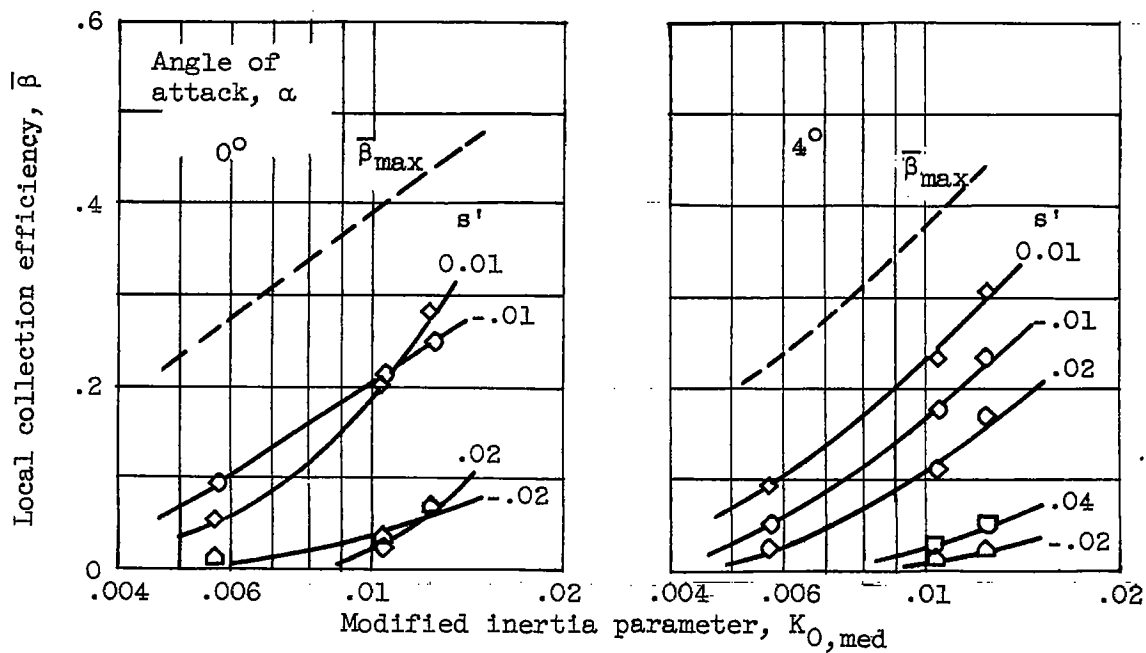
(e) NACA 65,2-216 airfoil. Chord, 96 inches.

Figure 9. - Continued. Local collection efficiency of airfoils as function of modified inertia parameter and surface location.

3689
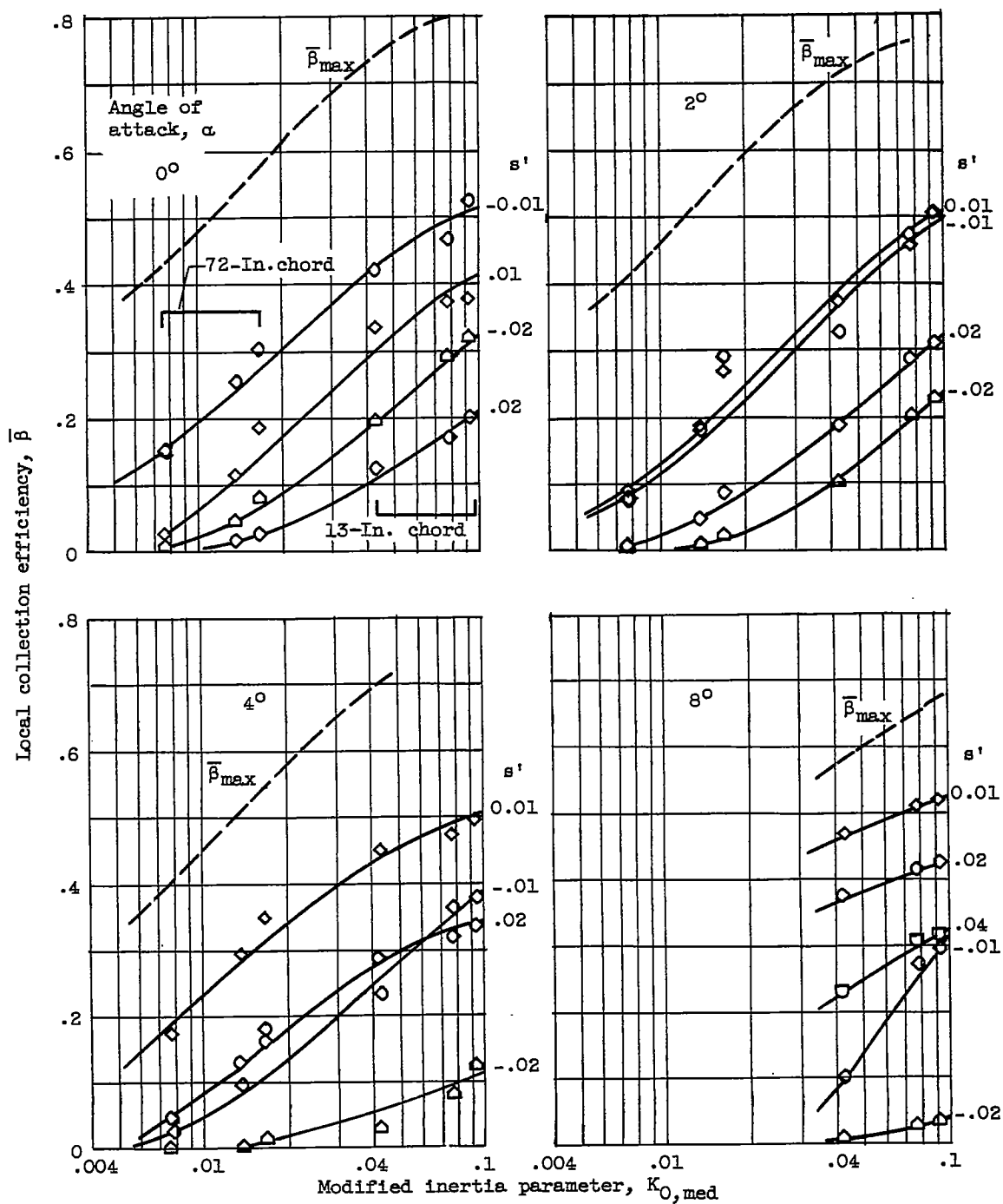
(f) and (g) NACA 65_1-212 airfoils. Chord, 13 and 72 inches.

Figure 9. - Continued. Local collection efficiency of airfoils as function
of modified inertia parameter and surface location.
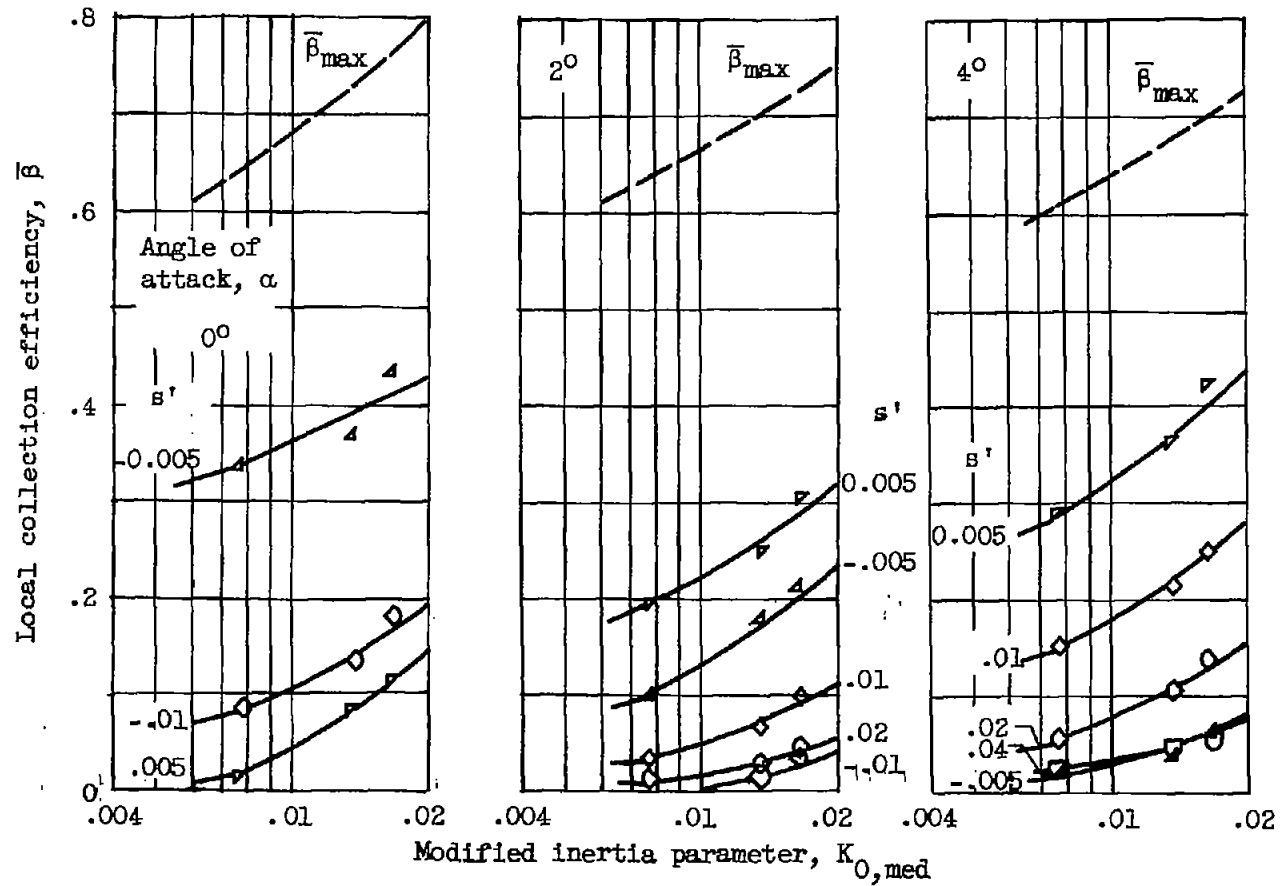
(h) NACA 65_1-206 airfoil. Chord, 72 inches.

Figure 9. - Continued. Local collection efficiency of airfoils as function of modified inertia parameter and surface location.
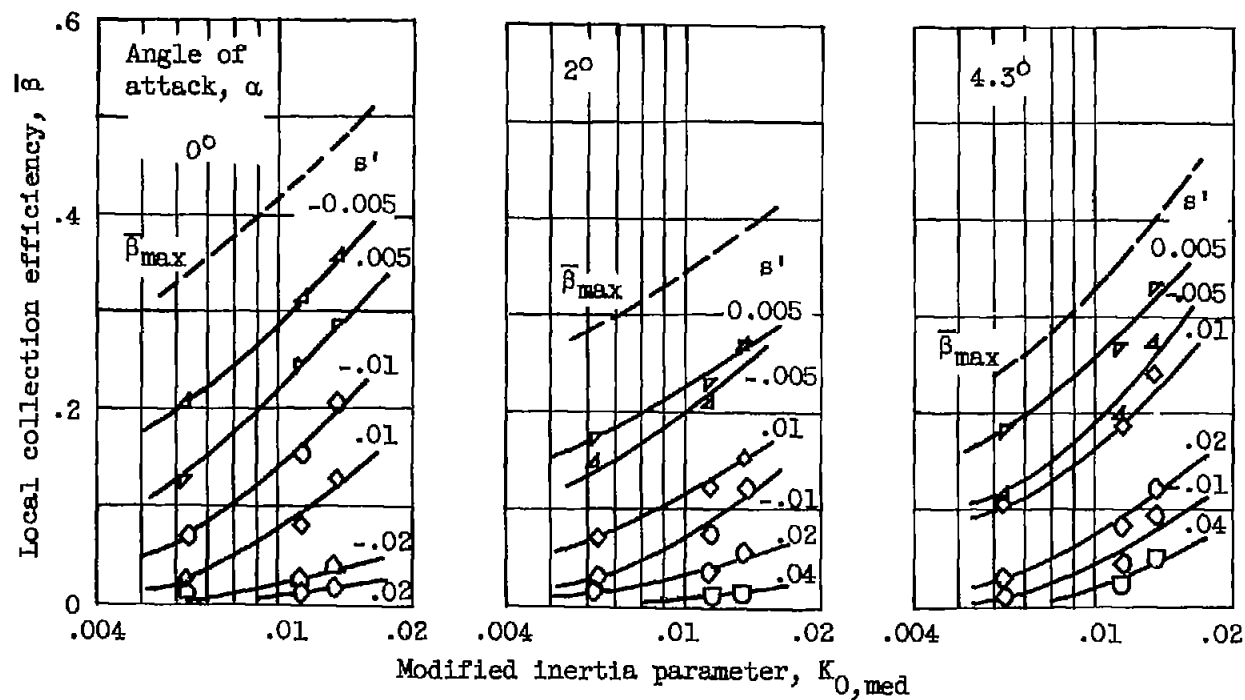
(i) NACA 65_1-212 airfoil, swept 35° (data in free-stream direction). Chord, 87.9 inches.

Figure 9. - Continued. Local collection efficiency of airfoils as function of modified inertia parameter and surface location.
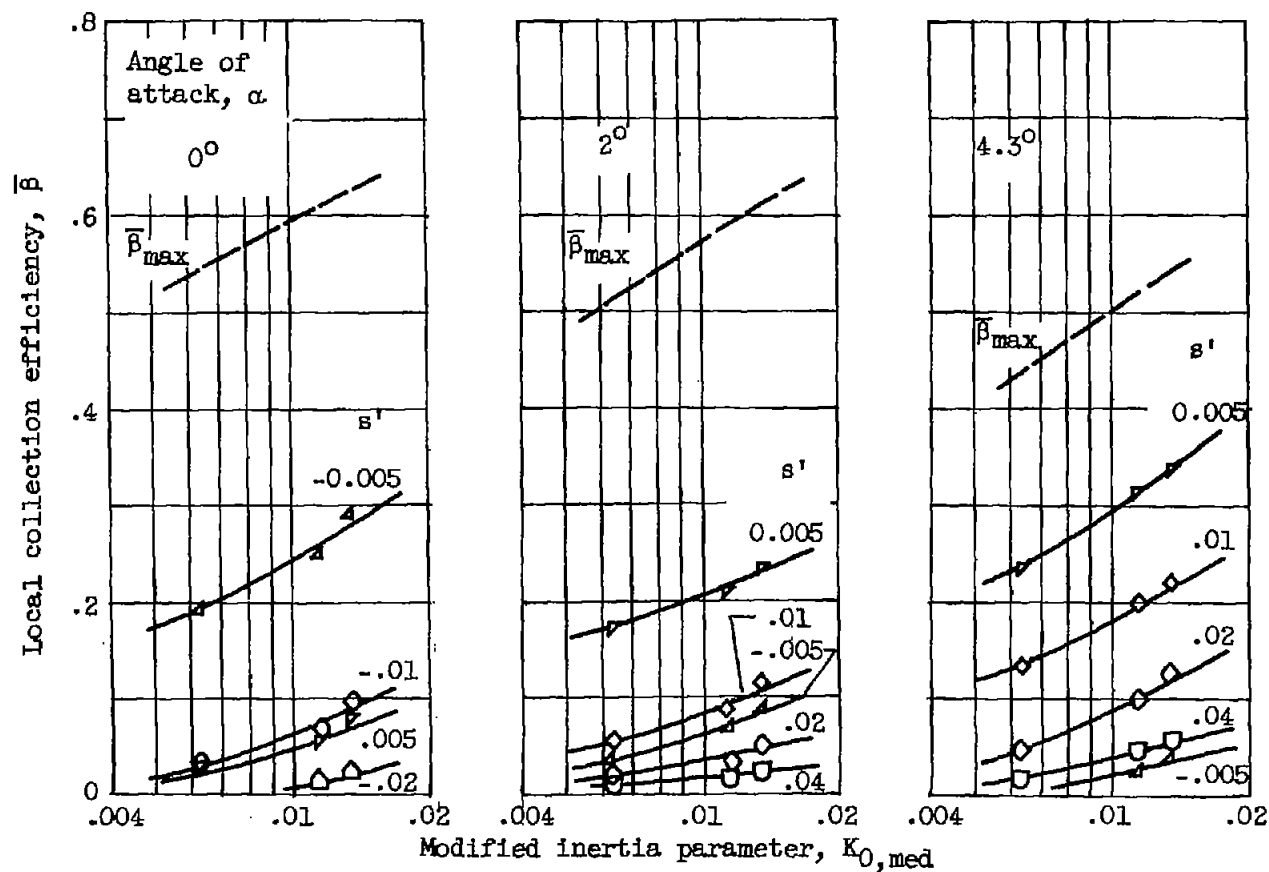
(j) NACA 65_1-206 airfoil, swept 35° (data in free-stream direction.)
Chord, 87.9 inches.

Figure 9. - Concluded. Local collection efficiency of airfoils as function of modified inertia parameter and surface location.

3689

CT-8

Surface location of $\bar{s}_{max}$, s''

α	Max.-pressure point	Foremost point on airfoil
2°	0.0065	0.00095
4°	.0130	.0019
8°	.0265	.0038

Angle of attack, α, deg

.014

.010

.006

.002 .01 .1

(a) and (b) Joukowski 0015

α	Max.-pressure point	Foremost point on airfoil
4°	0.011	0.0011
8°	.024	.0022
12°	.036	.0033

.03

.02

.01

0
.01 .1 .4

(c) NACA 63$_2$-015

α	Max.-pressure point	Foremost point on airfoil
4°	0.009	0.00105
8°	.018	.0021
12°	.027	.00315

.02

.01

0
.01 .1 .2

(d) NACA 65$_2$-015.

.012

.008

.004

0

-.004
.002 .01 .1

α	Max.-pressure point	Foremost point on airfoil
0°	0.0005	-0.0014
4°	.011	-.00025

Modified inertia parameter, $K_{0,med}$

(e) NACA 65,2-216.

Figure 10. - Surface location of maximum local collection efficiency as function of modified inertia parameter (max. and foremost points tabulated as s distance).

(f) and (g) NACA 65₁-212.

(h) NACA 65₁-206.

(i) NACA 65₁-212; 35° sweep.

(j) NACA 65₁206; 35° sweep.

Figure 10. - Concluded. Surface location of maximum local collection efficiency as function of modified inertia parameter (max. and foremost points tabulated as s distance.

(a) and (b) Joukowski 0015.

(c) NACA 63_2-015.   Chord, 13 inches.

(d) NACA 65_2-015.   Chord, 13 inches.

(e) NACA 65,2-216.   Chord, 96 inches.
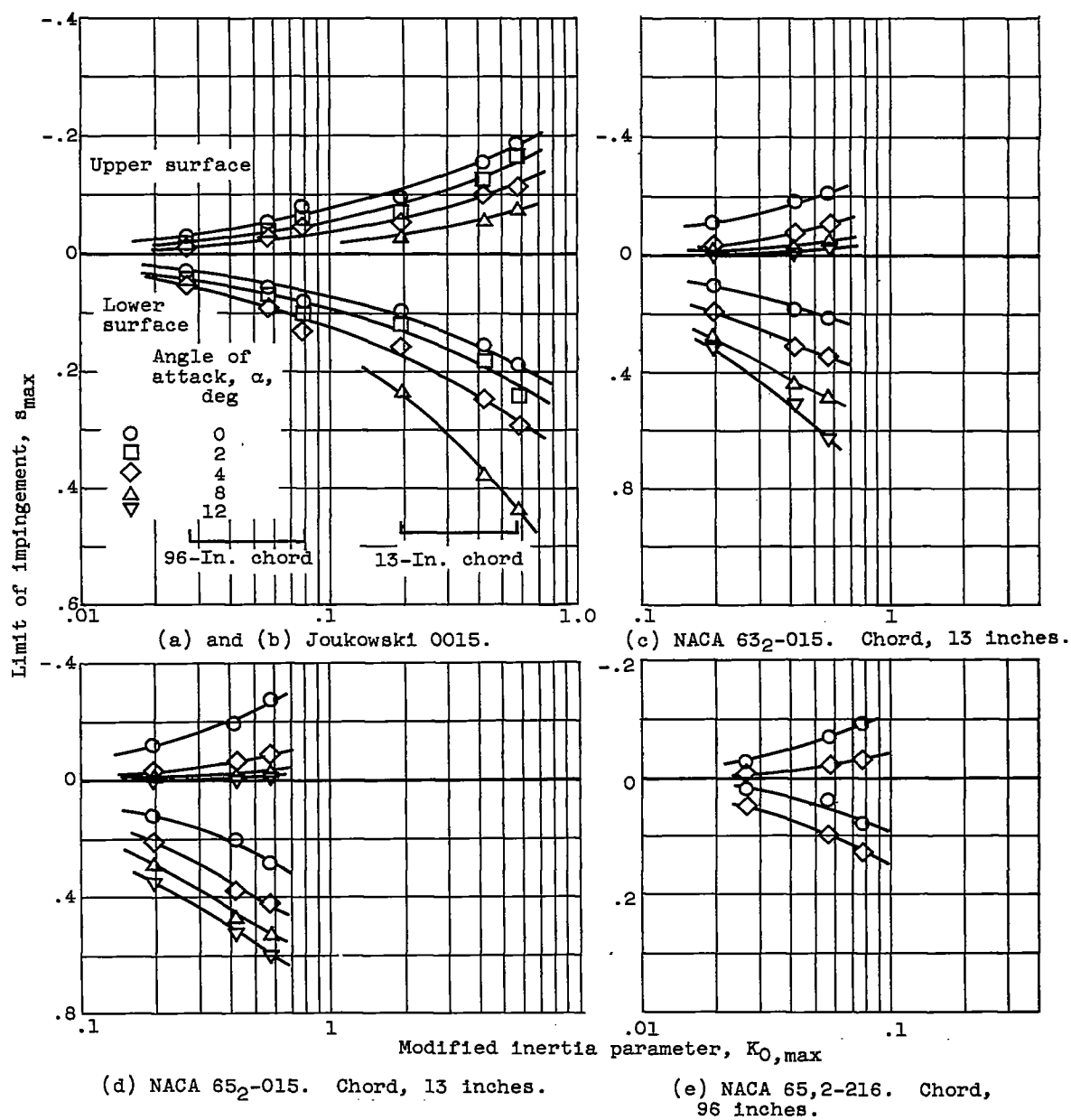
Figure 11. - Limits of impingement on airfoils as function of modified inertia parameter.

(f) and (g) NACA 65_1-212.

(h) NACA 65_1-206. Chord, 72 inches.

Angle of
attack,
α, deg

○   0
□   2
◇   4
◇   4.3
△   8
▽   12

Modified inertia parameter, $K_{O,max}$

(i) NACA 65_1-212, 35° sweep.
   Chord, 87.9 inches.

(j) NACA 65_1-206, 35° sweep.
   Chord, 87.9 inches.
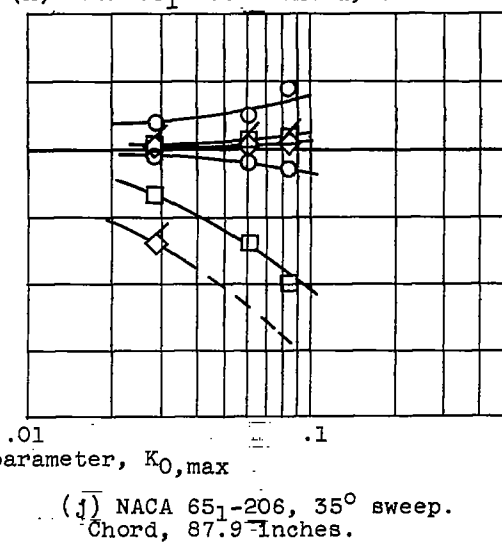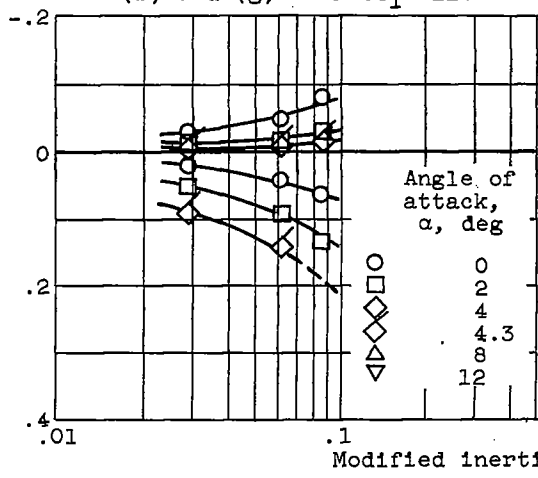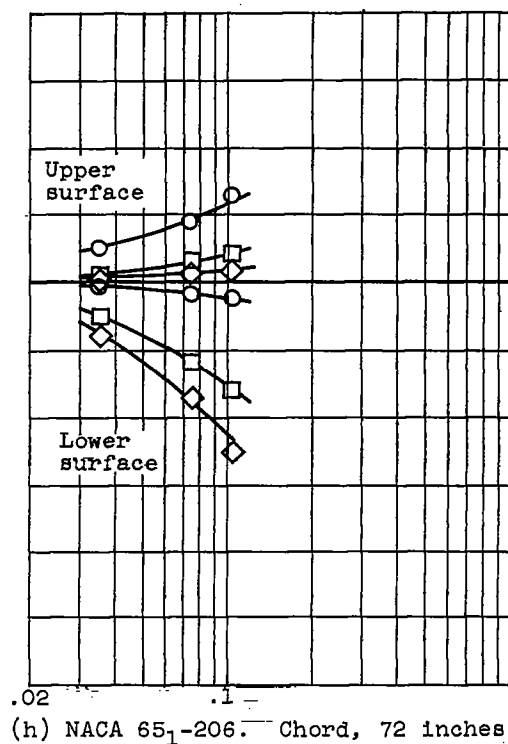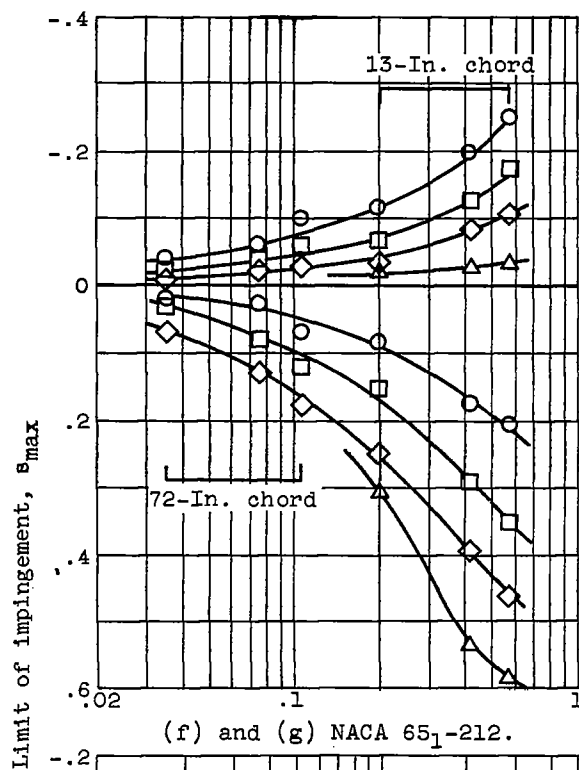
Figure 11. - Concluded. Limits of impingement on airfoils as function of modified inertia parameter.
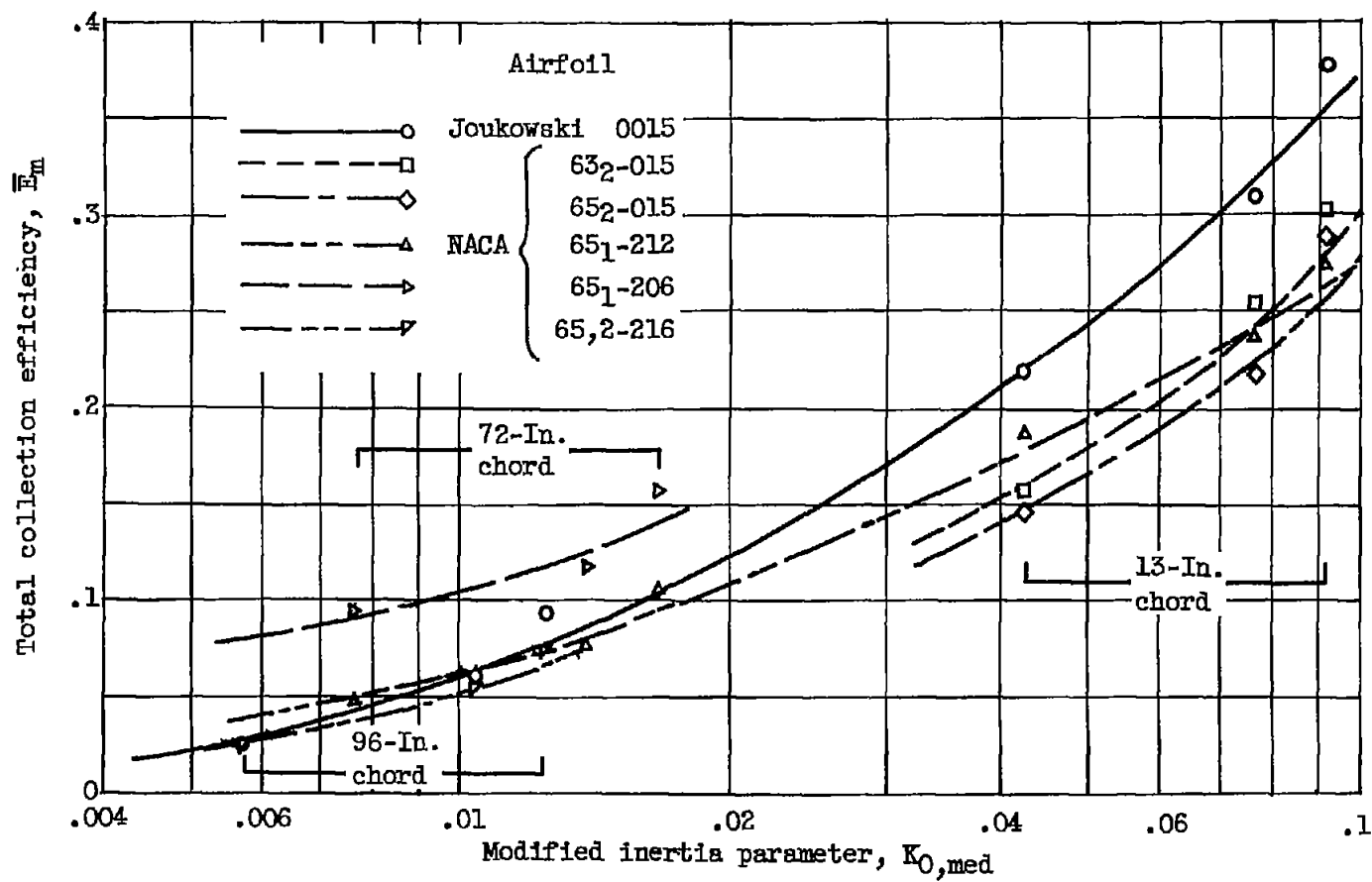
Figure 12. - Experimental total collection efficiency of six unswept airfoils at 0° angle of attack.

(a) Chord, 13 inches; $K_{0,med}$, 0.0769.

Airfoil

o	Joukowski 0015	
□		65_2-015
◇		63_2-015
△	NACA	65_1-212
▽	—	65_1-206
▼		65,2-216

(b) Chord, 72 inches; $K_{0,med}$, 0.01385.

(c) Chord, 87.9 inches; $K_{0,med}$, 0.01135; airfoils swept $35°$
(design sections in plane normal to leading edge).

(d) Chord, 96 inches; $K_{0,med}$, 0.0104
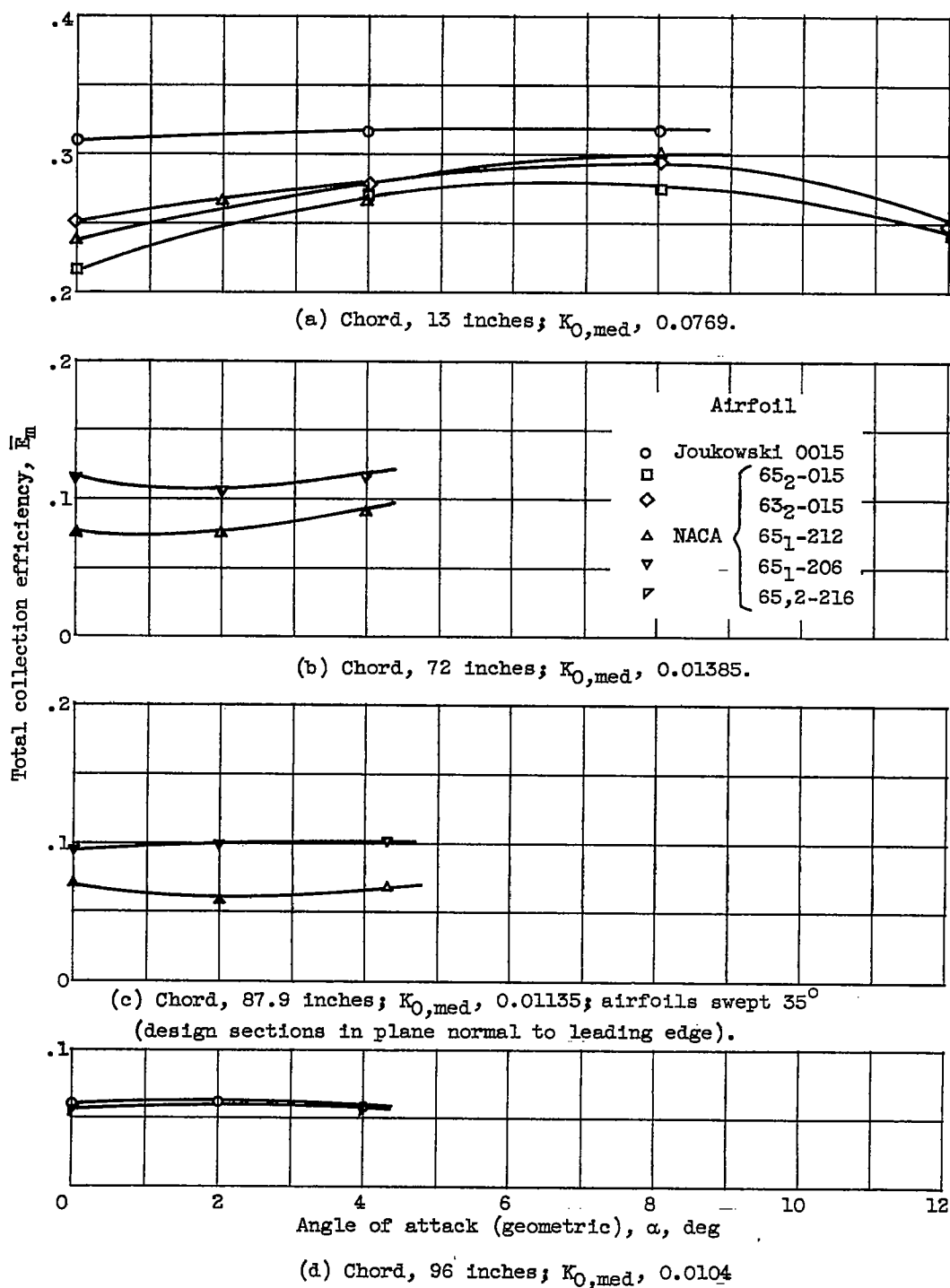
Figure 13. - Effect of angle of attack on experimental total collection
efficiency of six airfoil sections. Airspeed, 152 knots; volume-
median drop diameter, 16.7 microns.

3689
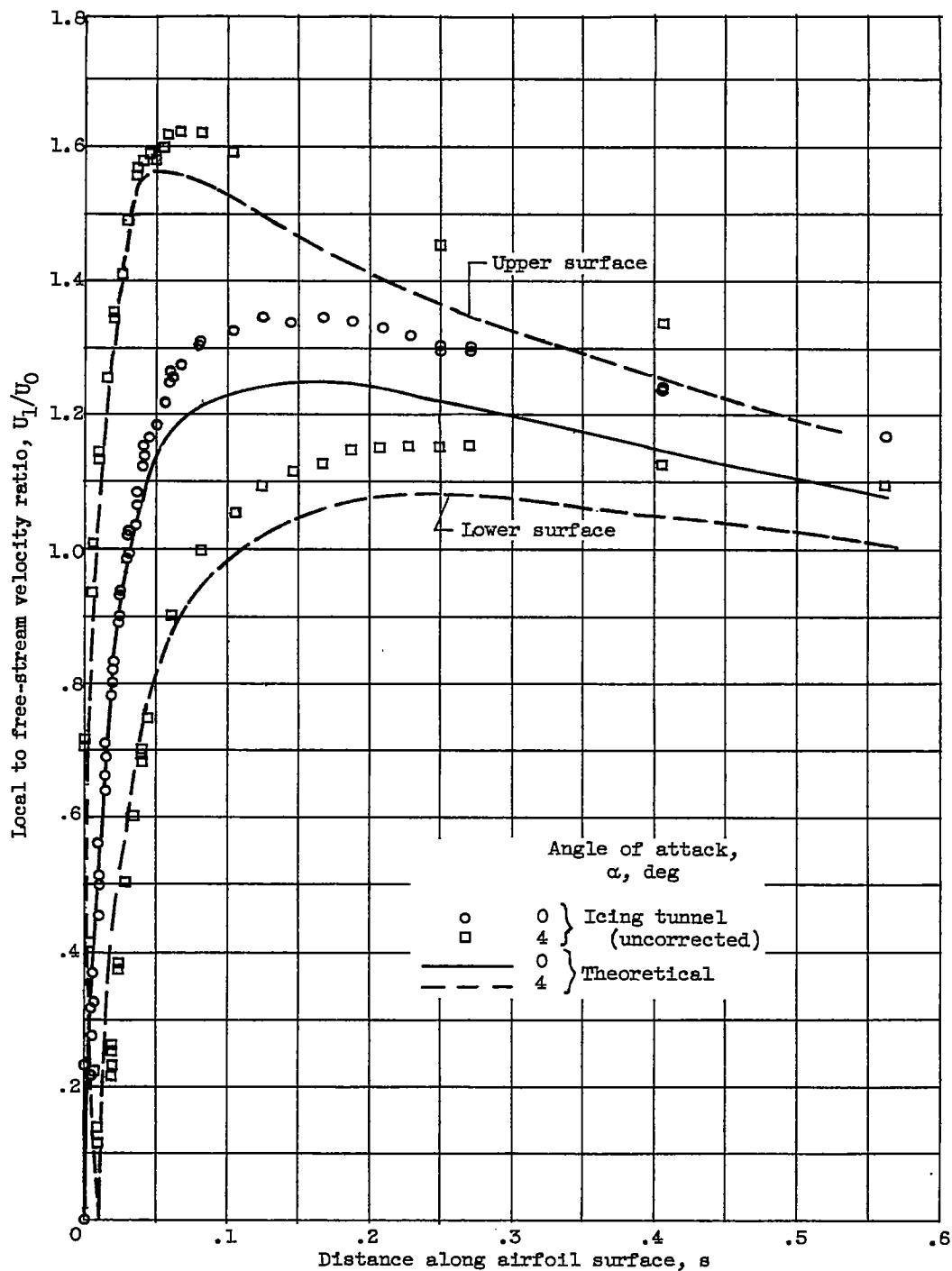
(a) Joukowski 0015 airfoil; 96-inch chord.

Figure 14. - Local velocity distribution on airfoil. Airspeed, 152 knots; pressure, 28.1 inches of mercury; temperature 50° F.
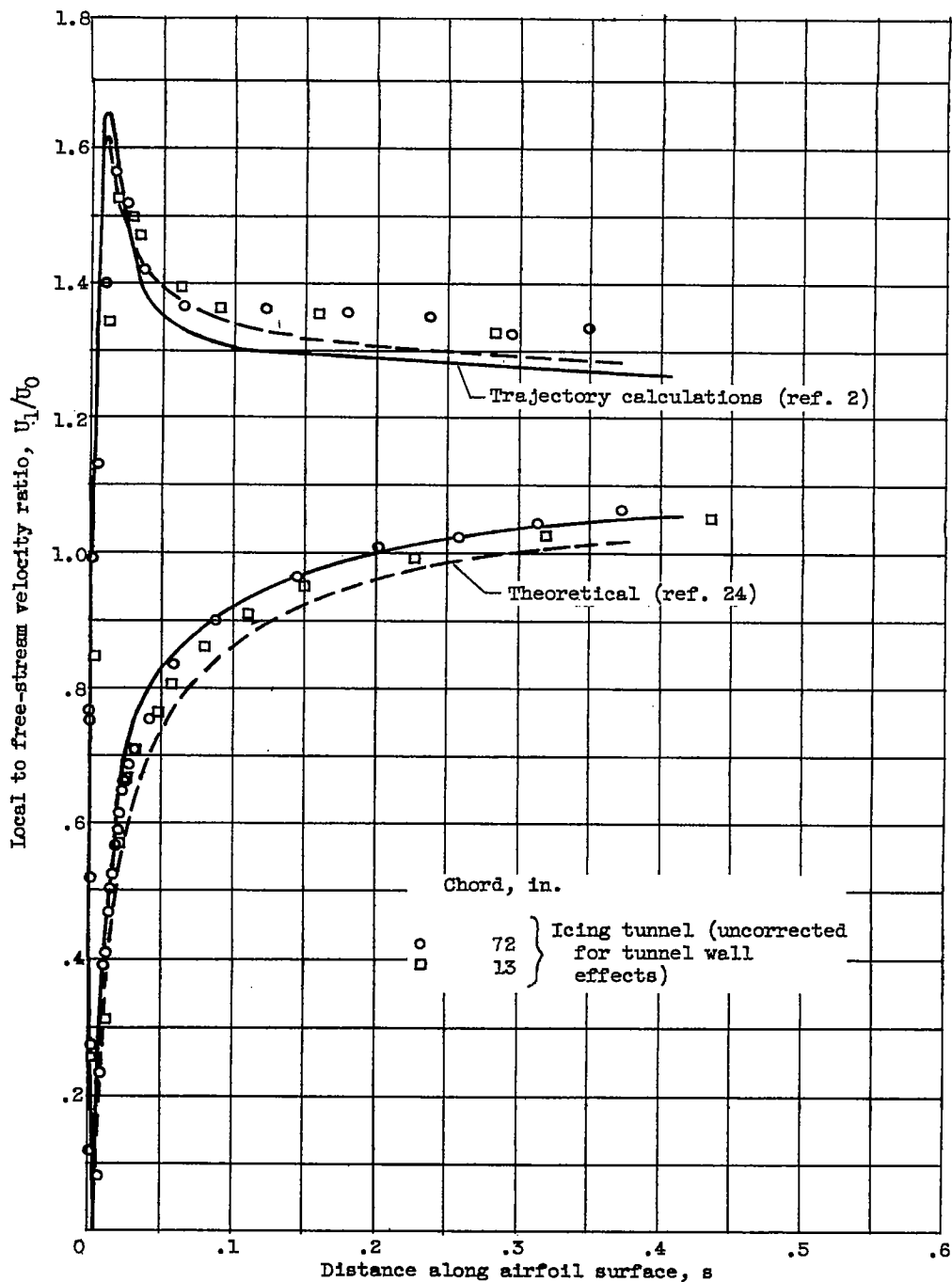
(b) NACA 65_1-212 airfoil; angle of attack, 4°.

Figure 14. - Concluded. Local velocity distribution on airfoil.
Airspeed, 152 knots; pressure, 28.1 inches of mercury; temperature, 50° F.
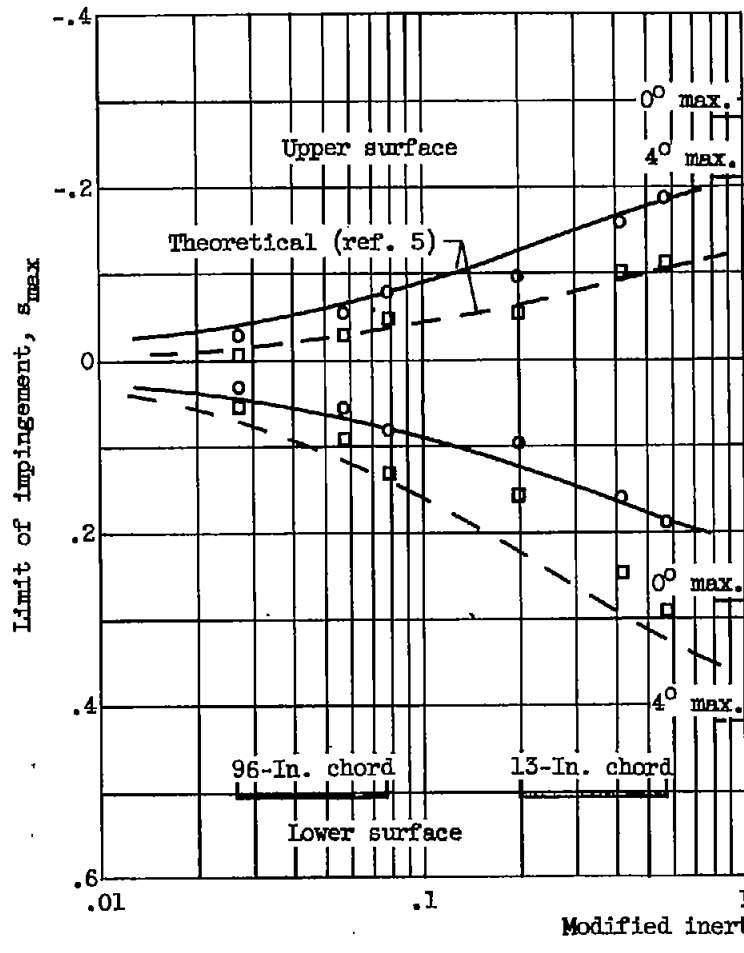
(a) Joukowski 0015 airfoil; angle of
attack, 0° and 4°.
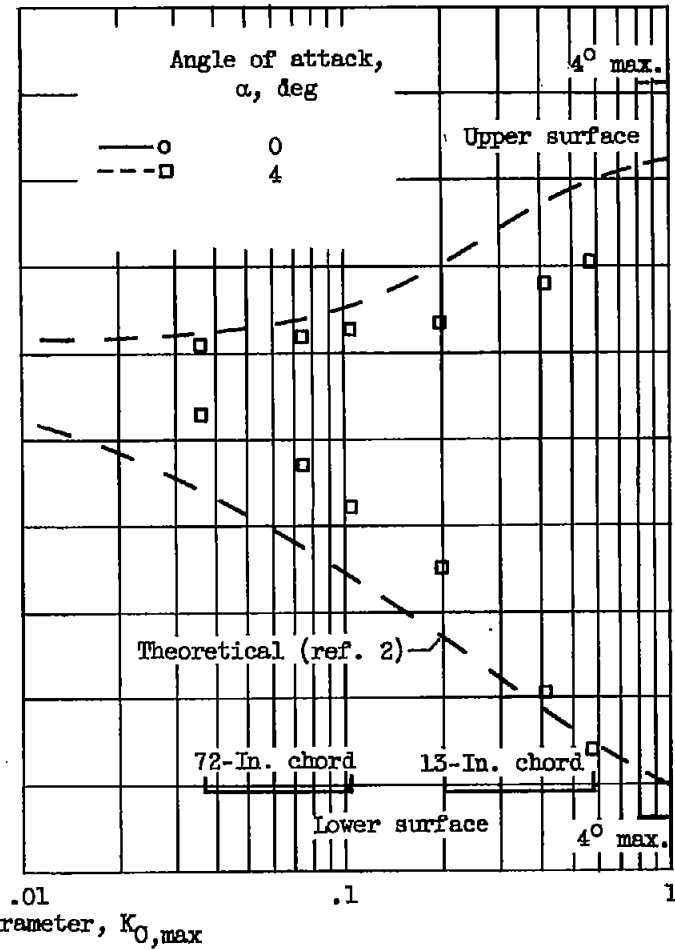
(b) NACA 65₁-212 airfoil; angle of
attack, 4°.

Figure 15. - Comparison of experimental and theoretical limits of impingement.

(a) Angle of attack, 0°.

(b) Angle of attack, 4°.
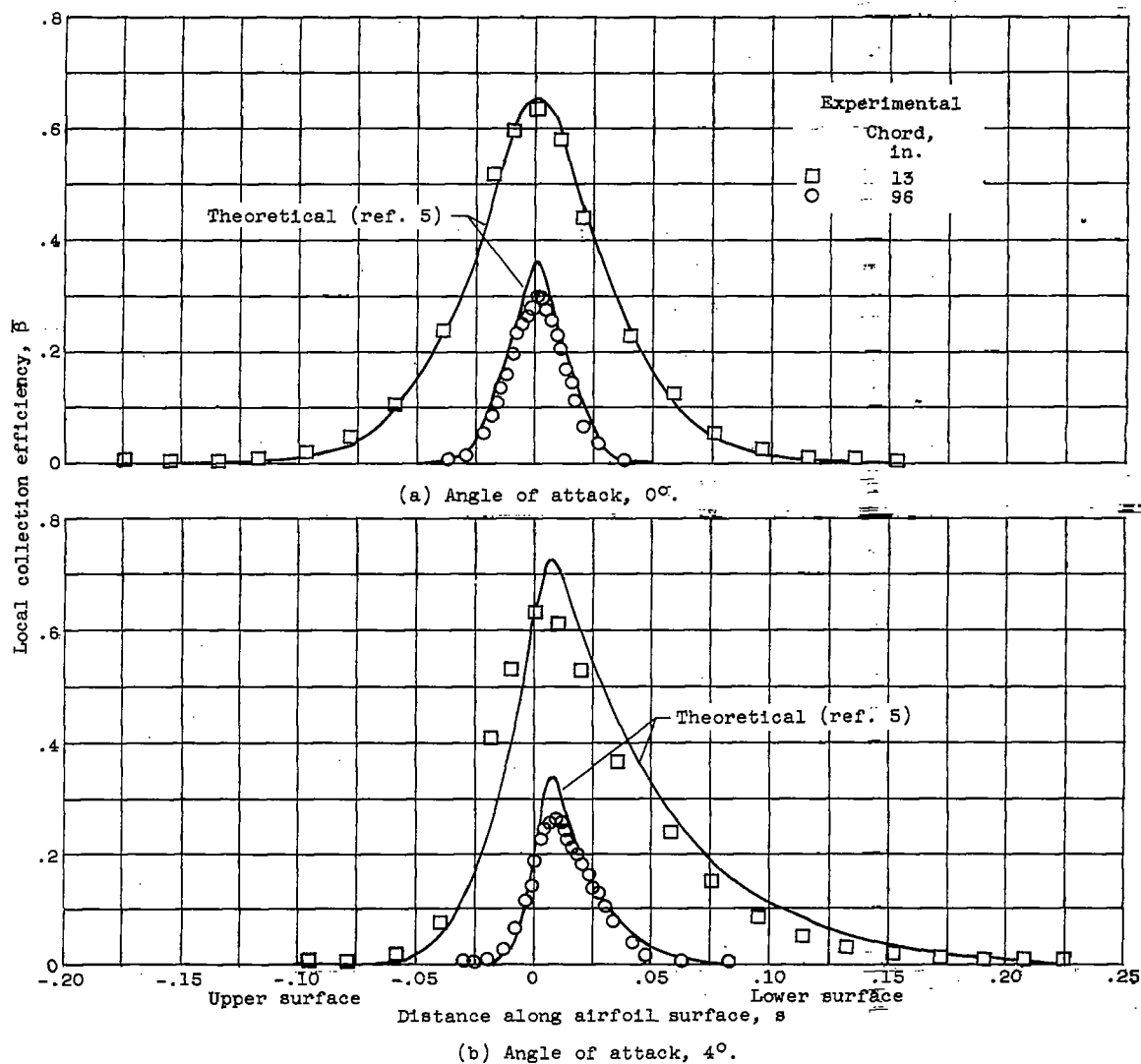
Figure 16. - Comparsion of experimental and theoretical local collection efficiency on 15-percent symmetrical Joukowski airfoil. Angles of attack, 0° and 4°; chord length, 13 and 96 inches; volume-median droplet size, 16.7 microns; airspeed, 152 knots.

(a) Joukowski 0015; angle of attack, 0°.

(b) Joukowski 0015; angle of attack, 4°.

(c) NACA 65_1-212; angle of attack, 4°.
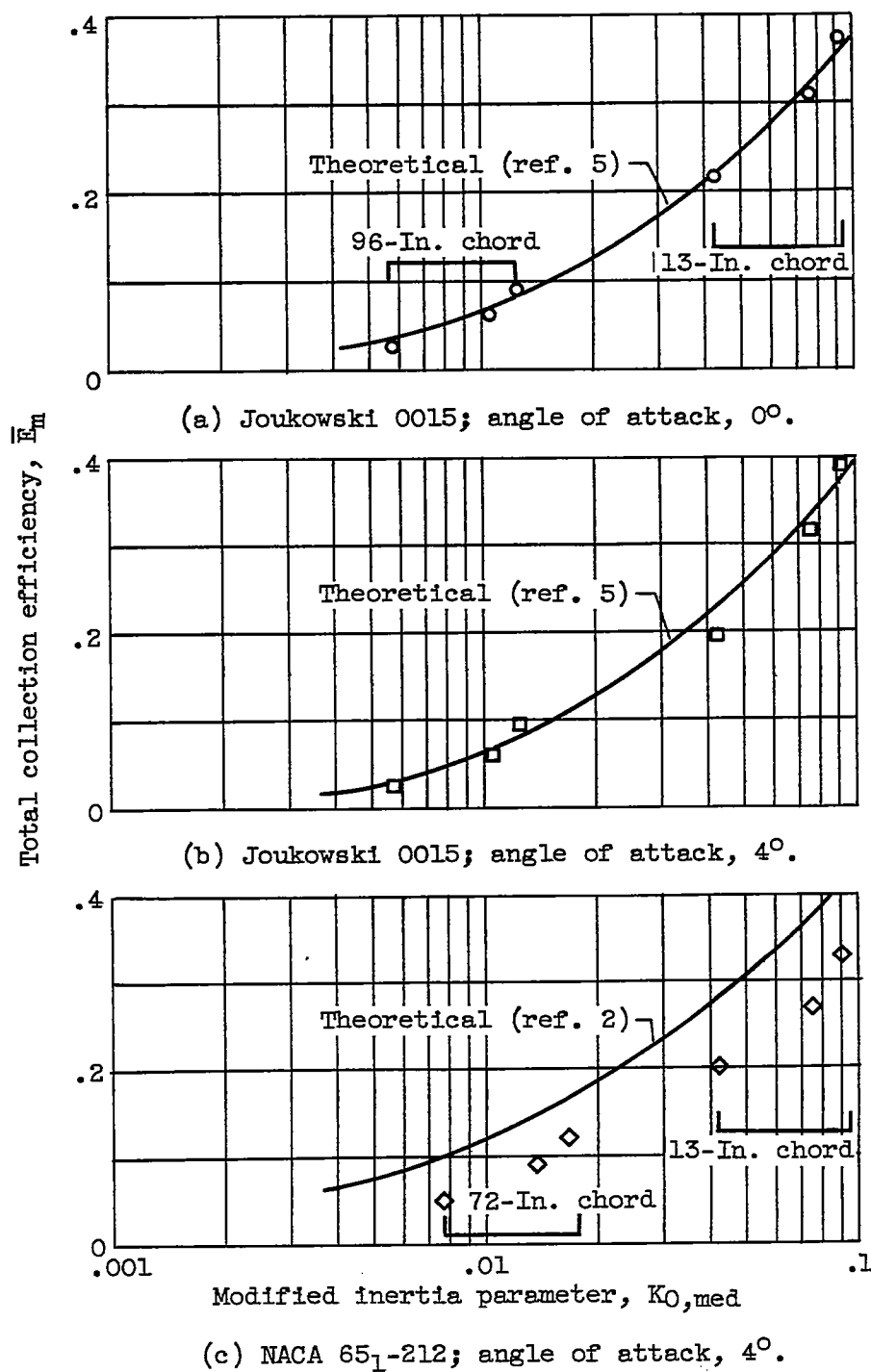
Figure 17. - Comparison of experimental and theoretical total collection efficiencies.
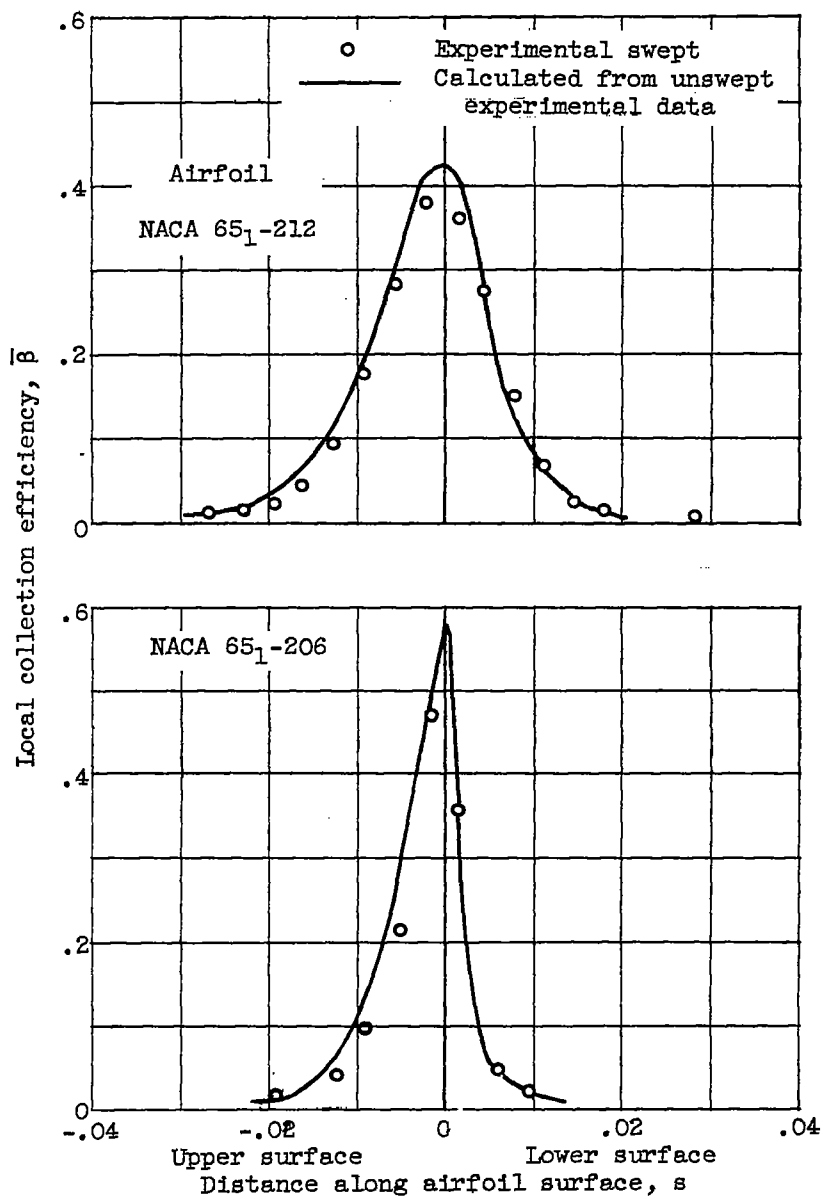
(a) Angle of attack, 0°.

Figure 18. - Comparison of local collection efficiency for 35° swept airfoils with values calculated from unswept-airfoil data (method of ref. 14). Speed, 152 knots; volume-median droplet size, 16.7 microns. (All values in terms of free-stream direction.)
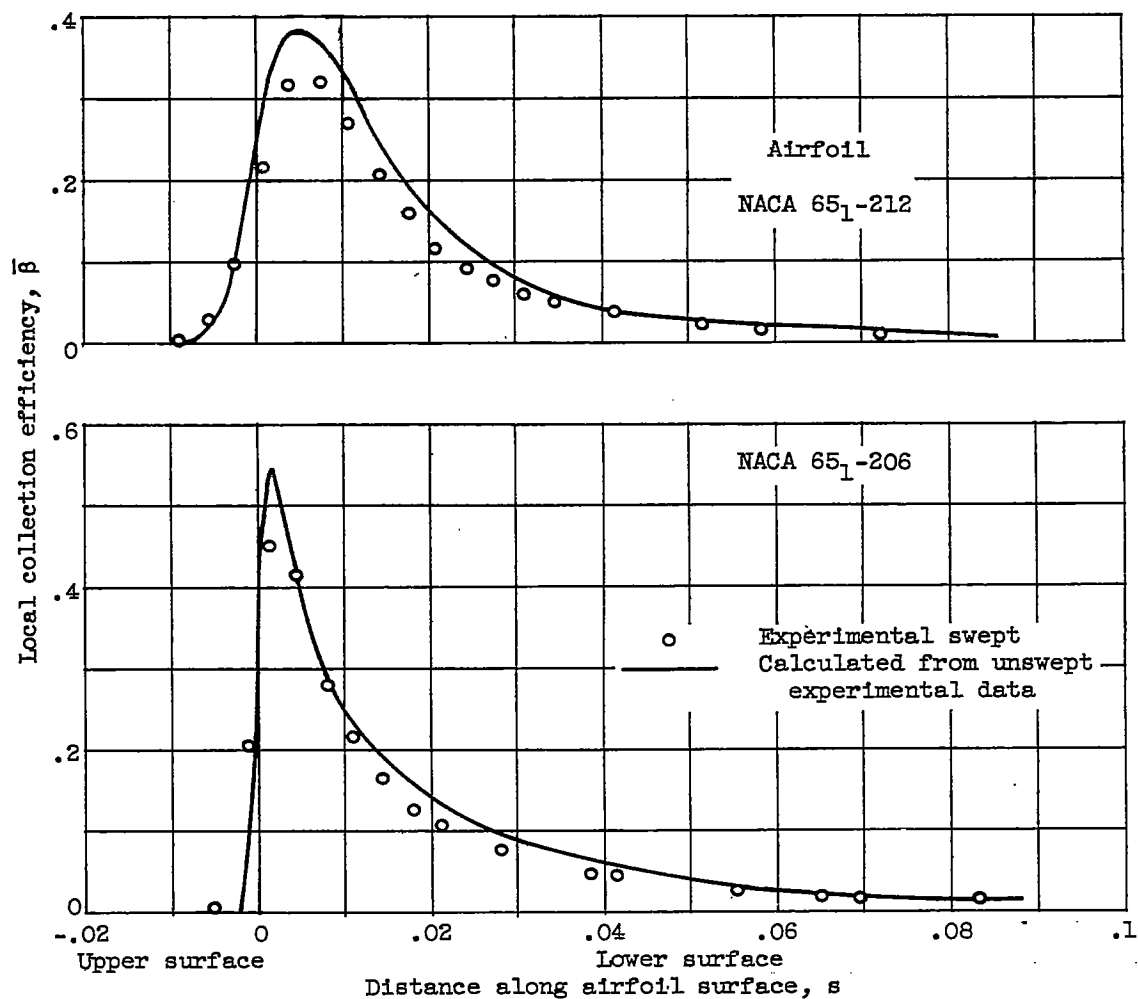
(b) Angle of attack, 4.3°.

Figure 18. - Concluded. Comparison of local collection efficiency for
35° swept airfoils with values calculated from unswept-airfoil data
(method of ref. 14). Speed, 152 knots; volume-median droplet size,
16.7 microns. (All values in terms of free-stream direction.)
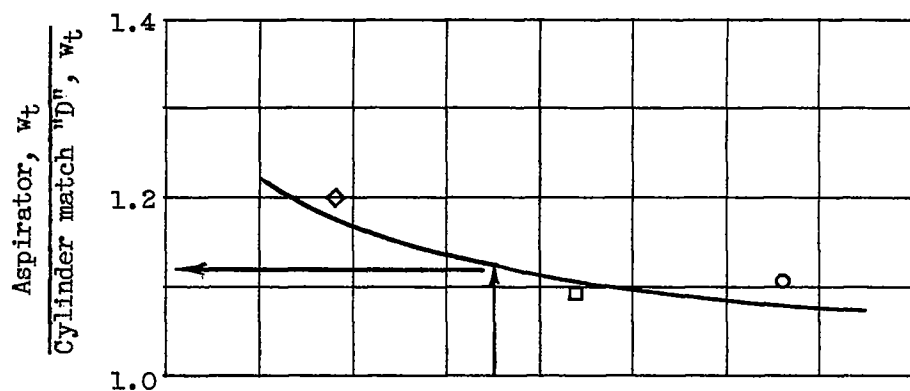
(a) Liquid-water-content ratio.
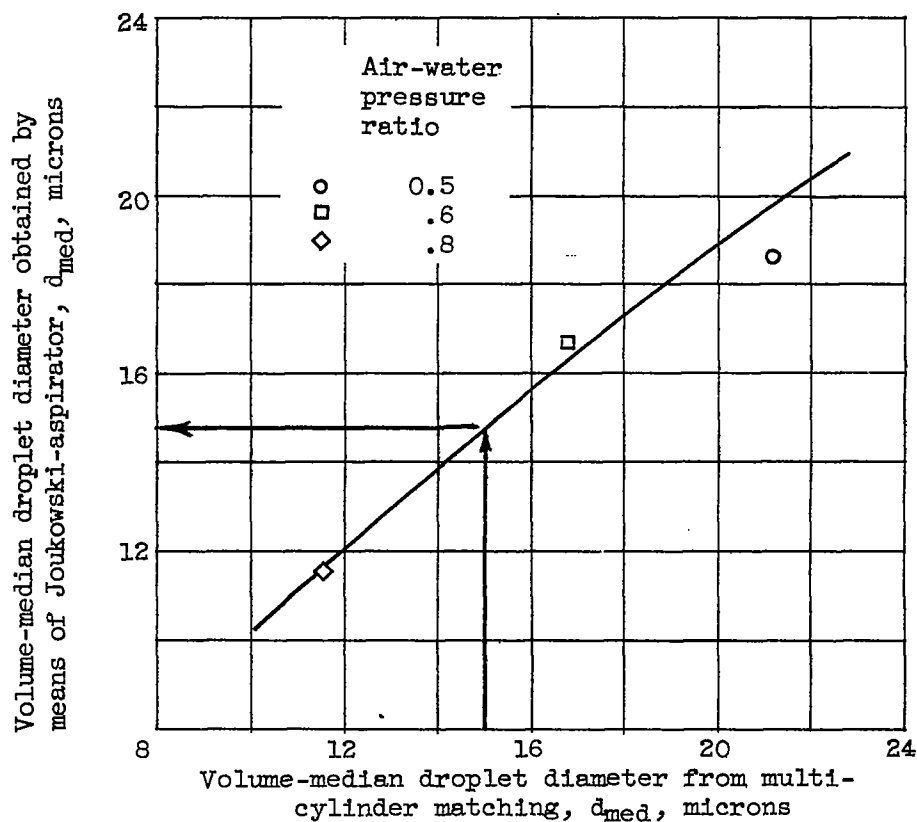
(b) Volume-median droplet diameter (Langmuir "D" distribution).

Figure 19. - Droplet diameter and liquid-water content by Joukowski-aspirator technique in terms of multicylinder matching to a Langmuir "D" distribution.

(a) Angle of attack, 0°.

(b) Angle of attack, 4°.
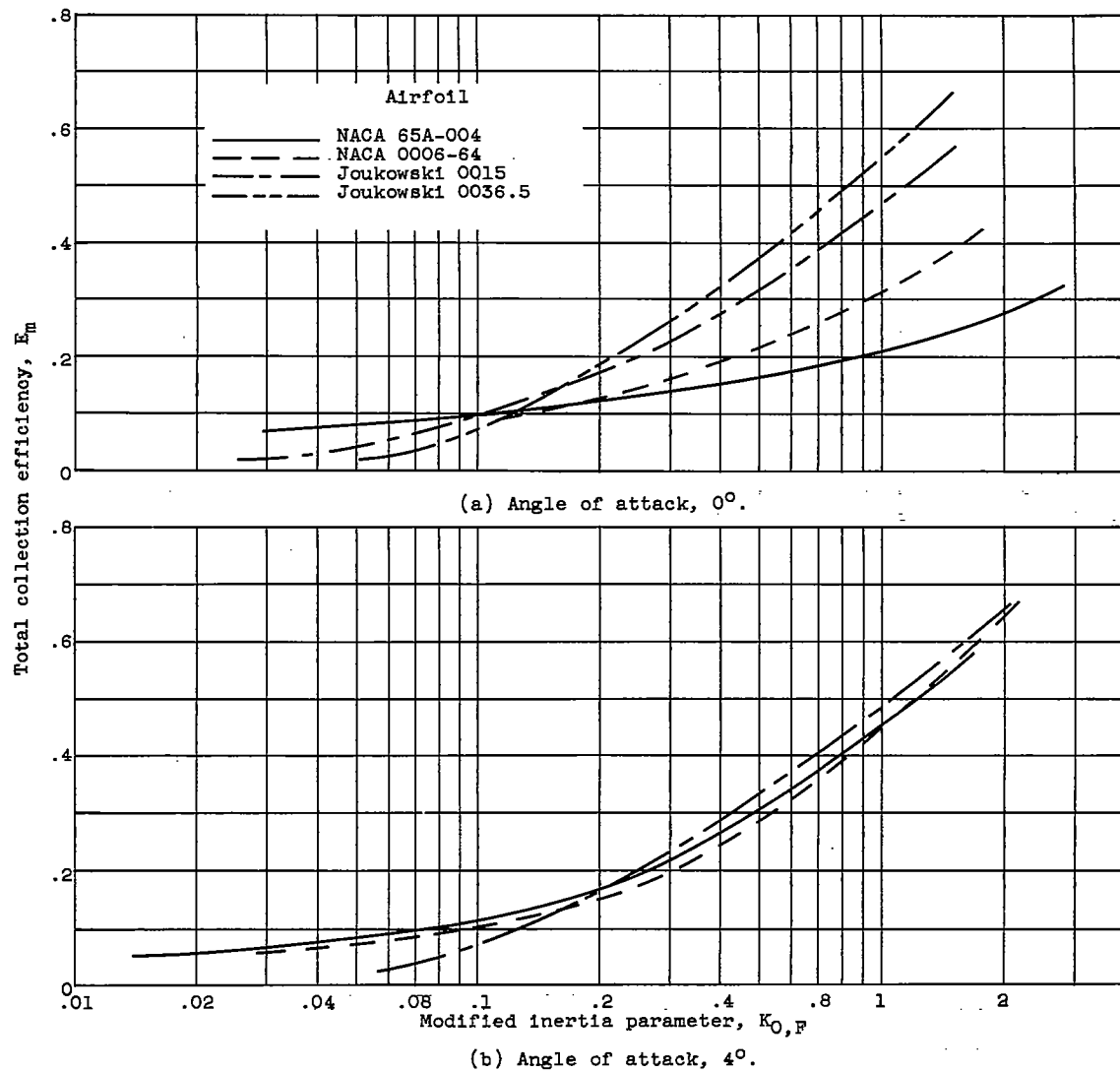
Figure 20. – Correlation of total collection efficiency with inertia parameter modified by projected height.
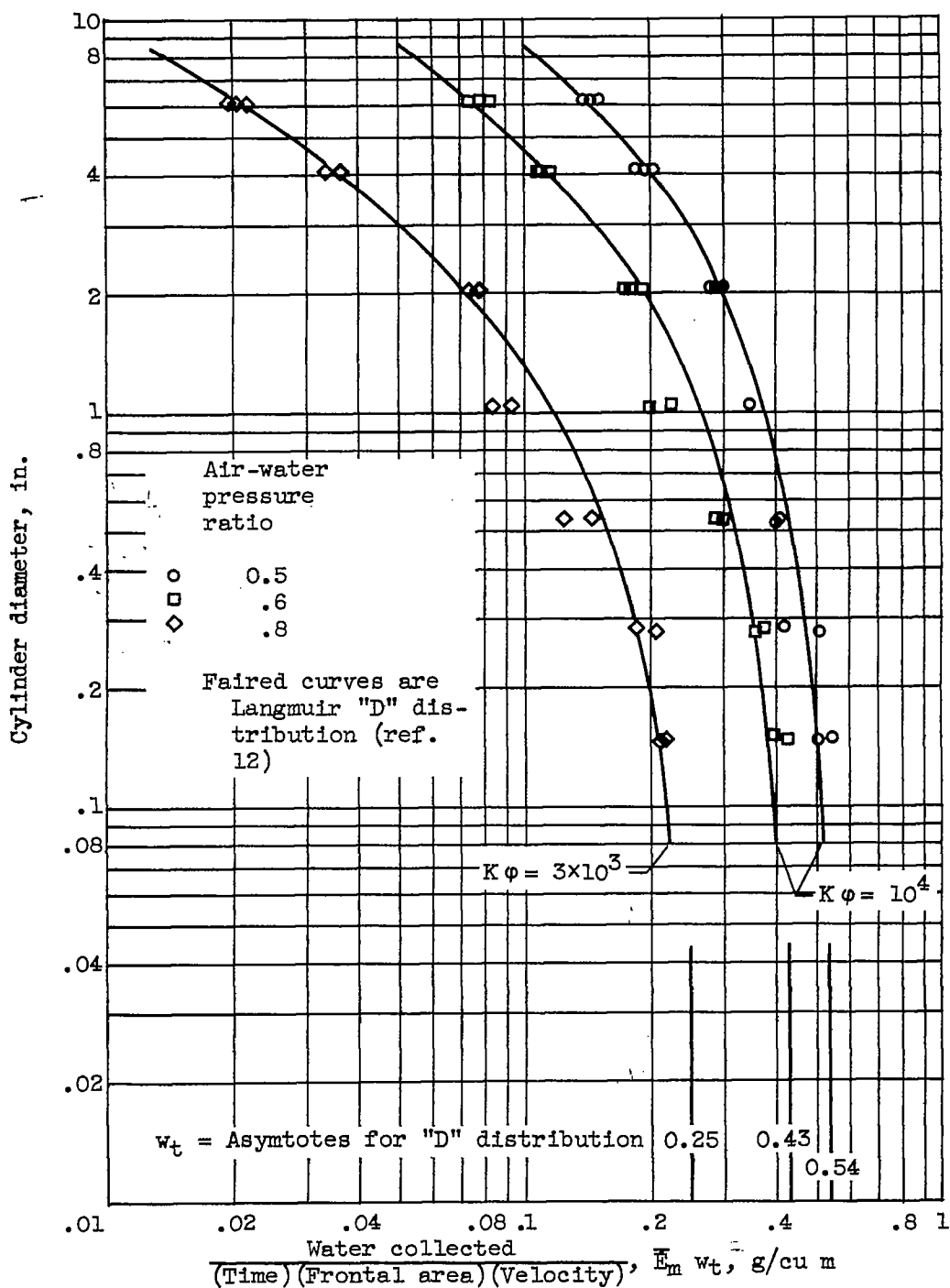
Figure 21. - Water collected by various cylinder sizes. Free-
stream velocity, 152 knots; air temperature, 50° F; air
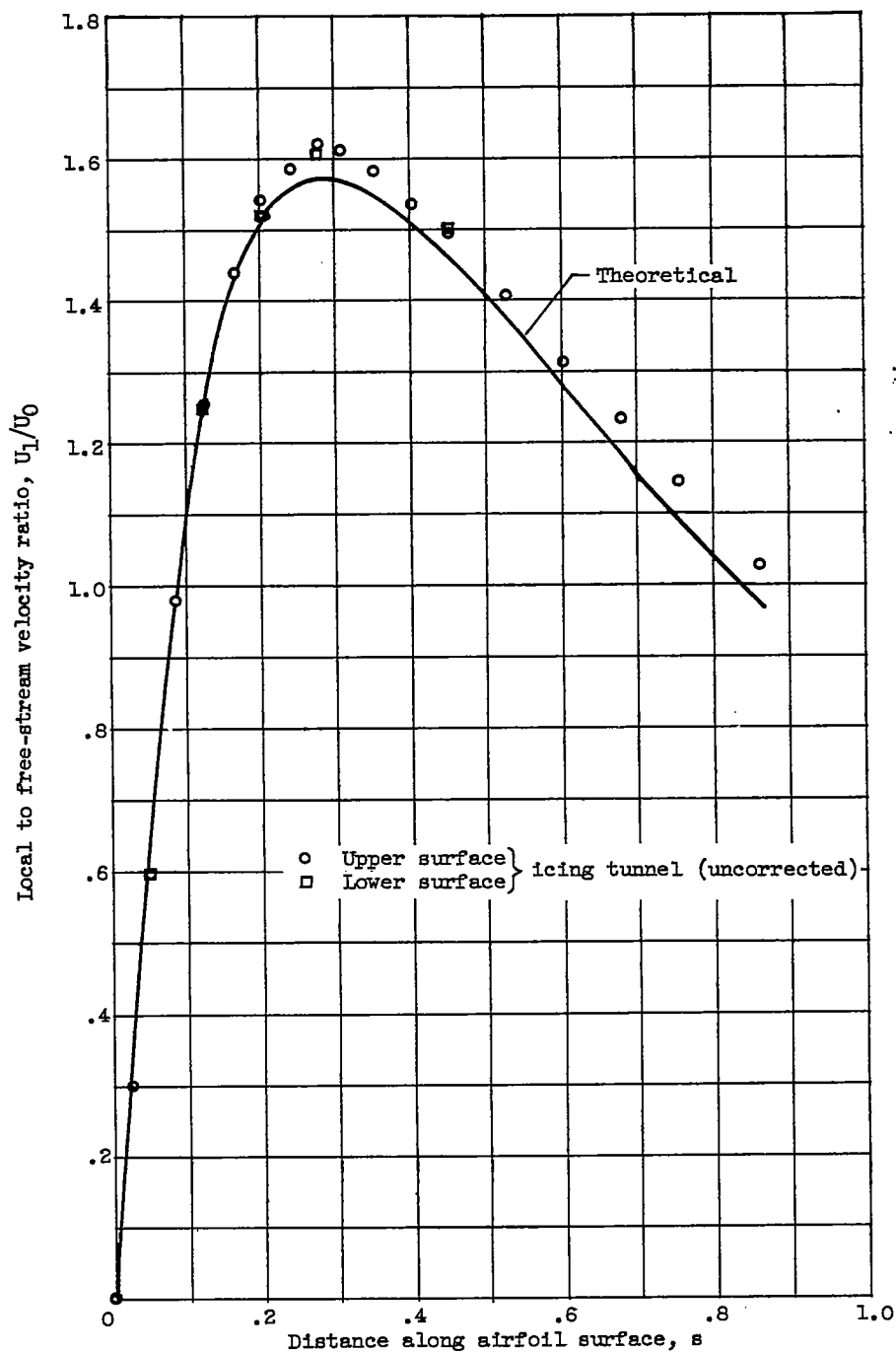pressure, 28.1 inches of mercury.

Figure 22. - Local velocity distribution on 36.5-percent-
thick symmetrical Joukowski airfoil. Angle of attack, 0°;
chord, 16.32 inches; airspeed, 152 knots; pressure, 28.1
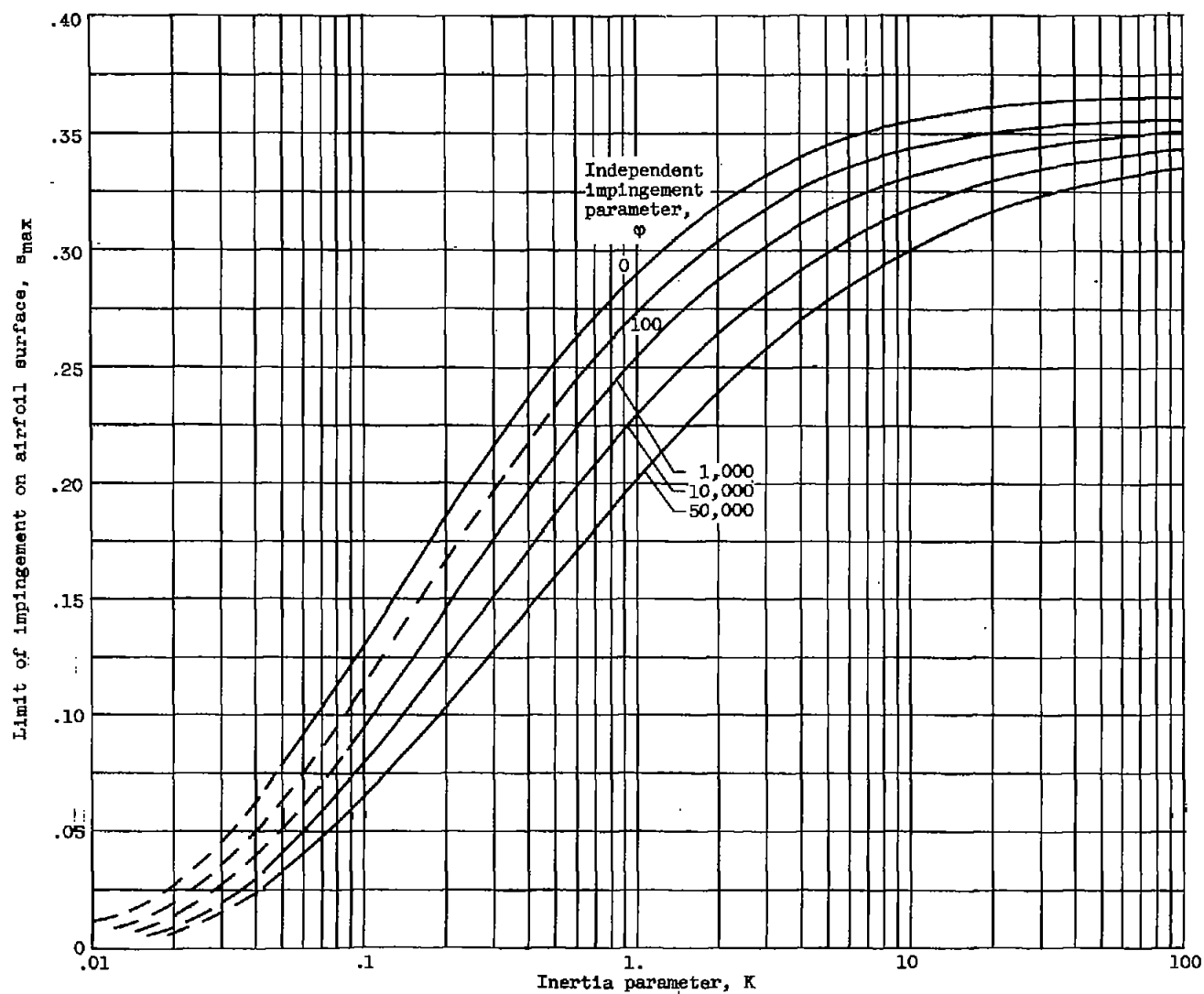inches of mercury; temperature, 50° F.

Figure 23. - Limit of impingement on upper or lower surface of 36.5-percent-thick symmetrical Joukowski airfoil. Angle of attack, 0°.
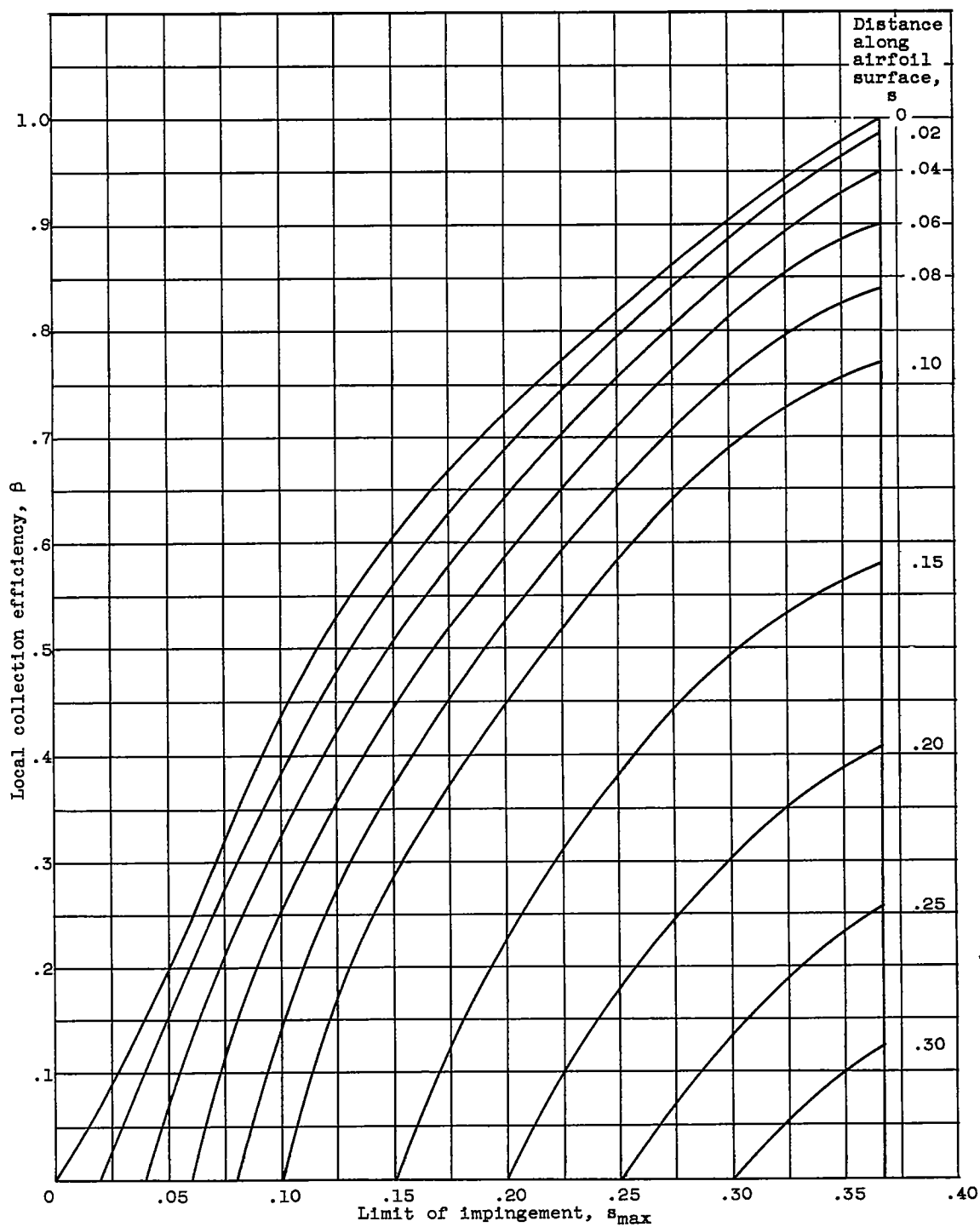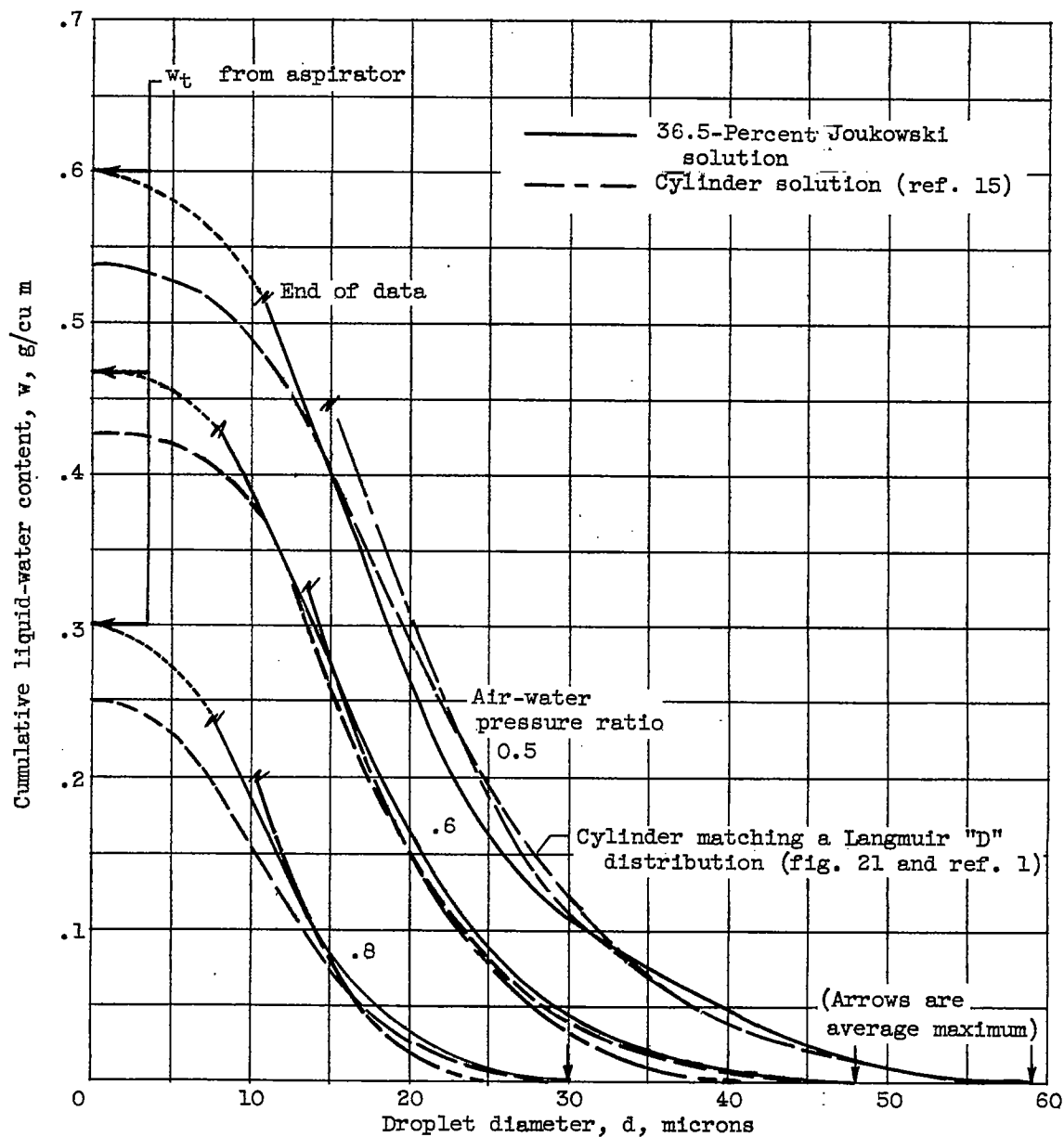
Figure 24. - Local collection efficiency of 36.5-percent-thick symmetrical
   Joukowski airfoil. Angle of attack, 0°.

(a) Average of data from several body sizes.

Figure 25. - Droplet-size distributions from experimental impingement
   rates on cylinders and 36.5-percent Joukowski airfoils. Comparison
   of methods of solution.

(b) Body size trends.

Figure 25. - Concluded. Droplet-size distributions from experimental impingement
rates on cylinders and 36.5-percent Joukowski airfoils. Comparison of methods
of solution.